Title	Study on Catalysis of Supported Platinum-Molybdenum Oxides in the Reductive Transformations of Carboxylic Acids and Esters
Author(s)	硲田, 捷将
Citation	大阪大学, 2025, 博士論文
Version Type	VoR
URL	https://doi.org/10.18910/101699
rights	
Note	

Study on Catalysis of Supported Platinum–Molybdenum Oxides

in the Reductive Transformations of Carboxylic Acids and Esters

Katsumasa SAKODA

MARCH 2025

Study on Catalysis of Supported Platinum–Molybdenum Oxides

in the Reductive Transformations of Carboxylic Acids and Esters

A dissertation submitted to

THE GRADUATE SCHOOL OF ENGINEERING SCIENCE

OSAKA UNIVERSITY

in partial fulfillment of the requirements for the degree of

DOCTOR OF PHILOSOPHY IN ENGINEERING

BY

Katsumasa SAKODA

MARCH 2025

Abstract

This thesis deals with studies on the catalysis of supported platinum–molybdenum oxide (Pt–MoO$_x$) in the reductive transformations of carboxylic acids and esters. The present thesis consists of four chapters.

In Chapter I, the author reviewed heterogeneous catalysts for the hydrogenation of carboxylic acids and esters to alcohols. In addition, reports on reductive transformations of carboxylic acids and esters to alkylamines and ethers were explained. Based on the literature survey, the purpose of the thesis was described.

In Chapter II, the author described an aluminum oxide-supported Pt–MoO$_x$ (Pt–MoO$_x$/γ-Al$_2$O$_3$) catalyst for the reductive amination of carboxylic acids to alkylamines. Alkylamines are important compounds used in pharmaceuticals, dyes, and surfactants. One of the well-known methods to synthesize them is the reductive amination of aldehydes, whereas the use of carboxylic acids will be a sustainable method for alkylamine production because carboxylic acids are abundant in nature. Previously reported heterogeneous catalysts required high H$_2$ pressures, such as 5 MPa, for the reductive amination of carboxylic acids. In sharp contrast, the Pt–MoO$_x$/γ-Al$_2$O$_3$ catalyst operated under 0.1 MPa H$_2$ for the first time. Moreover, the Pt–MoO$_x$/γ-Al$_2$O$_3$ catalyst was reusable without a significant loss of activity. This catalytic system exhibited a wide substrate scope with respect to both the carboxylic acids and amines, and biomass-derived fatty acids were successfully aminated to the corresponding fatty amines. A detailed investigation revealed that platinum nanoparticles (Pt NPs) cleave H$_2$ and molybdenum oxides (MoO$_x$) activate carboxylic acids. This cooperative catalysis facilitates the reductive amination of carboxylic acids under mild conditions.

In Chapter III, the author demonstrated that a titanium oxide-supported Pt–MoO$_x$ (Pt–MoO$_x$/TiO$_2$) can serve as a heterogeneous catalyst to promote the reductive amination of triglycerides

under mild conditions. Triglycerides are naturally abundant esters as oils and fats. The Pt–MoO$_x$/TiO$_2$ catalyst promoted the reductive amination of triglycerides under 1 MPa H$_2$, outperforming previously reported catalysts. The Pt–MoO$_x$/TiO$_2$ catalyst could be reused ten times without loss of activity. In addition, a broad substrate scope was demonstrated for both triglycerides and amines, and real cooking oils were successfully converted into their corresponding fatty amines. Detailed investigations revealed that the present catalytic reaction consists of the amidation of triglycerides to fatty amides and the subsequent hydrodeoxygenation of fatty amides to fatty amines. TiO$_2$ supports facilitate amidation reaction as acid catalysts, and Pt–MoO$_x$ species promote hydrodeoxygenation of fatty amides through activation of H$_2$ and fatty amides. Thus, the combination of TiO$_2$, Pt NPs, and MoO$_x$ efficiently catalyzes the reductive amination of triglycerides.

In Chapter IV, the author developed direct hydrodeoxygenation of esters to unsymmetrical ethers using a zirconium oxide-supported Pt–MoO$_x$ (Pt–MoO$_x$/ZrO$_2$) catalyst. Although unsymmetrical ethers are widely used as fragrances and pharmaceuticals, their traditional synthetic methods suffer from formation of waste. To overcome this problem, the author focused on the direct removal of carbonyl oxygen from esters as water using H$_2$ and achieved this reaction for the first time using the Pt–MoO$_x$/ZrO$_2$ catalyst. The Pt–MoO$_x$/ZrO$_2$ catalyst exhibited high activity under mild reaction conditions, such as 0.1 MPa H$_2$ and 100 °C. A wide range of esters, including triglycerides, was hydrodeoxygenated to the desired unsymmetrical ethers. Control experiments confirmed that the present reaction proceeded through the direct removal of the carbonyl oxygen from esters. Pt NPs activated H$_2$ and MoO$_x$ with oxygen vacancy sites abstracted the carbonyl oxygen of esters to produce ethers.

This thesis demonstrated a unique catalysis of supported Pt–MoO$_x$ in the reductive transformation of carboxylic acids and esters. This finding enhances the potential of carboxylic acids and esters as resources, and contributes to the establishment of a sustainable chemical process.

Preface

This dissertation is a collection of the author's studies which were carried out from 2019 to 2025 under the supervision of Professor Tomoo Mizugaki at the Division of Chemical Engineering, Department of Materials Engineering Science, Graduate School of Engineering Science, Osaka University.

The establishment of green and sustainable chemical processes using renewable resources is one of the ultimate goals of chemical industries. Carboxylic acids and esters are naturally abundant and regarded as renewable carbon sources. Therefore, it is highly desirable to develop an efficient method to transform carboxylic acids and esters into value-added compounds. In reduction reactions, the hydrogenation of carboxylic acids and esters to alcohols using heterogeneous catalysts has been widely developed. However, reductive transformations to synthesize other value-added compounds except for alcohols are less explored.

In this thesis, the author demonstrates that supported Pt–MoO$_x$ exhibits high catalytic activity in various reductive transformations of carboxylic acids and esters. Furthermore, the catalysis of supported Pt–MoO$_x$ in these reactions is extensively studied.

The author believes that this study will contribute to the establishment of green sustainable chemical processes by providing a simple and facile method for the transformation of carboxylic acids and esters into a wide variety of value-added compounds.

Contents

Chapter I.

General Introduction

1 Preliminary

Chemicals, produced in the chemical industry, have been applied in a wide range of fields, such as the agricultural, medical, electronics, and automotive industries, enhancing our quality of life. However, the chemical industry also has negative aspects, such as environmental pollution caused by the production of large amounts of waste, which threatens human lives. Solving this problem will lead to realizing an ideal society. In this context, the concept of "Green Chemistry" has gained significant attention. Green Chemistry is defined as the "design of chemical products and processes to reduce or eliminate the use and generation of hazardous substances" [1,2]. To establish an environmentally benign chemical process, P. Anastas and J. Warner introduced the Twelve Principles of Green Chemistry in 1998 as follows:

1. Prevention
2. Atom economy
3. Less Hazardous Chemical Syntheses
4. Designing Safer Chemicals
5. Safer Solvents and Auxiliaries
6. Design for Energy Efficiency
7. Use of Renewable Feedstocks
8. Reduce Derivatives
9. Catalysis
10. Design for Degradation
11. Real-time analysis for Pollution Prevention
12. Inherently Safer Chemistry for Accident Prevention

These principles are not independent but interrelated. For example, in organic chemistry textbooks, hydride reagents, such as lithium aluminum hydride, are used in the reduction of carbonyl compounds to alcohols. Lithium aluminum hydride is difficult-to-handle due to its moisture sensitivity and produce stoichiometric amounts of metal waste. In contrast, catalytic hydrogenation of carbonyl compounds using molecular hydrogen (H_2) as a reductant produces alcohols without the formation of metal waste. Moreover, highly active catalysts provide an alternative reaction pathway with a lower activation energy, enabling reactions at lower temperatures. Thus, the development of (9) catalytic

reactions leads to the use of (3) less hazardous and (12) safe reagents, (1) prevention of waste formation, and (6) energy savings, and is extremely important in green chemistry.

There are two types of catalysts: homogeneous and heterogeneous catalysts. Homogeneous catalysts, which are soluble in the reaction mixture, exhibit high catalytic activity because homogeneous catalysts easily interact with substrate and electronic state of metal centers is controlled by ligands. However, recovering homogeneous catalysts from a reaction mixture is difficult, resulting in high energy consumption. In contrast, heterogeneous catalysts, insoluble in the reaction mixture, can be easily recovered by filtration or centrifugation, with low energy consumption. Therefore, heterogeneous catalysts have been widely used in chemical industries, such as petrochemicals, and have been improved for the desired reactions. Recently, the replacement of fossil resources with renewable resources is a great interest in the pursuit of sustainable chemical processes. This corresponds to (7) of the Twelve Principles of Green Chemistry. Among renewable resources, the use of non-edible biomass, such as lignocellulose and used cooking oil, has attracted particular attention. Since the chemical structures of biomass-derived compounds differ from those of fossil-based compounds, the present heterogeneous catalyst systems cannot be applied to the transformation of biomass-derived compounds. Therefore, it is desired to develop new heterogeneous catalysts that can efficiently convert biomass-derived compounds into value-added chemicals.

2   Background

Carboxylic acids and esters are naturally abundant and regarded as renewable carbon sources (Figure 1-1). For example, acetic acid is the main component of vinegar, and abietic acid is obtained from pine resin. Methyl butyrate is contained in various fruits, and trilaurin with three ester moieties is found in coconut oil. Moreover, among the biomass-derived building blocks reported by the US Department of Energy, the majority of them contain carboxylic acid or ester moieties [3–5].
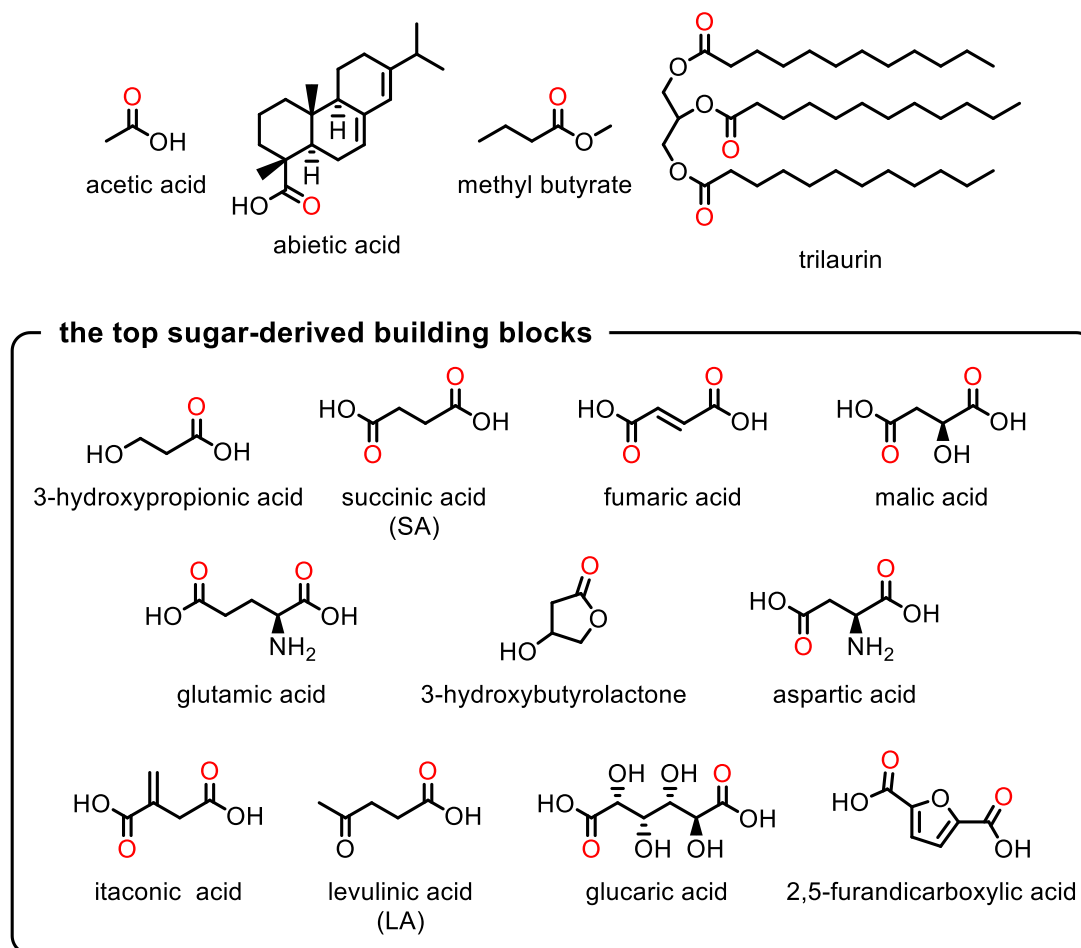

Figure 1-1 Carboxylic acids and esters in nature.

Carboxylic acids and esters can be transformed into various compounds, such as acid chlorides, acid anhydrides, amides, thioesters, aldehydes, and alcohols through nucleophilic acyl substitution (Figure 1-2). The oxidation states of the carbonyl carbons in carboxylic acids and esters are relatively high; therefore, the reduction of carboxylic acids and esters is important to convert them to a broader range of compounds. Carboxylic acid and ester moieties can be expressed in a resonant form between neutral and zwitterionic configurations (Figure 1-3). The electrophilicity of their carbonyl carbon decreases because of the delocalization of the lone pair of oxygen atoms [6]. As a result, the reactivity in the reduction of carbonyl compounds followed the order: acid chlorides > aldehydes and ketones > acid anhydrides > esters > carboxylic acids > amides [7]. Due to the difficulty of reduction of carboxylic acids and esters, strong reducing agents such as sodium metal (Bouveault–Blanc reduction) [8,9] and LiAlH$_4$ [10], have been used. However, these reductants are difficult-to-handle and generate large amounts of metal waste. From the viewpoints of environmental protection and atom economy, catalytic hydrogenation is attractive. To date, various homogeneous and heterogeneous catalysts have been developed [11–13]. In particular, the use of heterogeneous catalysts, which are easily recovered from reaction mixtures, contributes to the establishment of efficient hydrogenation processes.
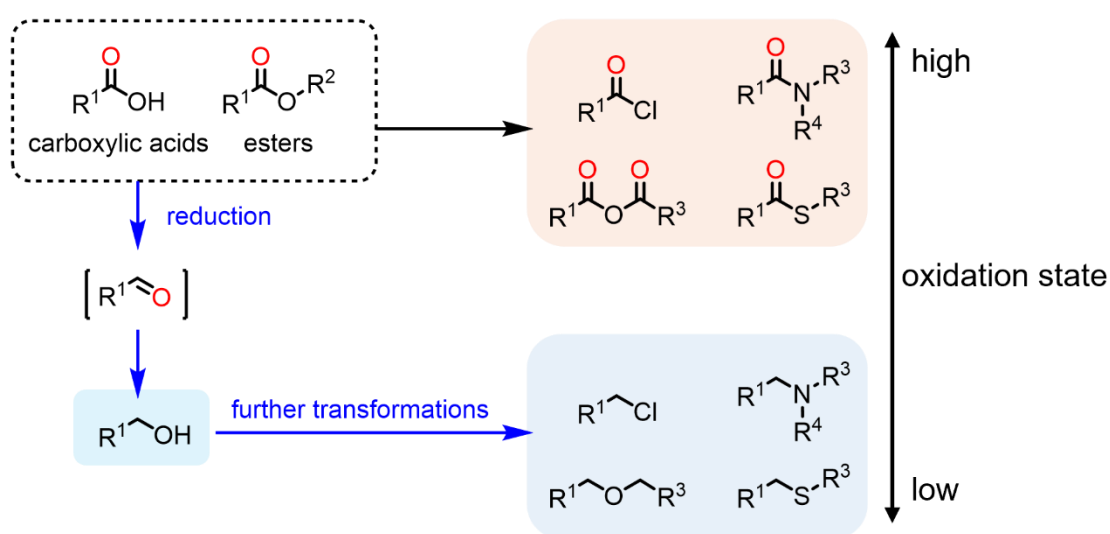

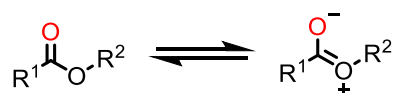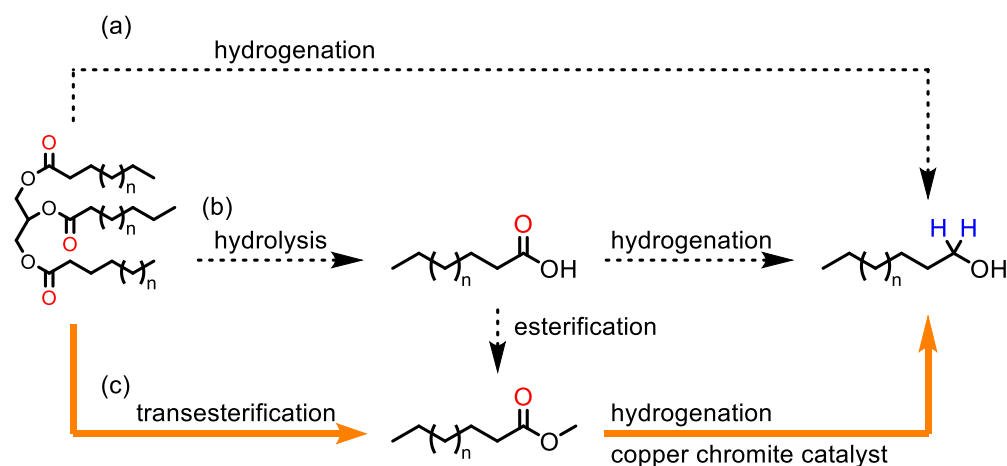**Figure 1-2** Transformation of carboxylic acids and esters.

Figure 1-3 Resonant form of carboxylic acids and esters.

2.1 Industrial hydrogenation of carboxylic acids and esters

In 1930, H. Adkins *et al.* reported that a copper chromite catalyst promoted hydrogenation of esters to the corresponding alcohol under 22 MPa H_2 at 250 °C [14–17]. The copper chromite catalysts have been used for the industrial production of fatty alcohols from natural oils and fats [18]. Scheme 1-1 shows various routes to convert natural oils and fats to fatty alcohols: hydrogenation of oils and fats (Scheme 1-1a); hydrolysis of oils and fats followed by hydrogenation of fatty acids (Scheme 1-1b); and transesterification followed by hydrogenation of fatty acid alkyl esters (Scheme 1-1c). Among them, the hydrogenation of oils and fats (Scheme 1-1a) is the most straightforward and attractive method. However, this method requires harsh reaction conditions and suffers from the loss of H_2 and glycerol due to the over-hydrogenation of glycerol to propylene glycol and propanol. The process *via* fatty acids (Scheme 1-1b) is conducted using a copper chromite catalyst at approximately 300 °C, but there are problems such as over-hydrogenation of the desired fatty alcohols to hydrocarbons and catalyst degradation by fatty acids.

To avoid these problems, fatty alcohol is often produced through transesterification and hydrogenation processes (Scheme 1-1c). In this process, oils and fats are converted to fatty acid methyl esters (FAME) through transesterification with methanol in the presence of a base catalyst. FAMEs are then hydrogenated to fatty alcohols using a copper chromite catalyst under 20–30 MPa at 200–300 °C. Nevertheless, harsh reaction conditions are still required, and the leaching of toxic Cr may cause serious environmental problems. Therefore, the development of a green and efficient heterogeneous catalytic system for the hydrogenation of carboxylic acids and esters is desirable.

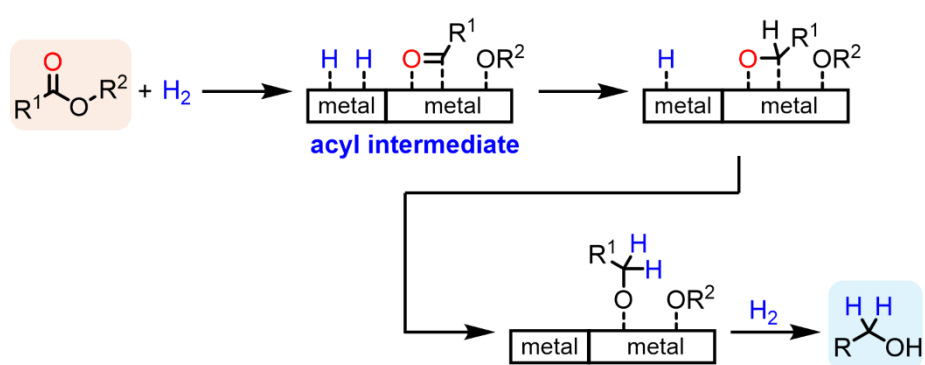**Scheme 1-1** Industrial hydrogenation of carboxylic acid and esters.

2.2 Mechanistic study of the hydrogenation of carboxylic acids and esters

To achieve the efficient hydrogenation of carboxylic acids and esters, it is crucial to understand the reaction mechanisms and develop a new catalyst based on the mechanism. In this section, the author summarized reports discussing the reaction mechanism of the hydrogenation of esters and carboxylic acids.

2.2.1 Mechanism of the hydrogenation of esters

M. S. Wainwright *et al.* investigated a reaction mechanism of the Raney Cu-catalyzed hydrogenation of ethyl acetate [19]. The reaction order was found to be −0.5 with respect to ethyl acetate, indicating the dissociative adsorption of ethyl acetate as surface acyl and alkoxide species (Scheme 1-2). This mechanism is supported by density functional theory (DFT) calculations [20]. Cu catalysts, including copper chromite catalysts, contain both Cu^0 and Cu^+ species, and it has long been discussed which are the actual active sites. To clarify the active species, X. Ma *et al.* prepared fourteen Cu/SiO_2 catalysts, and their catalytic activities were evaluated in the hydrogenation of methyl acetate [21]. Moreover, the Cu^0 and Cu^+ surface areas of these catalysts were estimated by N_2O adsorption,

X-ray photoelectron spectroscopy, X-ray absorption fine structure (XAFS), and CO Fourier Transform Infrared (FT-IR) analyses. As a result, Cu/SiO$_2$ with abundant Cu^0 and Cu$^+$ showed high activity, revealing that both species are important in the hydrogenation of esters. Cu^0 activates H$_2$, and Cu$^+$ stabilizes the surface acyl and alkoxyl species, thus cooperatively promoting the hydrogenation of esters to alcohols [22].

Scheme 1-2 Reaction mechanism of the hydrogenation of esters to alcohols.

2.2.2 Mechanism of the hydrogenation of carboxylic acids

In the hydrogenation of carboxylic acids using heterogeneous catalysts, three reaction mechanisms have been proposed [23]: dissociative adsorption of carboxylic acids to form surface acyl species followed by hydrogenation (acyl pathway; Scheme 1-3(I)); adsorption of carboxylic acids on the catalysts as carboxylates or molecular carboxylic acids followed by hydride addition to the carbonyl carbon atom (geminal diol pathway; Scheme 1-3(II)); and abstraction of oxygen from carboxylic acids to form aldehyde by metal oxides with oxygen vacancy sites followed by hydrogenation of aldehyde (deoxygenation pathway; Scheme 1-3(III)).
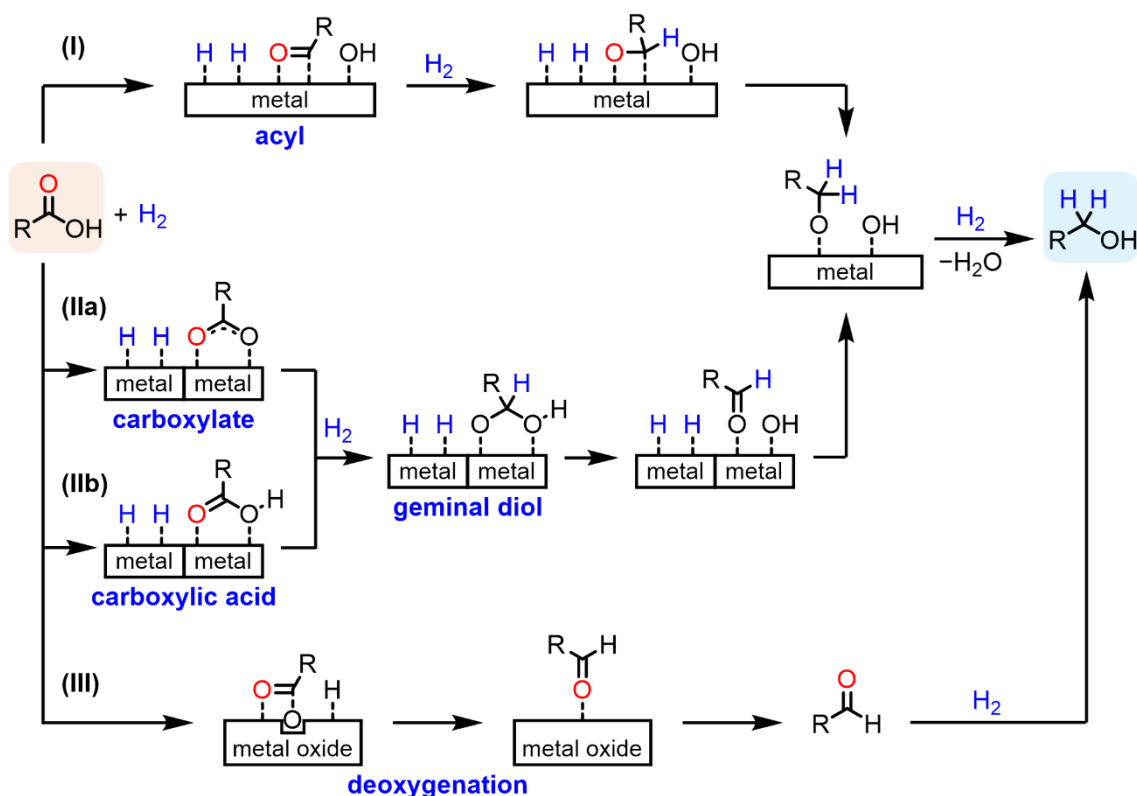
Scheme 1-3 Reaction mechanism of the hydrogenation of carboxylic acids to alcohols through the (I) acyl pathway, (II) geminal diol pathway, and (III) deoxygenation pathway.

Acyl pathway (Scheme 1-3(I))

M. A. Vannice *et al.* investigated the reaction mechanism of the hydrogenation of acetic acid over a Pt/TiO$_2$ catalyst using diffuse reflectance infrared Fourier transform spectroscopy (DRIFTS) and temperature-programmed reaction (TPR) [24]. The DRIFTS spectrum of acetic acid adsorbed on Pt/TiO$_2$ at room temperature exhibited various adsorption modes, including acyl species. When H$_2$ was introduced and the temperature increased, the peak of the acyl species disappeared at approximately 200 °C. In the TPR analysis, ethanol was detected at 217 °C, which was close to the temperature that the acyl species disappeared in the DRIFT analysis. Based on these results, acyl species were considered to be reaction intermediates. The acyl pathway was also supported by DFT calculations [25,26]. Moreover, W. Fan *et al.* developed a Co nanoparticle catalyst for hydrogenation

of carboxylic acids and investigated the mechanism using DRIFTS analysis and DFT calculations [27].

The DRIFTS spectrum of acetic acid adsorbed on the Co catalyst under H_2 showed a peak assigned to

the acyl species, which gradually disappeared as time passed, accompanied with appearance of a new

peak assigned to ethanol. Moreover, DFT calculations supported the preference for the acyl pathway.

It is reported that surface acyl species cause decarbonylation, resulting in a low selectivity for alcohols

[28]. L. Ma *et al.* contribute to solve this problem by employing metal–Lewis acid bifunctional catalyst

[29,30]. The catalytic activities of supported Ru catalysts were tested in the hydrogenation of propionic

acid. Ru/Al_2O_3, which has abundant Lewis acid sites and strong metal–support interactions (SMSI),

afforded the desired propyl alcohol by suppressing C–C bond cleavage. Lewis acid activated carbonyl

moiety of surface acyl species, and SMSI decreased bare Ru sites which cause decarbonylation.

Geminal diol pathway (Scheme 1-3(II))

The geminal diol pathway can be further divided into the carboxylate pathway (Scheme 1-

3(IIa)) and molecular carboxylic acid pathway (Scheme 1-3(IIb)). M. A. Vannice *et al.* studied the

reaction mechanism of the Fe/SiO_2-catalyzed hydrogenation of acetic acids using DRIFTS and TPR

[31], similar to their study of Pt/TiO_2 system mentioned in the previous paragraph. The DRIFTS

spectrum of acetic acid adsorbed on Fe/SiO_2 exhibited various peaks, including acetate and molecular

acetic acid, but no peak assigned to acyl species was observed. As the temperature increased under H_2,

the intensity of the observed peaks gradually decreased. In the TPR analysis, acetaldehyde and ethanol

were detected at approximately 300 °C. This was close to the temperature at which the acetate peak

decreased in the DRIFTS measurements. Based on these results, acetate was proposed as a plausible

intermediate in this system (Scheme 1-3(IIa)). M. Zhang *et al.* reported hydrogenation of acetic acid

using Cu–In/SBA-15 and investigated the reaction mechanism [32]. *In situ* FT-IR analysis of acetic

acid adsorbed on the catalyst revealed the presence of acyl and acetate species on the catalyst surface.

As the temperature increased, the acyl peak disappeared at 100 °C, which was significantly lower than the actual reaction temperature (350 °C), indicating that acetate was likely to be an intermediate in this system.

The hydrogenation of carboxylate species is difficult and requires a high reaction temperature [24]. In contrast, the pathway *via* molecularly adsorbed carboxylic acid can be operated at lower temperatures (Scheme 1-3(IIb)). D. R. Vardon *et al.* conducted hydrogenation of propionic acid using Ru and Ru–Sn catalysts [33]. The Ru catalyst provided propanol in 10% selectivity under 10 MPa H_2 at 160 °C, whereas the Ru–Sn catalyst showed 95% selectivity. DFT calculations revealed that hydrogenation proceeded through both acyl and geminal diol pathways on the Ru surface, as well as side reactions such as decarbonylation, decarboxylation, and over-hydrogenation. For the Ru–Sn catalyst, the geminal diol pathway is dominant. Molecular adsorption of propionic acid occurred on Lewis acidic SnO, and hydrogen species activated on the Ru surface attack to propionic acid. Therefore, geminal diol pathway is also efficiently promoted by the metal–Lewis acid bifunctional catalysts.

Deoxygenation pathway (Scheme 1-3(III))

Finally, the deoxygenation pathway is introduced. This pathway is often used for the selective deoxygenation of carboxylic acids to aldehydes. V. Ponec *et al.* conducted the hydrogenation of acetic acid using various metal oxides [34]. As a result, copper, iron, tin, and vanadium oxides provided acetaldehyde. A volcano-shape dependence between the obtained acetaldehyde amount and the metal–oxygen bond strength was observed. Moreover, the X-ray diffraction (XRD) and Mössbauer spectroscopy analyses revealed that the used catalysts were partially reduced. Based on these results, a reverse Mars–van Krevelen mechanism was proposed [35]: metal oxides are reduced by H_2, and lattice oxygens are removed as water to form oxygen vacancies. Then, the oxygen vacancies are

refilled by abstracting oxygen atom of acetic acid, which forms acetaldehydes. A higher metal–oxygen bond strength prevents the formation of oxygen vacancies, and a lower metal–oxygen bond strength does not promote the deoxygenation of acetic acid. K. Wada *et al.* developed a Pd/Fe$_2$O$_3$ catalyst for the hydrogenation of acetic acid to acetaldehyde and investigated the reaction mechanism using *in situ* XAFS measurement [36]. Pd/Fe$_2$O$_3$ were reduced to Pd^0 and Fe^0 during H$_2$ treatment to form Pd–Fe alloy nanoparticles. When acetic acid was fed into the catalyst in the absence of H$_2$, Pd^0 was maintained, and Fe^0 was oxidized to FeO. These observations revealed that the deoxygenation of acetic acid to acetaldehyde occurs on the Fe^0 site *via* a reverse Mars–van Krevelen mechanism.

2.3 Efficient hydrogenation using a bifunctional catalyst

2.3.1 Hydrogenation of aliphatic carboxylic acids and esters

As described above, the metal–Lewis acid bifunctional catalysts are effective for the hydrogenation of carboxylic acids and esters, and highly efficient catalyst systems have been developed based on these combinations. One example of them is the metal oxide-supported metal nanoparticle catalyst, in which metal nanoparticles activate H$_2$ and the supports with oxygen vacancies adsorb carboxylic acids and esters as Lewis acids. Pt/TiO$_2$ facilitated hydrogenation of various fatty acids under 2 MPa H$_2$ at 130 °C, providing the corresponding alcohols in over 70% yield [37]. Co/ZrO$_2$ showed high activity in the hydrogenation of methyl laurate to produce lauryl alcohol in 91% yield under 2 MPa H$_2$ and 180 °C [38]. Another type of the metal–Lewis acid bifunctional catalyst is the supported metal–metal oxide. Pd–Re/SiO$_2$ converted carboxylic acids under 8 MP H$_2$ at 140 °C [39]. Ru–Sn/C produced alcohols from fatty acids, FAME, and natural oils under 5 MP H$_2$ at 140–180 °C [40]. Table 1-1 summarized the heterogeneous catalysts that provide high yields (>80%) under mild reaction temperatures (<200 °C).

Table 1-1 Reported heterogeneous catalysts for hydrogenation of carboxylic acids and esters under mild conditions (over 80% yield, lower than 200 °C).

catalyst	substrate	condition	yield	ref.
Re/TiO$_2$	stearic acid	4 MPa, 200 °C	93	41
Co/HAP	stearic acid	4 MPa, 190 °C, 10 h	97	42
Co/ZrO$_2$	methyl laurate	2 MPa, 130 °C, 24 h	91	38
Pd–Re/SiO$_2$	stearic acid	8 MPa, 140 °C, 16 h	94	39
Cu–FeO$_x$/SiO$_2$	stearic acid	3 MPa, 180 °C, 3 h	95	43
Pd/Nb$_2$O$_5$/SiO$_2$	palmitic acid	2.5 MPa, 180 °C, 24 h	97	44
Pd/Re/C	stearic acid	2 MPa, 130 °C, 2 h	87	45
Ru–Sn/C	stearic acid	5 MPa, 140 °C, 6 h	96	40
Ni–Re/SBA-15	stearic acid	4 MPa, 150 °C, 5 h	95	46
Ni–ReO$_x$/TiO$_2$	stearic acid	4 MPa, 165 °C, 5.5 h	95	47
NiMoO$_x$@C	stearic acid	4 MPa, 160 °C, 4 h	97	48
Ru–FeO$_x$/SiO$_2$	octanoic acid	4 MPa, 140 °C, 36 h	96	49

2.3.2 Valorization of biomass-derived functionalized carboxylic acids

Most biomass-derived building blocks reported by the US Department of Energy contain carboxylic acids [4,5,6], and it is desirable to convert them into value-added compounds. Therefore, highly active catalysts for the hydrogenation of carboxylic acids are often applied to the biomass conversion. Herein, the hydrogenation of particularly attractive biomass-derived carboxylic acids, i.e. levulinic acid (LA) and succinic acid (SA), is described.

Levulinic acid

LA is the one of the most important compounds obtained from lignocellulose. In the hydrogenation of LA, the carbonyl moiety is firstly hydrogenated to form 4-hydroxypentanoic acid, which is immediately converted to γ-valerolactone (GVL) by intramolecular dehydration (Scheme 1-4). Then, hydrogenation of GVL affords 1,4-pentanediol (PDO). The rate-determining step in the hydrogenation of LA to PDO is the transformation from GVL to PDO, because hydrogenation of the ester moiety is more difficult than that of the carbonyl moiety. The first report on the hydrogenation of LA to PDO was performed using a copper chromite catalyst in 1947 [50]. Under 20 MPa H_2 at 300 °C, PDO was obtained in a 44% yield with GVL in an 11% yield. Although there were no reports for a while, since 2013, metal–Lewis acid bifunctional catalysts, such as Ru–Re/C [51], Rh–Mo/SiO$_2$ [52], Pt–Mo/hydroxyapatite [53], and Ru–Mo/C [54], have been developed to achieve high yields (<97%) under mild reaction conditions (>3 MPa H_2, >70 °C).
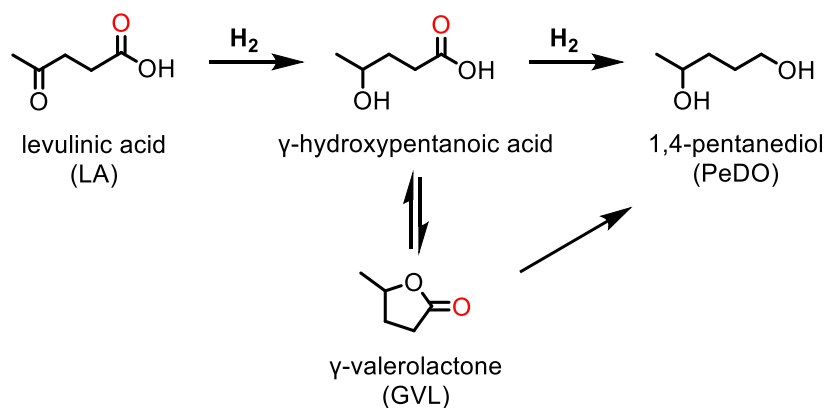
Scheme 1-4 Hydrogenation of levulinic acid (LA) to 1,4-pentandiol (PeDO).

Succinic acid

SA can be obtained by sugar fermentation. 1,4-butanediol (BDO), produced by the hydrogenation of SA, is used as a monomer for polyesters, polyurethanes, and polyethers. In the hydrogenation of SA, one carboxylic acid moiety is hydrogenated to give γ-hydroxybutyric acid, which is immediately transformed into γ-butyrolactone (GBL; Scheme 1-5). The subsequent hydrogenation of GBL produces BDO. Efficient hydrogenation of SA to give BDO in high yields (>70%) has been achieved using metal–Lewis acid bifunctional catalysts, for example Re–Ru/C [55], Re–Pd/SiO$_2$ [56], and Cu–Pd/HAP [57], under 8 MPa H$_2$ at 140–200 °C.
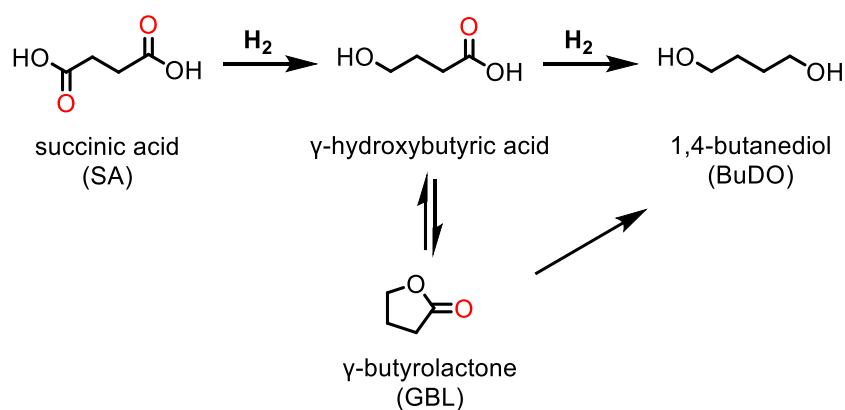

Scheme 1-5 Hydrogenation of succinic acid (SA) to 1,4-butanediol (BuDO).

2.4 Applications beyond traditional synthesis and productions

Heterogeneous catalyst systems for conversion of carboxylic acids and esters into alcohols were introduced. The obtained alcohols are an important class of chemicals that can be used as surfactants, lubricants, as well as intermediates to synthesize other value-added compounds. The development of a reductive transformation that synthesizes the desired value-added compounds, except for alcohols, will contribute to the construction of a simple and facile reaction process, and enhance the potential of carboxylic acids and esters as resources.

15

2.4.1 Amines

Amines are important compounds used as pharmaceuticals and surfactants, and are attractive candidates produced in the reductive transformation of carboxylic acids and esters [58,59]. In 1969, the reductive amination of coconut oil to fatty amines was performed using $ZnO–Al_2O_3$ under 25 MPa H_2 at 310 °C [60]. After that, in 1994, copper chromite-catalyzed reductive amination of FAME was reported under 5 MPa H_2 and 250 °C [61]. Recently, two heterogeneous catalyst systems, Re/TiO_2 [62] and Pt/ZrO_2 [63], were developed (Scheme 1-6). Re/TiO_2 promoted the reductive amination of 3-phenylpropionic acid and methyl 3-phenylpropionate to 3-phenylpropyl-dimethylamine at 5 MPa H_2 and 200 °C, where the hydrogenation of the substrates to alcohol intermediates was followed by the amination of alcohol intermediates (Scheme 1-6a). In the Pt/ZrO_2 system, a wide range of triglycerides was converted to amides and then hydrogenated to form fatty amines (Scheme 1-6b). It is reported that aliphatic amines poison metal catalysts [64]. Therefore, reductive transformations in the presence of aliphatic amines as substrates or products are challenging and require harsh reaction conditions.

Scheme 1-6 Reductive amination of carboxylic acid and esters.

2.4.2 Ethers

Ethers are widely used as fragrances, surfactants, and lubricants. In 1986, it was reported that

Re/γ-Al$_2$O$_3$ produced a small amount of diethyl ether in the hydrogenation of ethyl acetate [65,66].

The major product of this reaction is ethanol, and γ-Al$_2$O$_3$ is known to promote the dehydrative

condensation of ethanol to diethyl ether [67,68]. M. Lemaire *et al.* found that Pd/C and solid acid

(Amberlyst 35) transformed monoglyceride to 1-*O*-alkyl glycerol in glycerol solvent with formation

of 2-*O*-alkyl glycerol as byproduct [69,70]. Since 2022, D. W. Flaherty *et al.* performed a reductive

transformation of propyl acetate to ethyl propyl ether using Pd/WO$_3$ [71], Pd/Nb$_2$O$_5$ [72], or Pt/FAU

[73,74] catalysts. These catalytic systems require an acidic support, and ethanol and propanol were

detected. Furthermore, not only ethyl propyl ether but also symmetric ethers, such as diethyl ether and

dipropyl ether, were produced.

There are two possible reaction pathways in the transformation of esters to ethers:

hydrogenation of esters to alcohols followed by acid-catalyzed intermolecular dehydration of alcohols

(Scheme 1-7a); and direct hydrodeoxygenation of carbonyl oxygen (Scheme 1-7b). In the pathway *via*

alcohols shown in Scheme 1-7a, undesired symmetric ethers are by-produced, resulting in low

selectivity. In contrast, the direct hydrodeoxygenation pathway (Scheme 1-7b) has the advantage in

high selectivity for unsymmetrical ethers.
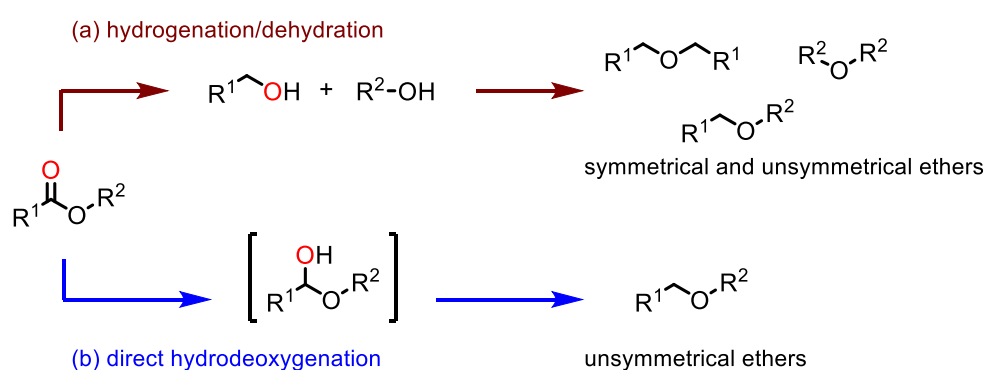
Scheme 1-7 Conversion of ester to ether through (a) hydrogenation/dehydration and (b) direct hydrodeoxygenation.

17

3   Purpose of this thesis

Since the catalytic hydrogenation of esters was reported in 1931, highly active bifunctional catalysts for hydrogenation of carboxylic acids and esters have been developed. These catalysts provide alcohols through C–O bond cleavage by cooperative catalysis between metal and Lewis acid activating H_2 and substrates, respectively. In contrast, catalysts for the reductive transformations to produce other value-added compounds have been less explored. To achieve this, development of heterogeneous catalysts to promote deoxygenative functionalization of carbonyl oxygen is desirable [75].

It is reported that low-valent oxophilic metal complexes such as Mo complex remove carbonyl oxygen of ketones to achieve deoxygenative functionalization [76]. However, in this reaction, low-valent Mo acts as a stoichiometric reductant and oxidized Mo is formed as waste. To prevent formation of metal waste, the use of Mo as a catalyst by reduction of the oxidized Mo species to reproduce low-valent Mo in the reaction system is essential. Especially, H_2 reduction of oxidized Mo is an attractive method because water is produced as a sole co-product [77], and it is efficiently promoted in the presence of hydrogenation catalysts such as Pt [78]. Based on this knowledge, the author envisaged that cooperative catalysis of Pt and Mo would achieve reductive transformations of carboxylic acids and esters through deoxygenation of carbonyl oxygen using H_2 as terminal reductant. The main purpose of this thesis is to develop supported platinum–molybdenum oxide (Pt–MoO$_x$) catalysts for the reductive transformation of carboxylic acids and esters. This study provides a simple and facile method to convert carboxylic acids and esters into a wide variety of value-added compounds, enhancing their potential as resources.

4   Outline of this thesis

The present thesis describes the reductive transformation of carboxylic acids and esters using supported Pt–MoO$_x$ catalysts.

In Chapter II, the author introduced the reductive amination of carboxylic acids using an aluminum oxide-supported Pt–MoO$_x$ (Pt–MoO$_x$/γ-Al$_2$O$_3$) catalyst (Figure 1-4). Pt–MoO$_x$/γ-Al$_2$O$_3$ exhibits a high activity under mild reaction conditions. This is the first example that promotes the reductive amination of a carboxylic acid at atmospheric pressure of H$_2$. The catalyst is easily recovered from the reaction mixture and reused without significant loss of its high activity and selectivity. A wide range of amines and carboxylic acids, including triglyceride-derived fatty acids, are successfully transformed into the desired alkylamines. Characterizations and DFT calculations reveal that the high activity of Pt–MoO$_x$/γ-Al$_2$O$_3$ originates from cooperative catalysis, in which platinum nanoparticles (Pt NPs) and molybdenum oxides with oxygen vacancies (MoO$_x$) activate H$_2$ and carboxylic acids, respectively.
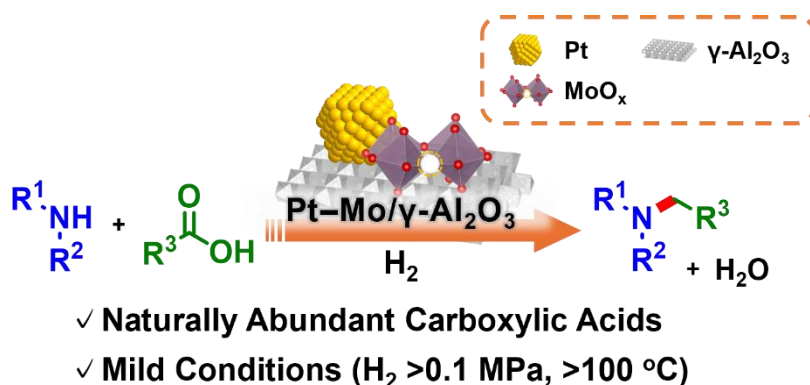
Figure 1-4 Reductive amination of carboxylic acids over a Pt–MoO$_x$/γ-Al$_2$O$_3$ catalyst.

In Chapter III, the author introduced reductive amination of triglycerides to fatty amines over a titanium oxide-supported Pt–MoO$_x$ (Pt–MoO$_x$/TiO$_2$) catalyst (Figure 1-5). Pt–MoO$_x$/TiO$_2$ can be operated under 1 MPa H$_2$, which is significantly lower than that of the reported catalyst systems. Moreover, Pt–MoO$_x$/TiO$_2$ is reusable 10 times maintaining its high activity, demonstrating high

durability. Various amines and triglycerides, including a real cooking oil, are converted to the corresponding fatty amines. Investigations of the reaction pathways reveal that this reaction consisting of the amidation of triglycerides and the hydrodeoxygenation of fatty amides to fatty amines. The TiO_2 support promotes amidation as a solid acid catalyst, and Pt and Mo species facilitate the hydrogenation of amides by activating H_2 and amides, respectively.
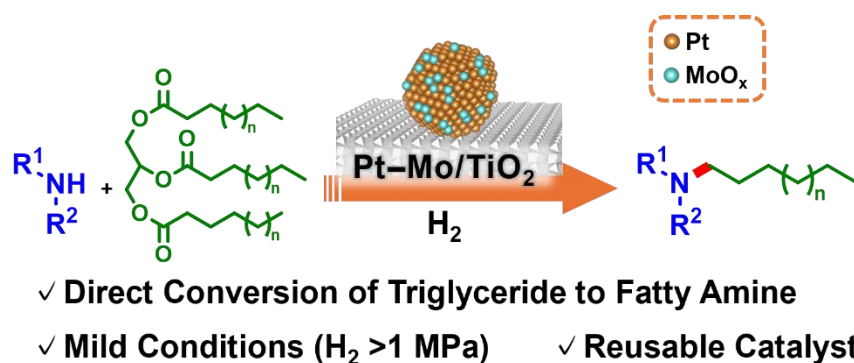
Figure 1-5 Reductive amination of triglycerides to fatty amines using a Pt–MoO$_x$/TiO$_2$ catalyst.

In Chapter IV, the author presented direct hydrodeoxygenation of esters to unsymmetrical ethers catalyzed by a zirconium oxide-supported Pt–MoO$_x$ (Pt–MoO$_x$/ZrO$_2$; Figure 1-6). This is the first example that promotes direct hydrodeoxygenation of esters to ethers. Pt–MoO$_x$/ZrO$_2$ efficiently converts a wide range of esters, including biomass-derived FAME and triglycerides, into the corresponding unsymmetrical ethers in high yields. The catalyst is reusable and applicable to a gram-scale reaction.
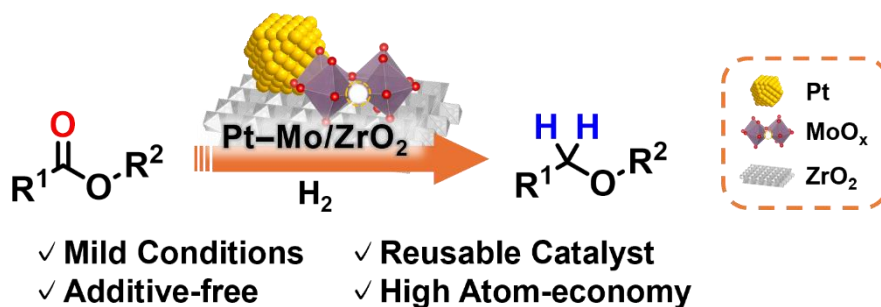
Figure 1-6 Direct hydrodeoxygenation of esters to unsymmetrical ethers catalyzed by Pt–MoO$_x$/ZrO$_2$.

5   Reference

1. Anastas, P. T.; Warner, J. C. *Green Chemistry: Theory and Practice*, Oxford University Press, 1998.

2. Anastas, P. T.; Eghbali, N. Green Chemistry: Principles and Practice. *Chem. Soc. Rev.* **2010**, *39*, 301–312.

3. Werpy, T.; Petersen, G. *Top Value Added Chemicals from Biomass: Volume I – Results of Screening for Potential Candidates from Sugars and Synthesis Gas*, 2004, DOI: 10.2172/15008859.

4. Bozell, J. J.; Petersen, G. R. Technology Development for the Production of Biobased Products from Biorefinery Carbohydrates—the US Department of Energy's "Top 10" Revisited. *Green Chem.* **2010**, *12*, 539–554.

5. Tomishige, K.; Yabushita, M.; Cao, J.; Nakagawa, Y. Hydrodeoxygenation of Potential Platform Chemicals Derived from Biomass to Fuels and Chemicals. *Green Chem.* **2022**, *24*, 5652–5690.

6. Qu, R.; Junge, K; Beller, M. Hydrogenation of Carboxylic Acids, Esters, and Related Compounds over Heterogeneous Catalysts: A Step toward Sustainable and Carbon-Neutral Processes. *Chem. Rev.* **2023**, *123*, 1103–1165.

7. McAlees, A. J.; McCrindle, R. Catalytic Hydrogenations of Cyclic Imides and Ayhydrides. *J. Chem. Soc. C* **1969**, 2425–2435.

8. Bouveault, L.; Blanc, G. Preparation of Primary Alcohols by Means of the Corresponding Acids. *Compt. Rend.* **1903**, *136*, 1676–1678.

9. Bouveault, L.; Blanc, G. Transformation des Acides Monobasiques Saturés dans les Alcools Primaires Correspondants. *Bull. Soc. Chim. Fr.* **1904**, *31*, 666–672.

10. Nystrom, R. F.; Brown, W. G. Reduction of Organic Compounds by Lithium Aluminum Hydride. I. Aldehydes, Ketones, Esters, Acid Chlorides and Acid Anhydrides. *J. Am. Chem. Soc.* **1947**, *69*, 1197–1199.

11. Werkmeister, S.; Junge, K.; Beller, M. Catalytic Hydrogenation of Carboxylic Acid Esters, Amides, and Nitriles with Homogeneous Catalysts. *Org. Process Res. Dev.* **2014**, *18*, 289–302.

12. Pritchard, J.; Filonenko, G. A.; van Putten, R.; Hensen, E. J. M.; Pidko, E. A. Heterogeneous and Homogeneous Catalysis for the Hydrogenation of Carboxylic Acid Derivatives: History, Advances and Future Directions. *Chem. Soc. Rev.* **2015**, *44*, 3808–3833.

13. Yoshioka, S.; Saito, S. Catalytic Hydrogenation of Carboxylic Acids Using Low-Valent and High-Valent Metal Complexes. *Chem. Commun.* **2018**, *54*, 13319–13330.

14. Adkins, H.; Folkers, K. The Catalytic Hydrogenation of Esters to Alcohols. *J. Am. Chem. Soc.*, **1931**, *53*, 1095–1097.

15. Adkins, H.; Cramer, H. I.; Connor, R. The Rate of Hydrogenation of Acetoacetic Ester, Dehydroacetic Acis, Benzene, Phenol and Aniline over Nickel at Pressures from 27 to 350 Atmospheres. *J. Am. Chem. Soc.* **1931**, *53*, 1402–1405.

16. Connor, R.; Folkers, K.; Adkins, H. The Preparation of Copper-Chromium Oxide Catalysts for Hydrogenation. *J. Am. Chem. Soc.* **1932**, *54*, 1138–1145.

17. Folkers, K.; Adkins, H. The Catalytic Hydrogenation of Esters to Alcohols. II. *J. Am. Chem. Soc.* **1932**, *54*, 1145–1154.

18. Kreutzer, U. R. Manufacture of Fatty Alcohols based on Natural Fats and Oils. *J. Am. Oil Chem. Soc.* **1984**, *61*, 343–348.

19. Evans, J. W.; Wainwright, M. S.; Cant, N. W.; Trimm, D. L. Structural and Reactivity Effects in the Copper-Catalyzed Hydrogenolysis of Aliphatic Esters. *J. Catal.* **1984**, *88*, 203–213.

20. Natal Santiago, M. A.; Sanchez-Castillo, M. A.; Cortright, R. D.; Dumesic, J. A. Catalytic Reduction of Acetic Acid, Methyl Acetate, and Ethyl Acetate over Silica-Supported Copper. *J. Catal.* **2000**, *193*, 16–28.

21. Wang, Y.; Shen, Y.; Zhao, Y.; Lv, J.; Wang, S.; Ma, X. Insight into the Balancing Effect of Active Cu Species for Hydrogenation of Carbon–Oxygen Bonds. *ACS Catal.* **2015**, *5*, 6200–6208.

22. Poels, E. K.; Brands, D. S. Modification of $Cu/ZnO/SiO_2$ Catalysts by High Temperature Reduction. *Appl. Catal., A* **2000**, *191*, 83–96.

23. Karam, L.; Neumann, C. N. Heterogeneously Catalyzed Carboxylic Acid Hydrogenation to Alcohols. *ChemCatChem* **2022**, *14*, e202200953.

24. Rachmady, W.; Vannice, M. A. Acetic Acid Reduction by H_2 over Supported Pt Catalysts: A DRIFTS and TPD/TPR Study. *J. Catal.* **2002**, *207*, 317–330.

25. Pallassana, V.; Neurock, M. Reaction Paths in the Hydrogenolysis of Acetic Acid to Ethanol over Pd(111), Re(0001), and PdRe Alloys. *J. Catal.* **2002**, *209*, 289–305.

26. Olcay, H.; Xu, L.; Xu, Y.; Huber, G. W. Aqueous-Phase Hydrogenation of Acetic Acid over Transition Metal Catalysts. *ChemCatChem* **2010**, *2*, 1420–1424.

27. Gao, X.; Zhu, S.; Dong, M.; Fan, W. MOF-derived hcp-Co Nanoparticles Encapsulated in Ultrathin Graphene for Carboxylic Acids Hydrogenation to Alcohols. *J. Catal.* **2021**, *399*, 201–211.

28. Mavrikakis, M.; Barteau, M. A. Oxygenate Reaction Pathways on Transition Metal Surfaces. *J. Mol. Catal. A Chem.* **1998**, *131*, 135–147.

29. Chen, L.; Zhu, Y.; Zheng, H.; Zhang, C.; Li, Y. Aqueous-Phase Hydrodeoxygenation of Propanoic Acid over the Ru/ZrO$_2$ and Ru–Mo/ZrO$_2$ Catalysts. *Appl. Catal. A* **2012**, *411–412*, 95–104.

30. Chen, L.; Li, Y.; Zhang, X.; Zhang, Q.; Wang, T.; Ma, L. Mechanistic Insights into the Effects of Support on the Reaction Pathway for Aqueous-Phase Hydrogenation of Carboxylic Acid over the Supported Ru Catalysts. *Appl. Catal. A* **2014**, *478*, 117–128.

31. Rachmady, W.; Vannice, M. A. Acetic Acid Reduction to Acetaldehyde over Iron Catalysts: II. Characterization by Mössbauer Spectroscopy, DRIFTS, TPD, and TPR. *J. Catal.* **2002**, *208*, 170–179.

32. Dong, X.; Lei, J.; Chen, Y.; Jiang, H.; Zhang, M. Selective Hydrogenation of Acetic Acid to Ethanol on Cu-In Catalyst Supported by SBA-15. *Appl. Catal. B* **2019**, *244*, 448–458.

33. Vorotnikov, V.; Eaton, T. R.; Settle, A. E.; Orton, K.; Wegener, E. C.; Yang, C.; Miller, J. T.; Beckham, G. T.; Vardon, D. R. Inverse Bimetallic RuSn Catalyst for Selective Carboxylic Acid Reduction. *ACS Catal.* **2019**, *9*, 11350–11359.

34. Pestman, R.; Koster, R. M.; Pieterse, J. A. Z.; Ponec, V. Reactions of Carboxylic Acids on Oxides 1. Selective Hydrogenation of Acetic Acid to Acetaldehyde. *J. Catal.* **1997**, *168*, 255–264.

35. Mars, P.; van Krevelen, D. W. Oxidations Carried Out by Means of Vanadium Oxide Catalysts. *Chem. Eng. Sci.* **1954**, *3*, 41–59.

36. Hosokawa, S.; Fukuzumi, N.; Nakatani, T.; Honma, T.; Mizugaki, T.; Tanaka, T.; Wada, K. Catalytic Selective Hydrogenation of Acetic Acid to Acetaldehyde over the Surface of the Iron Shell on Pd–Fe Alloy Nanoparticles. *Catal. Sci. Technol.* **2022**, *12*, 5604–5610.

37. Manyar, H. G.; Paun, C.; Pilus, R.; Rooney, D. W.; Thompson, J. M.; Hardacre, C. Highly Selective and Efficient Hydrogenation of Carboxylic Acids to Alcohols Using Titania Supported Pt Ccatalysts. *Chem. Commun.* **2010**, *46*, 6279–6281.

38. Zhou, Y.; Liu, L.; Li, G.; Hu, C. Insights into the Influence of ZrO$_2$ Crystal Structures on Methyl Laurate Hydrogenation over Co/ZrO$_2$ Catalysts. *ACS Catal.* **2021**, *11*, 7099–7113.

39. Takeda, Y.; Nakagawa, Y.; Tomishige, K. Selective Hydrogenation of Higher Saturated Carboxylic Acids to Alcohols Using a ReO$_x$–Pd/SiO$_2$ Catalyst. *Catal. Sci. Technol.* **2012**, *2*, 2221–2223.

40. Ali, A.; Li, B.; Lu, Y.; Zhao, C. Highly Selective and Low-Temperature Hydrothermal Conversion of Natural Oils to Fatty Alcohols. *Green Chem.* **2019**, *21*, 3059–3064.

41. Rozmysłowicz, B.; Kirilin, A.; Aho, A.; Manyar, H.; Hardacre, C.; Wärnå, J.; Salmi, T.; Murzin, D. Y. Selective Hydrogenation of Fatty Acids to Alcohols over Highly Dispersed ReO_x/TiO_2 Catalyst. *J. Catal.* **2015**, *328*, 197–207.

42. Jia, W.; Xu, G.; Liu, X.; Zhou, F.; Ma, H.; Zhang, Y.; Fu, Y. Direct Selective Hydrogenation of Fatty Acids and Jatropha Oil to Fatty Alcohols over Cobalt-Based Catalysts in Water. *Energy Fuels* **2018**, *32*, 8438–8446.

43. Kandel, K.; Chaudhary, U.; Nelson, N. C.; Slowing, I. I. Synergistic Interaction between Oxides of Copper and Iron for Production of Fatty Alcohols from Fatty Acids. *ACS Catal.* **2015**, *5*, 6719–6723.

44. Shao, Y.; Xia, Q.; Liu, X.; Lu, G.; Wang, Y. $Pd/Nb_2O_5/SiO_2$ Catalyst for the Direct Hydrodeoxygenation of Biomass-Related Compounds to Liquid Alkanes under Mild Conditions. *ChemSusChem* **2015**, *8*, 1761–1767.

45. Ullrich, J.; Breit, B. Selective Hydrogenation of Carboxylic Acids to Alcohols or Alkanes Employing a Heterogeneous Catalyst. *ACS Catal.* **2018**, *8*, 785–789.

46. Cao, X.; Zhao, J.; Long, F.; Liu, P.; Jiang, X.; Zhang, X.; Xu, J.; Jiang, J. Efficient Low-Temperature Hydrogenation of Fatty Acids to Fatty Alcohols and Alkanes on a Ni-Re Bimetallic Catalyst: The Crucial Role of NiRe Alloys. *Appl. Catal. B* **2022**, *312*, 121437.

47. Long, F.; Chen, Y.; Chen, H.; Cao, X.; Wu, S.; Lu, Y.; Liu, P.; Jiang, J.; Zhang, X.; Xu, J. ReO_x Promotes Ni Cluster Interactions on TiO_2 to Improve the Activity and Durability for Green Alkane and Alcohol Production at Low Temperature. *J. Mater. Chem. A* **2023**, 19591–19604.

48. Wu, S.; Long, F.; Cao, X.; Liu, P.; Lu, Y.; Xu, J. Highly Selective and Efficient Hydrogenation of Fatty Acids to Alcohols Using NiMo@C Catalyst. *Fuel* **2024**, *357*, 129830.

49. Tamura, M.; Chen, P.; Umehara, Y.; Onodera, W.; Akatsuka, M.; Kita, Y. Low-Temperature Hydrogenation of Carboxylic Acids to Alcohols over Heterogeneous FeO_x-Modified Ru Catalyst. *ChemCatChem* **2024**, e202400708.

50. Christian, R. V.; Brown, Jr., H. D.; Hixon, R. M. Derivatives of γ-Valerolactone, 1,4-Pentanediol and 1,4-Di-(β-cyanoethoxy)-pentane. *J. Am. Chem. Soc.* **1947**, *69*, 1961–1963.

51. Corbel-Demailly, L.; Ly, B.-K.; Minh, D.-P.; Tapin, B.; Especel, C.; Epron, F.; Cabiac, A.; Guillon, E.; Besson, M.; Pinel, C. Heterogeneous Catalytic Hydrogenation of Biobased Levulinic and Succinic Acids in Aqueous Solutions. *ChemSusChem* **2013**, *6*, 2388–2395.

52. Li, M.; Li, G.; Li, N.; Wang, A.; Dong, W.; Wang, X.; Cong, Y. Aqueous Phase Hydrogenation of

Levulinic Acid to 1,4-Pentanediol. *Chem. Commun.* **2014**, *50*, 1414–1416.

53. Mizugaki, T.; Nagatsu, Y.; Togo, K.; Maeno, Z.; Mitsudome, T.; Jitsukawa, K.; Kaneda K. Selective Hydrogenation of Levulinic Acid to 1,4-Pentanediol in Water Using a Hydroxyapatite-Supported Pt–Mo Bimetallic Catalyst. *Green Chem.* **2015**, *17*, 5136–5139.

54. Cui, J.; Tan, J.; Zhu, Y.; Cheng, F. Aqueous Hydrogenation of Levulinic Acid to 1,4-Pentanediol over Mo-Modified Ru/Activated Carbon Catalyst. *ChemSusChem* **2018**, *11*, 1316–1320.

55. Kang, K. H.; Hong, U. G.; Bang, Y.; Choi, J. H.; Kim, J. K.; Lee, J. K.; Han, S. J.; Song, I. K. Hydrogenation of Succinic Acid to 1,4-Butanediol over Re–Ru Bimetallic Catalysts Supported on Mesoporous Carbon. *Appl. Catal. A* **2015**, *490*, 153–162.

56. Takeda, Y.; Tamura, M.; Nakagawa, Y.; Okumura, K.; Tomishige, K. Hydrogenation of Dicarboxylic Acids to Diols over Re–Pd Catalysts. *Catal. Sci. Technol.* **2016**, *6*, 5668–5683.

57. Le, S. D.; Nishimura, S. Highly Selective Synthesis of 1,4-Butanediol via Hydrogenation of Succinic Acid with Supported Cu–Pd Alloy Nanoparticles. *ACS Sustain. Chem. Eng.* **2019**, *7*, 18483–18492.

58. Cabrero-Antonino, J. R.; Adam, R.; Beller, M. Catalytic Reductive N-Alkylations Using CO_2 and Carboxylic Acid Derivatives: Recent Progress and Developments. *Angew. Chem., Int. Ed.* **2019**, *58*, 12820–12838.

59. Dong, J.; Yang, Z. Catalytic One-Pot Reductive Amination of Carboxylic Acids. *ChemCatChem* **2024**, *16*, e202301427.

60. Rutzen, H.; Process for the Production of Saturated and/or Unsaturated Aliphatic Amines. DE Pat., 1288595B, 1969.

61. Barrault, J.; Brunet, S.; Suppo-Essayem, N.; Piccirilli, A.; Guimon, C. Selectivity Control in Substituted Fatty Amines Synthesis from Esters or Nitriles in the Presence of Bifunctional Catalysts. *J. Am. Oil Chem. Soc.* **1994**, *71*, 1231–1238.

62. Toyao, T.; Siddiki, S. M. A. H.; Morita, Y.; Kamachi, T.; Touchy, A. S.; Onodera, W.; Kon, K.; Furukawa, S.; Ariga, H.; Asakura, K.; Yoshizawa, K.; Shimizu, K. Rhenium-Loaded TiO_2: A Highly Versatile and Chemoselective Catalyst for the Hydrogenation of Carboxylic Acid Derivatives and the N-Methylation of Amines Using H_2 and CO_2. *Chem. Eur. J.* **2017**, *23*, 14848–14859.

63. Jamil, M. A. R.; Siddiki, S. M. A. H.; Touchy, A. S.; Rashed, M. N.; Poly, S. S.; Jing, Y.; Ting, K. W.; Toyao, T.; Maeno, Z.; Shimizu, K. Selective Transformations of Triglycerides into Fatty

Amines, Amides, and Nitriles by using Heterogeneous Catalysis. *ChemSusChem* **2019**, *12*, 3115–3125.

64. Devereux, J. M.; Payne, K. R.; Peeling, E. R. A. Catalytic Hydrogenation. Part I. The Hydrogenation of Unsaturated Amines over Platinic Oxide. *J. Chem. Soc.* **1957**, 2845–2851.

65. Minachev, K. M.; Avaev, V. I.; Ryashentseva, M. A. Hydrogenation of Ethyl Acetate on Re/γ-Al$_2$O$_3$ Catalyst. *Bull. Acad. Sci. USSR, Div. Chem. Sci.* **1986**, *35*, 280–283.

66. Avaev, V. I.; Ryashentseva, M. A.; Minachev, K. M. Effect of the Nature of the Carrier and Reduction Conditions on the Properties of Rhenium Catalysts of Hydrogenation of Ethyl Acetate. *Bull. Acad. Sci. USSR, Div. Chem. Sci.* **1988**, *37*, 15–19.

67. Knözinger, H. Dehydration of Alcohols on Aluminum Oxide. *Angew. Chem., Int. Ed.* **1968**, *7*, 791–805.

68. Kang, M.; Bhan, A. Kinetics and Mechanisms of Alcohol Dehydration Pathways on Alumina Materials. *Catal. Sci. Technol.* **2016**, *6*, 6667–6678.

69. Sutter, M.: Dayoub, W.; Metay, E.; Raoul, Y.; Lemaire, M. Selective Synthesis of 1-*O*-Alkyl(poly)glycerol Ethers by Catalytic Reductive Alkylation of Carboxylic Acids with a Recyclable Catalytic System. *ChemSusChem* **2012**, *5*, 2397–2409.

70. Sutter, M.: Dayoub, W.; Metay, E.; Raoul, Y.; Lemaire, M. 1-*O*-Alkyl (di)glycerol Ethers Synthesis from Methyl Esters and Triglycerides by Two Pathways: Catalytic Reductive Alkylation and Transesterification/Reduction. *Green Chem.* **2013**, *15*, 786–797.

71. Yun, Y. S.; Berdugo-Díaz, C. E.; Luo, J.; Barton, D. G.; Chen, I.; Lee, J.; Flaherty, D. W. The Importance of Brønsted Acid Sites on C–O Bond Rupture Selectivities during Hydrogenation and Hydrogenolysis of Esters. *J. Catal.* **2022**, *411*, 212–225.

72. Berdugo-Díaz, C. E.; Yun, Y. S.; Manetsch, M. T.; Luo, J.; Barton, D. G.; Chen, X.; Flaherty, D. W. Pathways for Reactions of Esters with H$_2$ over Supported Pd Catalysts: Elementary Steps, Site Requirements, and Particle Size Effects. *ACS Catal.* **2022**, *12*, 9717–9734.

73. Berdugo-Díaz, C. E.; Manetsch, M. T.; Yun, Y. S.; Lee, J.; Luo, J.; Chen, X.; Flaherty, D. W. Ester Reduction with H$_2$ on Bifunctional Metal-Acid Catalysts: Implications of Metal Identity on Rates and Selectivities. *Angew. Chem., Int. Ed.* **2023**, e202216165.

74. Berdugo-Díaz, C. E.; Manetsch, M. T.; Lee, J.; Yun, Y. S.; Yancey, D. F.; Rozeveld, S. J.; Luo, J.; Chen, X.; Flaherty, D. W. Ester Reduction on Bifunctional Metal-acid Catalysts: Effect of Metal to Acid Ratio, *J. Catal.* **2024**, *430*, 115346.

75. Li, J.; Huang, C.-Y.; Li, C.-J. Deoxygenative Functionalizations of Aldehydes, Ketones and Carboxylic Acids. *Angew. Chem., Int. Ed.*, **2022**, *61*, e202112770.

76. Asako, S.; Ishihara, S.; Hirata, K.; Takai, K. Deoxygenative Insertion of Carbonyl Carbon into a C(sp^3)–H Bond: Synthesis of Indolines and Indoles. *J. Am. Chem. Soc.* **2019**, *141*, 9832–9836.

77. Prasomsri, Y.; Nimmanwudipong, T.; Roman-Leshkov, Y. Effective Hydrodeoxygenation of Biomass-Derived Oxygenates into Unsaturated Hydrocarbons by MoO_3 Using Low H_2 Pressures. *Energy Environ. Sci.* **2013**, *6*, 1732–1738.

78. Kuwahara, Y.; Yoshimura, Y.; Haematsu, K.; Yamashita, H. Mild Deoxygenation of Sulfoxides over Plasmonic Molybdenum Oxide Hybrid with Dramatic Activity Enhancement under Visible Light. *J. Am. Chem. Soc.* **2018**, *140*, 9203–9210.

79. Nishimura, S. *Handbook of Heterogeneous Catalytic Hydrogenation for Organic Synthesis*; John Wiley & Sons Inc., 2001.

Chapter II.

Reductive Amination of Carboxylic Acids by Pt–MoO$_x$/γ-Al$_2$O$_3$ Catalyst

1   Introduction

Alkylamines are important compounds with broad applications in polymers, surfactants, agrochemicals, dyes, and pharmaceuticals [1]. There are numerous methods for the synthesis of alkylamines, such as *N*-alkylation using organohalides, hydroamination of alkenes [2–4], Buchwald–Hartwig cross coupling [5–7], and reductive amination [8,9]. In particular, reductive amination of carbonyl compounds is a reliable and important method widely applied in both research laboratories and industries. This reaction has been extensively studied using aldehydes and ketones with nitrogen nucleophiles in the presence of reductants. Recently, reductive amination of carboxylic acids has attracted attention [10–12] because of their abundance in nature [13–15]. Stoichiometric amounts of reductants, such as $NaBH_4$ [16,17] and hydrosilanes [18–22], have been employed (Scheme 2-1(I)). However, these methods have a significant disadvantage of generating large amounts of waste. From an environmental protection viewpoint, H_2 serves as an optimal reductant since water is produced as a sole co-product. Homogeneous Ru or Co catalysts with triphos ligands have been developed for the reductive amination of carboxylic acids using H_2 (Scheme 2-1(II)) [23–28]. However, these catalyst systems pose a difficulty in recovering the catalyst and sometimes require acid additives. To overcome these problems, Re/TiO_2, $Ru–WO_x/MgAlO_x$, and Au/TiO_2 have been developed as easily recoverable and additive-free heterogeneous catalysts (Scheme 2-1(III)) [29–31]. Nevertheless, these heterogeneous catalyst systems require high H_2 pressures and temperatures (3–5 MPa H_2 and 200 °C). Therefore, it is necessary to develop heterogeneous catalysts for reductive amination of carboxylic acids under mild conditions.

Catalysis by metal and metal oxide has attracted significant attention to promote various molecular transformations [32,33]. Among them, the combination of platinum nanoparticles (NPs) and molybdenum oxide species is highly effective for reductive transformations of acyl compounds [34–44], CO_2 [45–51], lignocellulosic oxygenates [52–54], and sulfoxides [55,56] using H_2. Based on

29

this knowledge, the author envisaged that catalysis of Pt–MoO$_x$ might be applicable to the reductive amination of carboxylic acids. In this chapter, the author reports the mild reductive amination of carboxylic acids with H$_2$ using an aluminum oxide-supported Pt–MoO$_x$ (Pt–MoO$_x$/γ-Al$_2$O$_3$) catalyst (Scheme 2-1(IV)). Pt–MoO$_x$/γ-Al$_2$O$_3$ is the first catalyst to promote the reductive amination of carboxylic acids under ambient H$_2$ pressure. A wide range of amines and carboxylic acids, including fatty acids abundant in biomass, were successfully transformed into alkylamines in high yields.
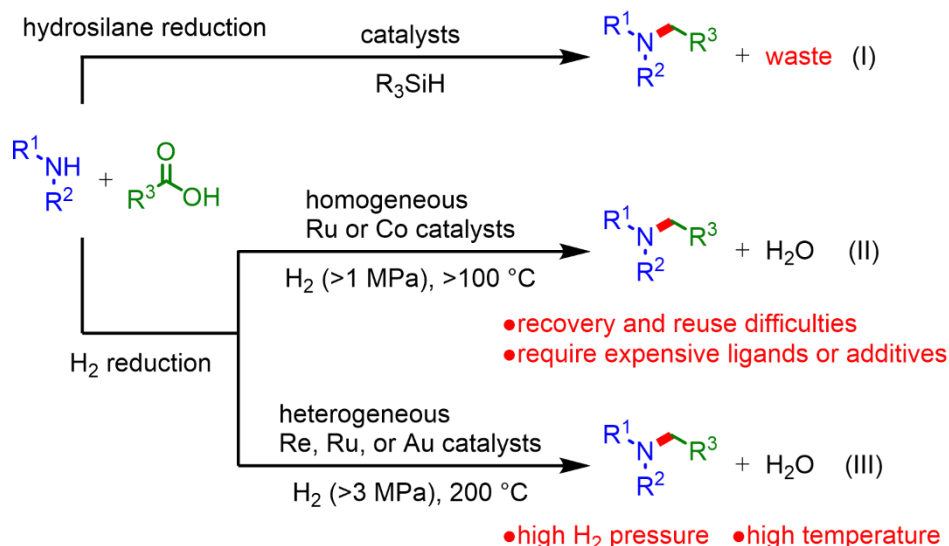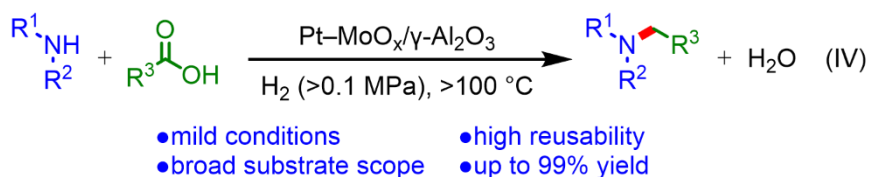
Scheme 2-1 Reductive amination of carboxylic acids.

2   Experimental section

2.1   General

Organic chemicals were purchased from Fujifilm Wako Pure Chemical Industries, Ltd., Tokyo Chemical Industry Co., Ltd., and Sigma-Aldrich, and were used as received. H_2PtCl_6, $RuCl_3$, K_3RhCl_6, and $Pd(NH_3)_4Cl_2$ hydrates were obtained from N. E. Chemcat. $(NH_4)_6Mo_7O_{24} \cdot 4H_2O$, NH_4VO_3, $(NH_4)_{10}(H_2W_{12}O_{42}) \cdot 4H_2O$, and $NaReO_4$ were purchased from Nacalai Tesque, Kishida Chemical, Sigma-Aldrich, and Alfa Aesar Co., Ltd., respectively. γ-Al_2O_3 was obtained from Sumitomo Chemical Co., Ltd. α-Al_2O_3 and WO_3 were purchased from Fujifilm Wako Pure Chemical Industries, Ltd. TiO_2 (JRC-TIO-2), Nb_2O_5 (JRC-NBO-2), ZrO_2 (JRC-ZRO-7), and CeO_2 (JRC-CEO-2) were supplied by the Catalyst Society of Japan as reference catalysts. SiO_2 (CARiACT, Q-6) was purchased from Fuji Silysia Chemical, Ltd. Gas chromatography (GC-FID) analyses were performed on a Shimadzu GC-2014 instrument equipped with a capillary column (InertCap for amines, GL Science, 30 m × 0.32 mm i.d.). Gas chromatography-mass spectrometry (GC-MS) analyses were performed on a Shimadzu QP-2010SE instrument equipped with a capillary column (SH-Rtx-200MS, Shimadzu, 30 m × 0.25 mm i.d. film thickness 0.25 μm). ^1H and ^{13}C nuclear magnetic resonance (NMR) spectra were recorded on a JEOL JNM-ECS400 spectrometer. Chemical shifts are reported as follows: 1,4-dioxane (3.76 ppm for ^1H NMR, 67.15 ppm for ^{13}C NMR) as an external standard in D_2O solvent, TMS (0 ppm for ^1H NMR), $CDCl_3$ (77.10 ppm for ^{13}C NMR). NMR multiplicities are reported using the following abbreviations: s, singlet; d, doublet; t, triplet; q, quartet; m, multiplet; br, broad; J, coupling constants in hertz. Transmission electron microscopy (TEM) images were obtained using FEI Titan Cubed G2 60-300 or FEI Tecnai G2 20ST. High-angle annular dark-field scanning TEM (HAADF-STEM) images with elemental maps were collected using a FEI Titan Cubed G2 60-300 instrument, operated at 300 kV and equipped with a Super-X energy-dispersive X-ray spectroscopy (EDX) detector. Pt L_3-edge and Mo K-edge X-ray absorption near-edge structure (XANES) analyses

were performed at room temperature in transmittance mode using Si (311) monochromators at the 14B2 and 01B1 beamline stations at SPring-8, Japan Atomic Energy Research Institute (JASRI), Harima, Japan (promotion numbers: 2021B1945, 2022B1699, 2022B0519, and 2022B0586). Data analysis was performed using the Demeter ver. 0.9.21. Inductively coupled plasma-atomic emission spectroscopy (ICP-AES) was performed using a Perkin Elmer Optima 8300 instrument. EDX measurements were performed using a Shimadzu EDX-7200 instrument. CO pulse chemisorption was measured using a BELCAT-A instrument (BEL Japan Inc.) equipped with a thermal conductivity detector.

2.2 Preparation of Pt–MoO$_x$/γ-Al$_2$O$_3$ catalyst

The Pt–MoO$_x$/γ-Al$_2$O$_3$ catalyst was prepared using a co-impregnation method. Aqueous solution of H$_2$PtCl$_6$ (6.00 mL, 100 mM), (NH$_4$)$_6$Mo$_7$O$_{24}$·4H$_2$O (0.0265 g), and γ-Al$_2$O$_3$ (1.000 g) was added to distilled water (50 mL) at room temperature. After stirring for 12 h in air, water was removed by rotary evaporation under reduced pressure, and the resulting powder was dried at 110 °C for 5 h. After drying, the powder was calcined at 500 °C for 3 h under static air atmosphere to obtain Pt–MoO$_x$/γ-Al$_2$O$_3$ as a black powder. As determined by ICP-AES, the Pt and Mo contents in Pt–MoO$_x$/γ-Al$_2$O$_3$ were 10.1 and 1.42 wt%, respectively. The other catalysts were prepared in a similar manner using various metal salts and supports. All catalysts were applied to the reaction without any pre-reduction steps.

2.3 Typical reductive amination procedure

The reductive amination of acetic acid (**2a**) with piperidine (**1a**) was carried out in a 50 mL stainless steel autoclave equipped with a Teflon vessel. The vessel was charged with **1a** (0.085 g, 1.0 mmol), **2a** (0.180 g, 3.0 mmol), Pt–MoO$_x$/γ-Al$_2$O$_3$ (0.150 g), *n*-hexane (3 mL), and a Teflon-coated

magnetic stir bar. The reactor was sealed, purged five times with 1.0 MPa H_2, pressurized (2.0 MPa), heated to 100 °C, and stirred at 900 rpm for 12 h. After the reaction, the autoclave was cooled in an ice-water bath, and H_2 gas was released. The resulting reaction mixture was diluted with 1-butanol and analyzed by GC-FID. Product yields were calculated based on **1a**.

Product yields were calculated by the following equation:

$$\textbf{3a} \text{ yield (based on } \textbf{1a}) = \frac{\text{amount of } \textbf{3a} \text{ (mmol)}}{\text{amount of loaded } \textbf{1a} \text{ (mmol)}} \times 100 \qquad \text{(eq. 2-1)}$$

The turnover frequency (TOF) in Table 2-2 were calculated by the following equation:

$$\text{TOF} = \frac{\text{amount of } \textbf{3a} \text{ (mmol)}}{W_{\text{catalyst}} \text{ (mg)} \times \frac{\text{Pt loading}}{\text{atomic weight of Pt}} \times \text{time (h)}} \qquad \text{(eq. 2-2)}$$

W_{catalyst}: the weight of catalyst used in the reductive amination

Pt loading: the loading amount of Pt measured by EDX analysis

2.4 Catalyst reuse experiment

After the reductive amination was complete, the catalyst was recovered from the reaction mixture by centrifugation, washed with ethanol, and then with *n*-hexane in air before reuse in subsequent reactions.

2.5 Reductive amination under atmospheric H_2 pressure

The reductive amination under atmospheric H_2 pressure was carried out in a Schlenk tube equipped with a balloon and condenser. The Schlenk tube was charged with **1a** (0.085 g, 1.0 mmol), **2a** (0.180 g, 3.0 mmol), Pt–MoO$_x$/γ-Al$_2$O$_3$ (0.150 g), *n*-dodecane (3 mL), and a Teflon-coated magnetic stir bar. The reaction mixture was degassed twice by the freeze-pump-thaw method, filled

with 0.1 MPa H_2, heated to 140 °C, and stirred at 900 rpm for 24 h. After the reaction, the reactor was cooled and H_2 gas was released. The resulting reaction mixture was diluted with 1-butanol and analyzed by GC-FID.

2.6 Gram-scale reaction

The gram-scale reductive amination was carried out in a 100 mL stainless steel autoclave equipped with a Teflon vessel. The vessel was charged with **1a** (1.00 g, 11.7 mmol), **2a** (2.00 g, 33.3 mmol), Pt–MoO$_x$/γ-Al$_2$O$_3$ (0.150 g), *n*-hexane (10 mL), and a Teflon-coated magnetic stir bar. The reactor was purged five times with 1.0 MPa H_2, pressurized to 4.0 MPa at room temperature, heated to 160 °C, and stirred at 1000 rpm for 48 h. After the reaction, the autoclave was cooled in an ice-water bath, and H_2 gas was carefully released. Pt–MoO$_x$/γ-Al$_2$O$_3$ was separated by filtration, and a hydrogen chloride solution (1.25 M, 1,4-dioxane) was added. The solvents were evaporated, washed with diethyl ether and water, then the water phase was gathered, evaporated, and dried to give pure hydrogen chloride salt **3a** (1.64 g, 10.9 mmol, 93%).

The turnover number (TON) based on the surface Pt atoms was described by the following equation:

$$\text{TON} = \frac{\text{amount of } \textbf{3a} \text{ (mmol)}}{W_{\text{catalyst}} \times \frac{\text{Pt loading}}{\text{atomic weight of Pt}} \times \text{dispersion}} \qquad \text{(eq. 2-3)}$$

dispersion: Pt dispersion measured by CO pulse chemisorption analysis (40.2%)

2.7 Pt–MoO$_x$/γ-Al$_2$O$_3$ pre-reduction

Pt–MoO$_x$/γ-Al$_2$O$_3$ was pre-reduced for characterizations under the typical reductive amination conditions without substrates: Pt–MoO$_x$/γ-Al$_2$O$_3$ (0.150 g), *n*-hexane (3 mL), 100 °C, H_2 (2.0 MPa), 2 h.

2.8 Synthesis of *N*-propionylpiperidine

N-Propionylpiperidine (**4b**) was prepared according to the literature procedure [57]. The Schlenk tube was charged with **1a** (2.00 g, 23.5 mmol), propionyl chloride (1.00 g, 10.8 mmol), CHCl$_3$ (10 mL), and a Teflon-coated magnetic stir bar in an ice-water bath. The reactor was heated to 80 °C and stirred at 900 rpm for 2 h. After the reaction, the solvents were evaporated, washed with diethyl ether and water, and the organic phase was gathered, evaporated, and distilled to obtain pure **4b** (0.827 g, 5.87 mmol, 54%).

2.9 Product identification
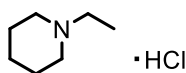
1-Ethylpiperidine hydrochloride

CAS registry No. [17874-60-1]. **^{1}H NMR** (400 MHz, D$_2$O): δ/ppm 3.52 (d, 2H, *J* = 12.4 Hz), 3.14 (dq, 2H, *J* = 7.2, 2.4 Hz), 2.90 (t, 2H, *J* = 12.4 Hz), 1.95 (d, 2H, *J* = 14.0 Hz), 1.86–1.78 (m, 1H), 1.78–1.63 (m, 2H), 1.54–1.41 (m, 1H), 1.30 (dt, 3H, *J* = 7.4 Hz, 3.2 Hz). **^{13}C NMR** (100 MHz, D$_2$O): δ/ppm 53.1, 52.7, 23.5, 21.8, 9.2. **GC-MS** (EI): 113.10.
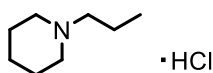
1-Propylpiperidine hydrochloride

CAS registry No. [17874-62-3]. **^{1}H NMR** (400 MHz, D$_2$O): δ/ppm 3.52 (d, 2H, *J* = 12.4 Hz), 3.12–2.96 (m, 2H), 2.91 (dt, 2H, *J* = 12.4, 1.6 Hz), 1.94 (d, 2H, *J* = 14.4 Hz), 1.87–1.64 (m, 5H), 1.55–1.41 (m, 1H), 0.96 (t, 3H, *J* = 7.4 Hz). **^{13}C NMR** (100 MHz, D$_2$O): δ/ppm 59.0, 53.6, 23.4, 21.8, 17.7, 10.8. **GC-MS** (EI): 127.15.
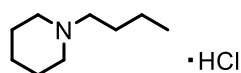
1-Butylpiperidine hydrochloride

CAS registry No. [80840-88-6]. **^{1}H NMR** (400 MHz, D$_2$O): δ/ppm 3.53 (d, 2H, *J* = 12.8 Hz), 3.12–3.04 (m, 2H), 2.91 (dt, 2H, *J* = 12.8, 2.0 Hz), 1.94 (d, 2H, *J* = 14.4 Hz), 1.86–1.64 (m, 5H), 1.54–1.30 (m, 3H), 0.93 (t, 3H, *J* = 7.4 Hz). **^{13}C NMR** (100 MHz, D$_2$O): δ/ppm 57.3, 53.6, 26.0, 23.4, 21.8, 19.9, 13.4. **GC-MS** (EI): 141.15.
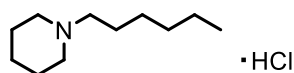
1-Hexylpiperidine hydrochloride

CAS registry No. [80840-90-0]. **^{1}H NMR** (400 MHz, D$_2$O): δ/ppm 3.52 (d, 2H, *J* = 12.4 Hz), 3.13–3.03 (m, 2H), 2.91 (dt, 2H, *J* = 12.6, 2.0 Hz), 1.94 (d, 2H, *J* = 14.4 Hz), 1.86–1.65 (m, 5H), 1.53–1.41 (m, 1H), 1.40–1.25 (m, 6H), 0.88 (t, 3H, *J* = 7.2 Hz). **^{13}C NMR** (100 MHz, D$_2$O): δ/ppm 57.6, 53.6, 31.0, 26.0, 23.9, 23.4, 22.3, 21.8, 13.9. **GC-MS** (EI): 169.20.
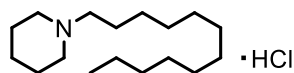
1-Dodecylpiperidine hydrochloride

CAS registry No. [71756-81-5]. **^{1}H NMR** (400 MHz, CDCl$_3$): δ/ppm 11.9 (br-s, 1H), 3.52 (d, 2H, *J* = 11.2 Hz), 2.99–2.87 (m, 2H), 2.76–2.60 (m, 2H), 2.38–2.20 (m, 2H), 2.00–1.79 (m, 5H), 1.52–1.18 (m, 19H), 0.88 (t, 3H, *J* = 6.8 Hz). **^{13}C NMR** (100 MHz, CDCl$_3$): δ/ppm 57.4, 53.0, 31.8, 29.50, 29.48, 29.40, 29.3, 29.2, 29.0, 26.8, 23.4, 22.6, 22.5, 22.1, 14.0. **GC-MS** (EI): 253.25.

1-Hexadecylpiperidine hydrochloride

CAS registry No. [89632-30-4]. **^{1}H NMR** (400 MHz, CDCl$_3$): δ/ppm 11.8 (br-s, 1H), 3.53 (d, 2H, $J =$ 10.8 Hz), 3.02–2.83 (m, 2H), 2.75–2.58 (m, 2H), 2.40–2.13 (m, 2H), 2.00–1.78 (m, 4H), 1.50–1.05 (m, 28H), 0.88 (t, 3H, $J =$ 7.0 Hz). **^{13}C NMR** (100 MHz, CDCl$_3$): δ/ppm 57.5, 53.0, 31.8, 29.63, 29.60, 29.57, 29.50, 29.4, 29.33, 29.28, 29.0, 26.8, 23.4, 22.6, 22.5, 22.1, 14.1. **GC-MS** (EI): 309.30.
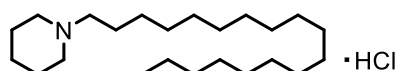
1-Octadecylpiperidine hydrochloride

CAS registry No. [89632-31-5]. **^{1}H NMR** (400 MHz, CDCl$_3$): δ/ppm 11.9 (br-s, 1H), 3.51 (d, 2H, $J =$ 10.4 Hz), 3.00–2.85 (m, 2H), 2.75–2.59 (m, 2H), 2.40–2.23 (m, 2H), 2.00–1.78 (m, 4H), 1.55–1.00 (m, 32H), 0.88 (t, 3H, $J =$ 7.0 Hz). **^{13}C NMR** (100 MHz, CDCl$_3$): δ/ppm 57.5, 53.0, 31.9, 29.63, 29.59, 29.5, 29.4, 29.33, 29.29, 29.0, 26.9, 23.4, 22.6, 22.5, 22.1, 14.1. **GC-MS** (EI): 337.40.
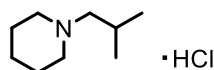
1-Isobutylpiperidine hydrochloride

CAS registry No. [858850-36-9]. **^{1}H NMR** (400 MHz, D$_2$O): δ/ppm 3.53 (d, 2H, $J =$ 12.0 Hz), 3.00–2.87 (m, 4H), 2.21–2.09 (m, 1H), 1.99–1.88 (m, 2H), 1.86–1.69 (m, 3H), 1.56–1.42 (m, 1H), 0.99 (d, 6H, $J =$ 7.2 Hz). **^{13}C NMR** (100 MHz, D$_2$O): δ/ppm 64.5, 54.0, 23.7, 23.0, 21.7, 19.9. **GC-MS** (EI): 141.15.
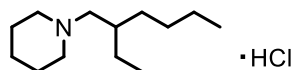
1-(2-Ethylhexyl)piperidine hydrochloride

CAS registry No. [1071548-49-6]. **^{1}H NMR** (400 MHz, D$_2$O): δ/ppm 3.57–3.47 (m, 2H), 3.02 (d, 2H, J = 7.2 Hz), 2.99–2.86 (m, 2H), 1.93 (d, 2H, J = 14.4 Hz), 1.88–1.67 (m, 4H), 1.58–1.22 (m, 9H), 0.99–0.80 (m, 6H). **^{13}C NMR** (100 MHz, D$_2$O): δ/ppm 61.5, 54.4, 54.0, 34.2, 30.3, 28.1, 23.8, 22.9, 22.8, 21.7, 13.9, 9.9. **GC-MS** (EI): 197.20.
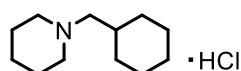
1-cyclohexylmethylpiperidine hydrochloride

CAS registry No. [5005-71-0]. **^{1}H NMR** (400 MHz, D$_2$O): δ/ppm 3.52 (d, 2H, J = 12.4 Hz), 3.02–2.82 (m, 4H), 2.01–1.60 (m, 11H), 1.56–1.41 (m, 1H), 1.38–1.11 (m, 3H), 1.09–0.94 (m, 2H). **^{13}C NMR** (100 MHz, D$_2$O): δ/ppm 63.4, 54.0, 32.7, 30.6, 26.0, 25.5, 23.0, 21.7. **GC-MS** (EI): 181.20.
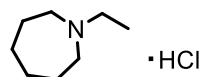
1-Ethylhexamethyleneimine hydrochloride

CAS registry No. [6763-92-4]. **^{1}H NMR** (400 MHz, D$_2$O): δ/ppm 3.50–3.39 (m, 2H), 3.28–3.12 (m, 4H), 2.00–1.89 (m, 2H), 1.89–1.76 (m, 2H), 1.76–1.62 (m, 4H), 1.31 (t, 3H, J = 7.2 Hz). **^{13}C NMR** (100 MHz, D$_2$O): δ/ppm 54.7, 53.2, 26.3, 24.1, 9.6. **GC-MS** (EI): 127.20.
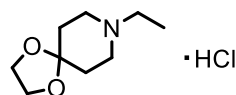
4-(Ethylenedioxy)-*N*-ethylpiperidine hydrochloride

CAS registry No. [3025972-37-3]. **^{1}H NMR** (400 MHz, D$_2$O): δ/ppm 4.08 (s, 4H), 3.67–3.60 (m, 2H), 3.28–3.09 (m, 4H), 2.14–1.98 (m, 4H), 1.33 (t, 3H, J = 7.4 Hz). **^{13}C NMR** (100 MHz, D$_2$O): δ/ppm 104.8, 65.2, 65.1, 52.2, 50.7, 32.1, 9.5. **GC-MS** (EI): 171.15.
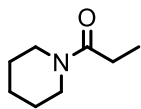
1-(1-Piperidinyl)-1-propane

CAS registry No. [14045-28-4]. **¹H NMR** (400 MHz, CDCl₃): δ/ppm 3.55 (t, 2H, J = 5.6 Hz), 3.40 (t, 2H, J = 5.6 Hz), 2.34 (q, 2H, J = 7.6 Hz), 1.68–1.60 (m, 2H), 1.60–1.49 (m, 4H), 1.14 (t, 3H, J = 7.6 Hz). **¹³C NMR** (100 MHz, CDCl₃): δ/ppm 172.0, 46.4, 42.5, 26.5, 26.4, 25.5, 24.5, 9.5. **GC-MS** (EI): 141.15.

3 Result and discussion

3.1 Catalyst performance in the reductive amination of acetic acid (2a) with piperidine (1a)

Various heterogeneous catalysts were prepared by the co-impregnation method. Their catalyst activities were evaluated in the reaction of piperidine (**1a**) with acetic acid (**2a**) under 2 MPa H_2 at 100 °C for 12 h (Table 2-1). Among the catalysts tested, the Pt–MoO_x/γ-Al_2O_3 catalyst exhibited the highest activity, affording 1-ethylpiperidine (**3a**) in a 98% yield (Table 2-1, entry 1). The combination of other noble metals (Rh, Pd, and Ru) with MoO_x were not effective (Table 2-1, entries 2–4). Pt with metal oxides, such as ReO_x, WO_x, and VO_x, provided low yields of **3a** (Table 2-1, entries 5–7). Catalysts with a single metal (Pt/γ-Al_2O_3 and MoO_x/γ-Al_2O_3) resulted in lower conversions (Table 2-1, entries 8 and 9). Physical mixture of Pt/γ-Al_2O_3 and MoO_x/γ-Al_2O_3 afforded **3a**, but the yield was lower than that of Pt–MoO_x/γ-Al_2O_3 (Table 2-1, entry 10). These results clearly demonstrate that co-loading of Pt and Mo species is important for efficient reductive amination.

Table 2-1. Reductive amination of **2a** with **1a** using various heterogeneous catalysts.

entry	catalyst	conv. of **1a** (%)	yield (%)	
			3a	**4a**
1	Pt–MoO$_x$/γ-Al$_2$O$_3$	>99	98	0
2	Rh–MoO$_x$/γ-Al$_2$O$_3$	28	18	3
3	Pd–MoO$_x$/γ-Al$_2$O$_3$	11	5	6
4	Ru–MoO$_x$/γ-Al$_2$O$_3$	9	0	4
5	Pt–ReO$_x$/γ-Al$_2$O$_3$	36	28	3
6	Pt–WO$_x$/γ-Al$_2$O$_3$	13	9	3
7	Pt–VO$_x$/γ-Al$_2$O$_3$	11	2	4
8	Pt/γ-Al$_2$O$_3$	7	2	3
9	MoO$_x$/γ-Al$_2$O$_3$	13	0	5
10[a]	Pt/γ-Al$_2$O$_3$ + MoO$_x$/γ-Al$_2$O$_3$	83	52	1

Reaction conditions: catalyst (0.15 g, Pt: 8 mol% and Mo: 2 mol%), **1a** (1 mmol), **2a** (3 mmol), *n*-hexane (3 mL), 100 °C, H$_2$ (2 MPa), 12 h. Conversion and yield were determined by GC-FID using an internal standard method and calculated based on **1a**. [a] Pt/γ-Al$_2$O$_3$ (0.15 g), MoO$_x$/γ-Al$_2$O$_3$ (0.15 g).

The support materials for the Pt–MoO$_x$ catalysts were then investigated (Table 2-2). The γ-Al$_2$O$_3$- and TiO$_2$-supported catalysts exhibited high yields in the reductive amination (Table 2-2, entries 1 and 2). Nb$_2$O$_5$-, WO$_3$-, ZrO$_2$-, and α-Al$_2$O$_3$-supported catalysts were also effective, but their yields were lower than those of γ-Al$_2$O$_3$- and TiO$_2$- supported catalysts (Table 2-2, entries 3–6). Pt–MoO$_x$ on CeO$_2$ and SiO$_2$ hardly promoted the reductive amination (Table 2-2, entries 7 and 8). Moreover, the Pt loading of active catalysts was measured by EDX and their TOF values werecompared based on Pt loading. Pt–MoO$_x$/TiO$_2$ exhibited the highest TOF of 2.3 (Table 2-2, entry 2), and other catalysts supported on γ-Al$_2$O$_3$, Nb$_2$O$_5$, WO$_3$, ZrO$_2$, and α-Al$_2$O$_3$ showed similar value (Table 2-2, entries 1 and 3–6). Subsequently, the reusability of the Pt–MoO$_x$ catalysts was evaluated. After the reductive amination, the Pt–MoO$_x$ catalysts were recovered from the reaction mixture, washed, and reused for the next reaction. Although Pt–MoO$_x$/TiO$_2$ provide **3a** in >99% yield in 1st run, the yield was significantly decreased to 42% in the 2nd run (Figure 2-1a). The EDX analysis revealed the leaching of Mo species from Pt–MoO$_x$/TiO$_2$ during the 1st run (Table 2-3). In sharp contrast, Pt–MoO$_x$/γ-Al$_2$O$_3$ catalyst, which showed high yield in Table 2-2, retained high activity even in the 6th run, suppressing Mo leaching compared to TiO$_2$ support (Figure 2-1b and Table 2-3). Therefore, the Pt–MoO$_x$/γ-Al$_2$O$_3$ catalyst was selected as a highly active and reusable heterogeneous catalyst in the reductive amination.

Table 2-2. Reductive amination of **2a** with **1a** over Pt–MoO$_x$ catalysts on various supports.

entry	catalyst	Pt loading (wt%)[a]	conv. of **1a** (%)	yield (%) 3a	yield (%) 4a	TOF[b]
1	Pt–MoO$_x$/γ-Al$_2$O$_3$	10.3	29	28	0	1.8
2	Pt–MoO$_x$/TiO$_2$	7.25	26	26	0	2.3
3	Pt–MoO$_x$/Nb$_2$O$_5$	9.24	30	22	0	1.5
4	Pt–MoO$_x$/WO$_3$	8.09	25	22	<1	1.8
5	Pt–MoO$_x$/ZrO$_2$	8.12	26	20	0	1.6
6	Pt–MoO$_x$/α-Al$_2$O$_3$	6.93	22	18	<1	1.7
7	Pt–MoO$_x$/CeO$_2$	9.91	59	6	0	0.4
8	Pt–MoO$_x$/SiO$_2$	8.08	18	5	0	0.4

Reaction conditions: catalyst (0.15 g, Pt: 8 mol% and Mo: 2 mol%), **1a** (1 mmol), **2a** (3 mmol), *n*-hexane (3 mL), 100 °C, H$_2$ (2 MPa), 2 h. Conversion and yield were determined by GC-FID using an internal standard for analysis and calculated based on **1a**. [a] Pt loading was measured by EDX. [b] TOF was calculated based on total Pt atoms.
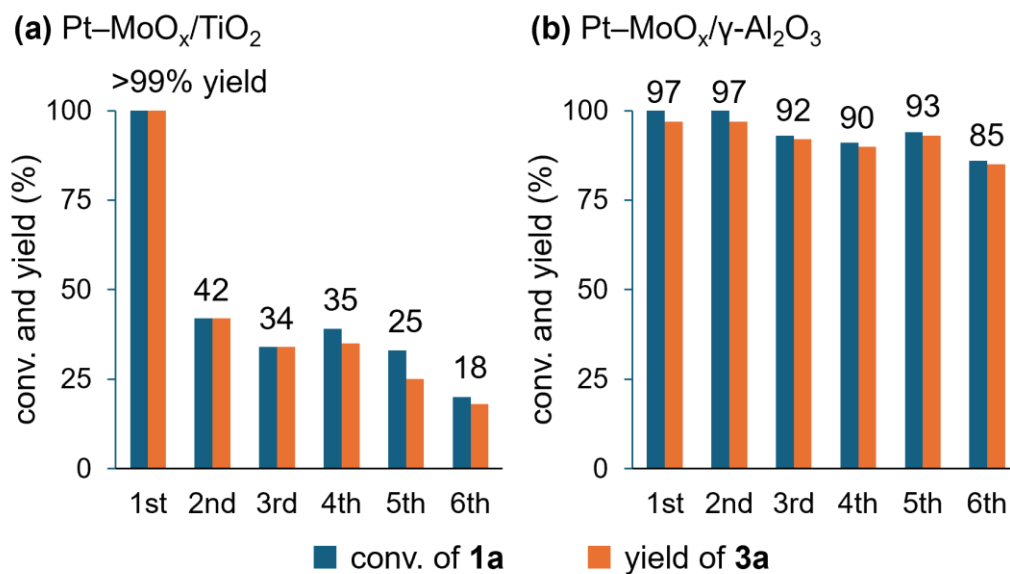
Figure 2-1 Reuse experiment in the (a) Pt–MoO$_x$/TiO$_2$- and (b) Pt–MoO$_x$/γ-Al$_2$O$_3$-catalyzed reductive amination. Reaction conditions: catalyst (0.15 g, Pt: 8 mol% and Mo: 2 mol%), **1a** (1 mmol), **2a** (3 mmol), *n*-hexane (3 mL), 100 °C, H$_2$ (2 MPa), 12 h. Conversion and yield were determined by GC-FID using an internal standard for analysis and calculated based on **1a**.

Table 2-3 EDX analyses of fresh, 1st used, and 6th used Pt–MoO$_x$/γ-Al$_2$O$_3$ and Pt–MoO$_x$/TiO$_2$

sample	atomic ratio				
	Pt/Ti	Mo/Ti	Pt/Al	Mo/Al	Mo/Pt
fresh Pt–MoO$_x$/TiO$_2$	0.034	0.014	-	-	0.40
1st used Pt–MoO$_x$/TiO$_2$	0.036	0.010	-	-	0.29
6th used Pt–MoO$_x$/TiO$_2$	0.034	0.006	-	-	0.16
fresh Pt–MoO$_x$/γ-Al$_2$O$_3$	-	-	0.041	0.011	0.26
1st used Pt–MoO$_x$/γ-Al$_2$O$_3$	-	-	0.041	0.011	0.25
6th used Pt–MoO$_x$/γ-Al$_2$O$_3$	-	-	0.042	0.006	0.14

Next, the outstanding performance of the Pt–MoO$_x$/γ-Al$_2$O$_3$ catalyst was demonstrated. Pt–MoO$_x$/γ-Al$_2$O$_3$ successfully catalyzed the reductive amination of **2a** with **1a** under 0.1 MPa H$_2$, providing a 71% yield of **3a** (Scheme 2-2a). This is the first example that promotes the reductive amination of carboxylic acid under ambient H$_2$ pressure. The Pt–MoO$_x$/γ-Al$_2$O$_3$ catalyst showed applicability in gram-scale amination (Scheme 2-2b). When the reductive amination using 2 g of **2a** and 1 g of **1a** was conducted under 4 MPa H$_2$ at 160 °C for 48 h, **3a** was produced in a 93% isolated yield, achieving an excellent TON of 363.
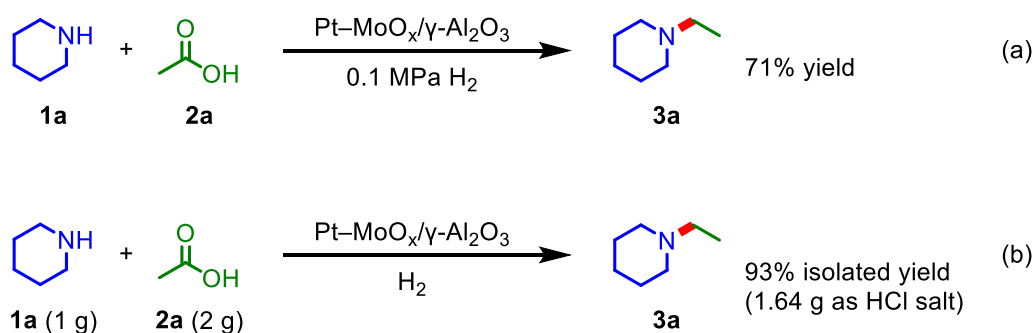
Scheme 2-2 (a) Pt–MoO$_x$/γ-Al$_2$O$_3$ catalyzed reductive amination under H$_2$ at atmospheric pressure. Reaction conditions: Pt–MoO$_x$/γ-Al$_2$O$_3$ (0.15 g, Pt: 8 mol% and Mo: 2 mol%), **1a** (1 mmol), **2a** (3 mmol), *n*-hexane (3 mL), 140 °C, H$_2$ (0.1 MPa), 24 h. (b) Gram-scale reductive amination. Reaction conditions: Pt–MoO$_x$/γ-Al$_2$O$_3$ (0.15 g, Pt: 0.68 mol% and Mo: 0.17 mol%), **1a** (1 g), **2a** (2 g), *n*-hexane (10 mL), 160 °C, H$_2$ (4 MPa), 48 h.

3.2 Substrate scope

With Pt–MoO$_x$/γ-Al$_2$O$_3$ in hand, the scope of carboxylic acids in the reductive amination with **1a** was explored (Scheme 2-3). The volatile fatty acids recoverable from the waste stream, such as **2a**, propionic acid (**2b**), and butyric acid (**2c**) [58], were smoothly aminated to their corresponding 1-alkylated amines in high yields. Medium- and long-chain fatty acids, abundant in oils and fats, were used in this catalyst system. Caproic acid (**2d**), lauric acid (**2e**), palmitic acid (**2f**), and stearic acid (**2g**) were converted to 1-hexyl (**3d**), 1-dodecyl (**3e**), 1-hexadecyl (**3f**), and 1-octadecylpiperidine (**3g**) in over 93% yield. Carboxylic acids with functional groups, such as trifluoromethyl (**2h**), ether (**2i** and **2j**), and heterocycles (**2k**), were aminated. In the amination of acetic acid-d_4 (**2l**), two products, with and without H–D scramble, were observed (to be discussed in Scheme 2-7). The Pt–MoO$_x$/γ-Al$_2$O$_3$ catalyst converted secondary carboxylic acids (**2m**, **2n**, and **2o**) into their corresponding alkylamines at 160 °C. When benzoic acid (**2p**) was used instead of **2o**, **2p** was aminated to **3o** in a 93% yield, with hydrogenation of the aromatic ring. The tertiary carboxylic acid (**2q**) was hardly aminated, indicating the sensitivity of Pt–MoO$_x$/γ-Al$_2$O$_3$ to steric hindrance around the acyl carbonyl carbon. Unfortunately, formic acid (**2r**) and sodium acetate (**2s**) were unfavorable for this catalyst system.

Next, the Pt–MoO$_x$/γ-Al$_2$O$_3$ catalyst was applied to the reductive amination of **2a** with various amines (Scheme 2-4). Secondary cyclic amines with five- and seven-membered rings (**1t** and **1u**) were successfully converted to *N*-ethyl amines in 99% and 93% yields, respectively. Notably, various functional groups, such as hydroxyl (**1v**), ester (**1w**), ether (**1x**), acetal (**1y**), amino (**1z**), amide (**1aa**), and carbamate (**1ab**), were tolerated. Amination with *cis*-2,6-dimethylpiperidine (**1ac**) afforded only 7% of the desired product. The Pt–MoO$_x$/γ-Al$_2$O$_3$ catalyst was effective for reactions involving primary amines; secondary amines were obtained in high yields from heptyl (**1ad**), tert-butyl (**1ae**), and cyclohexyl amines (**1af**). Furthermore, *N*-ethyl cyclohexylamine (**3af**) underwent additional alkylation to yield *N,N*-diethyl cyclohexylamine (**3ag**). The applicability of aromatic amines and

heteroaromatics was also investigated. Aniline (**1ah**) as aromatic amines was hydrogenated and aminated to **3af** in a 40%. Heteroaromatics, such as pyrrole (**1ai**), pyridine (**1aj**), and its derivatives (**1ak**–**1am**), were transformed into tertiary alicyclic amines in moderate yields. These results highlight the wide applicability of the Pt–MoO$_x$/γ-Al$_2$O$_3$ catalyst for the synthesis of various alkylamines from carboxylic acids and amines.
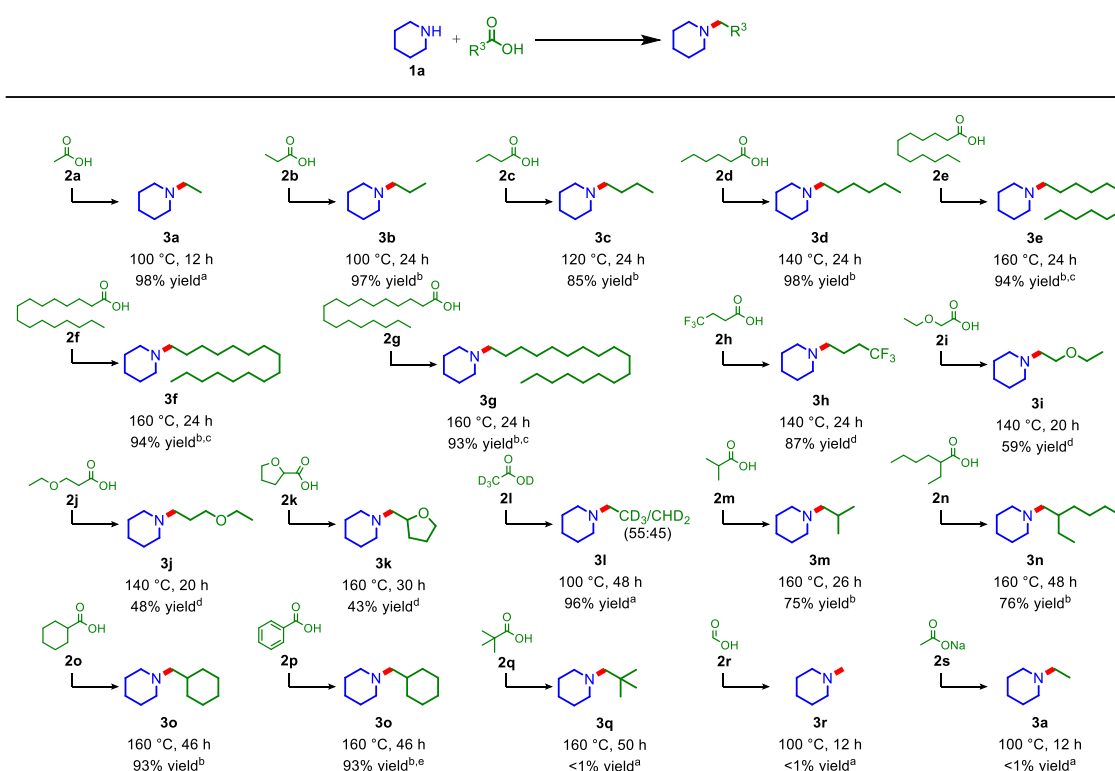
Scheme 2-3 Reductive amination of various carboxylic acids with **1a** under H$_2$. Reaction conditions: Pt–MoO$_x$/γ-Al$_2$O$_3$ (0.15 g, Pt: 8 mol% and Mo: 2 mol%), amine (1 mmol), carboxylic acid (3 mmol), *n*-hexane (3 mL), H$_2$ (2 MPa). [a] GC-FID yield. [b] Isolated yield as a hydrochloride salt. [c] Carboxylic acid (1.5 mmol). [d] ^{1}H NMR yield. [e] H$_2$ (3 MPa). [f] H$_2$ (4 MPa). [g] Carboxylic acid (4 mmol). [h] Carboxylic acid (5 mmol).
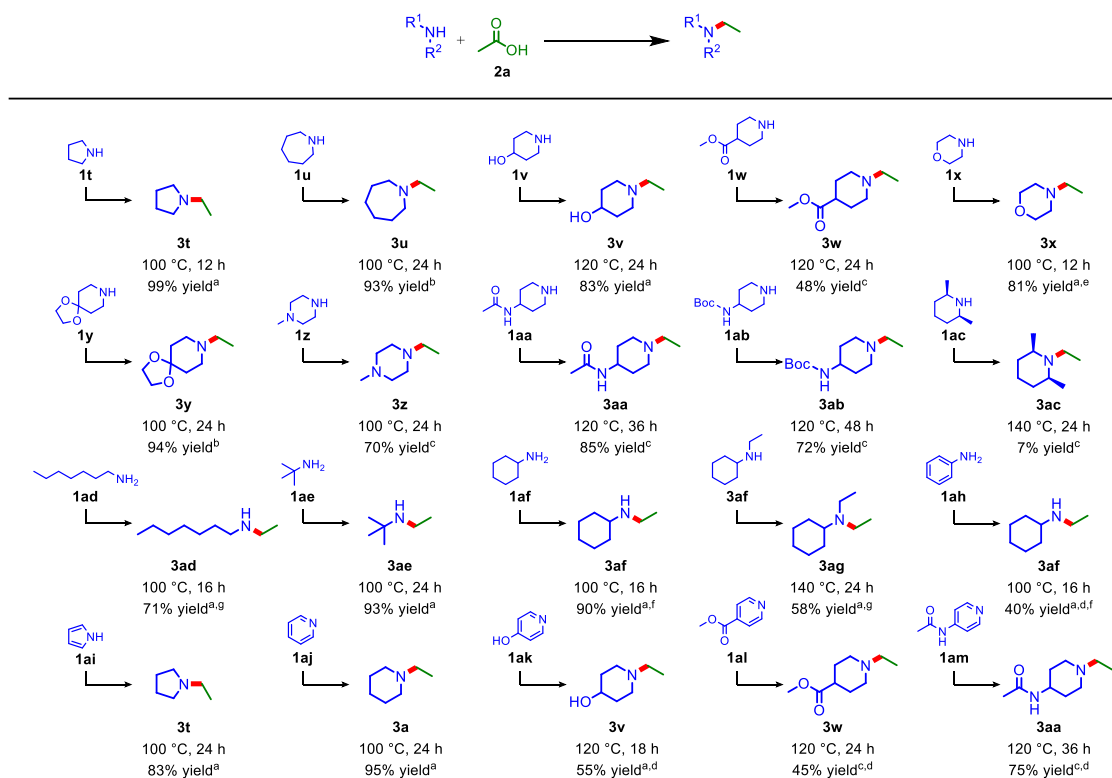
Scheme 2-4 Reductive amination of **2a** with various amines under H_2. Reaction conditions: Pt–MoO$_x$/γ-Al$_2$O$_3$ (0.15 g, Pt: 8 mol% and Mo: 2 mol%), amine (1 mmol), carboxylic acid (3 mmol), *n*-hexane (3 mL), H_2 (2 MPa). [a] GC-FID yield. [b] Isolated yield as a hydrochloride salt. [c] ^{1}H NMR yield. [d] H_2 (3 MPa). [e] H_2 (4 MPa). [f] Carboxylic acid (4 mmol). [g] Carboxylic acid (5 mmol).

3.3 Reaction pathway

The reductive amination can proceed through four potential pathways without stable intermediates (direct pathway), or involving amide, aldehyde, and alcohol intermediates (Scheme 2-5) [23–31]. To investigate reaction pathway of the Pt–MoO$_x$/γ-Al$_2$O$_3$-catalyzed reductive amination, time-course analysis was performed (Figure 2-2). The time-course data showed that the conversion of substrates (**1a** and **2a**) and **3a** yield increased as time-passed with formation of **4a** (<1%) and **5a** (<36%) as potential intermediates. As illustrated in Scheme 2-4, the amide and hydroxyl groups were tolerated (**3aa** and **3v**, respectively), indicating that amides or alcohols are unlikely to be the primary

reaction intermediates. Indeed, hydrogenation of 1-(1-piperidinyl)-1-propane (**4b**) in the presence of

2b and amination of 1-propanol with **1a** afforded poor amounts of **3b** (Schemes 2-6a and b). Therefore,

the Pt–MoO$_x$/γ-Al$_2$O$_3$-catalyzed reductive amination can occur through direct pathway without stable

intermediates. Although aldehyde intermediate is not detected in time-course, propionaldehyde was

smoothly aminated into **3b** in a 70% yield (Scheme 2-6c), suggesting that aldehyde pathway could not

be excluded. Overall, the present reaction can proceed through direct or aldehyde pathways.
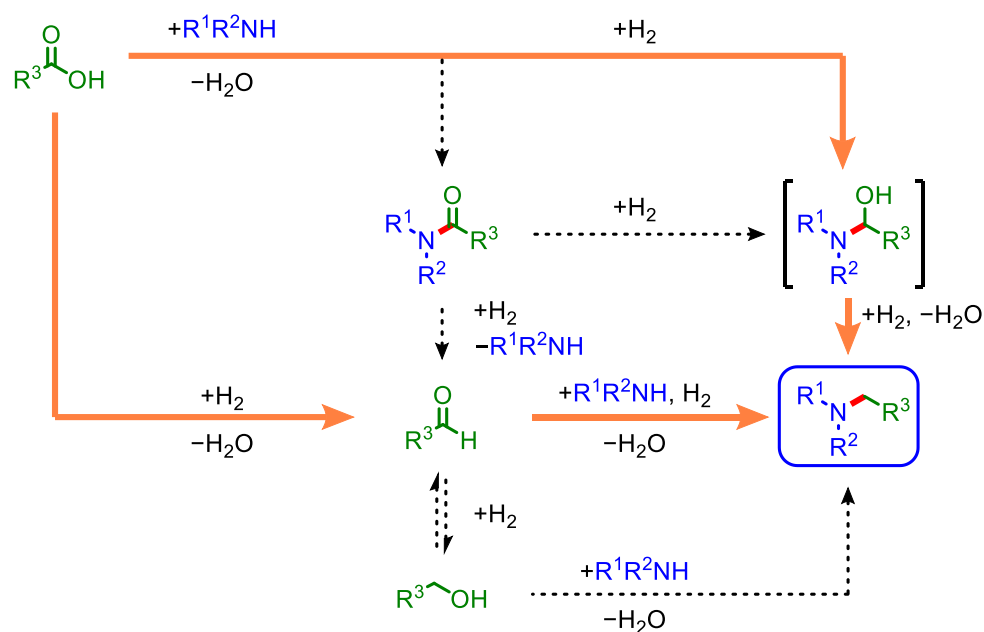
Scheme 2-5 Possible reaction pathways for the Pt–MoO$_x$/γ-Al$_2$O$_3$ catalyzed reductive amination of carboxylic acids.
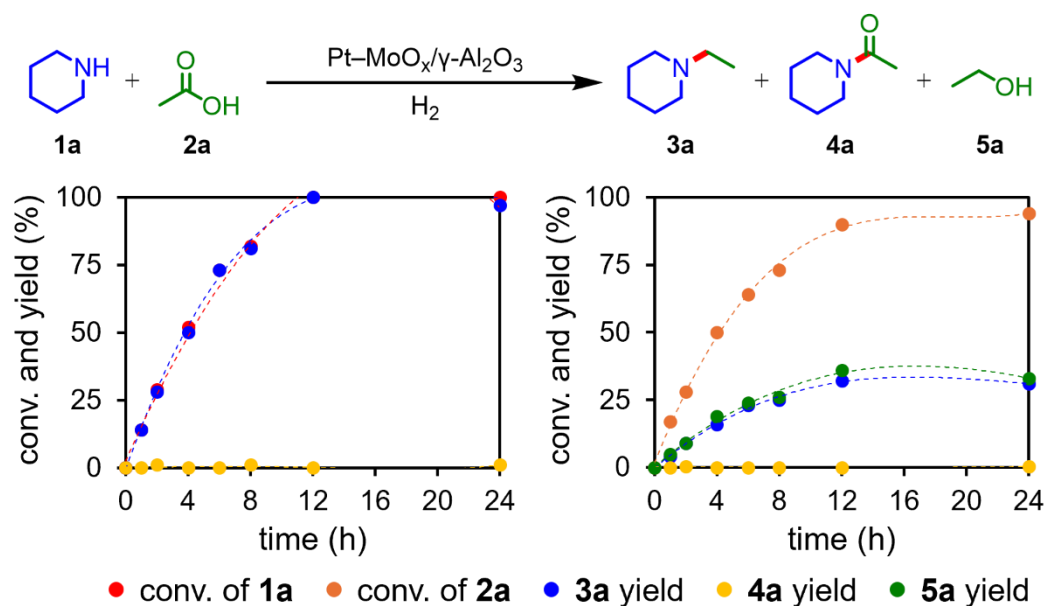
Figure 2-2 Time-course data of the Pt–MoO$_x$/γ-Al$_2$O$_3$ catalyzed reductive amination of **2a** with **1a** to **3a**. Product distribution was determined based on (a) **1a** and (b) **2a**. Reaction conditions: Pt–MoO$_x$/γ-Al$_2$O$_3$ (0.15 g, Pt: 8 mol% and Mo: 2 mol%), **1a** (1 mmol), **2a** (3 mmol), *n*-hexane (3 mL), 100 °C, H$_2$ (2 MPa).
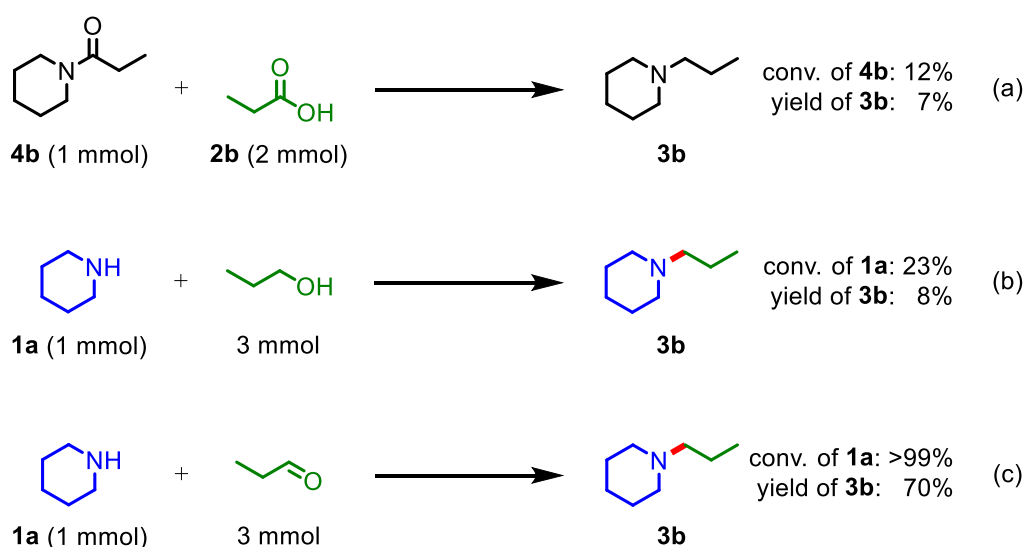
Scheme 2-6 Control experiments. (a) Hydrogenation of **4b**. (b) Amination of 1-propanol with **1a**. (c) Reductive amination of propionaldehyde with **1a**. Reaction conditions: Pt–MoO$_x$/γ-Al$_2$O$_3$ (0.15 g, Pt: 8 mol% and Mo: 2 mol%), *n*-hexane (3 mL), 100 °C, H$_2$ (2 MPa), 24 h.

3.4 Characterization

The structures of the Pt and Mo species in Pt–MoO$_x$/γ-Al$_2$O$_3$ were investigated using XANES analysis. The white line of the Pt L_3-edge XANES spectrum of fresh Pt–MoO$_x$/γ-Al$_2$O$_3$ was similar to that of PtO$_2$ (Figure 2-3a), and the Mo K-edge XANES spectrum of fresh Pt–MoO$_x$/γ-Al$_2$O$_3$ resembled that of MoO$_3$ (Figure 2-3b), revealing that the Pt and Mo species in fresh Pt–MoO$_x$/γ-Al$_2$O$_3$ were present as PtO$_2$ and MoO$_3$, respectively. After pre-reduction, the intensity of the white line in the Pt L_3-edge XANES spectrum and the absorption edge energy of the Mo K-edge XANES spectrum decreased (Figures 2-3a and b). These XAFS results suggested that PtO$_2$ and MoO$_3$ in fresh Pt–MoO$_x$/γ-Al$_2$O$_3$ were reduced *in situ* to form metallic Pt and partially reduced molybdenum oxide species (MoO$_x$). To obtain more information regarding the Mo valence state, the Mo K-edge XANES pattern fitting analysis of the reduced Pt–MoO$_x$/γ-Al$_2$O$_3$ was performed using Mo$_2$C, MoO$_2$, and MoO$_3$ as standards for the Mo^{2+}, Mo^{4+}, and Mo^{6+} oxidation states, respectively (Figure 2-3c). This result revealed that the ratio of Mo^{2+}, Mo^{4+}, and Mo^{6+} was 42:40:18.
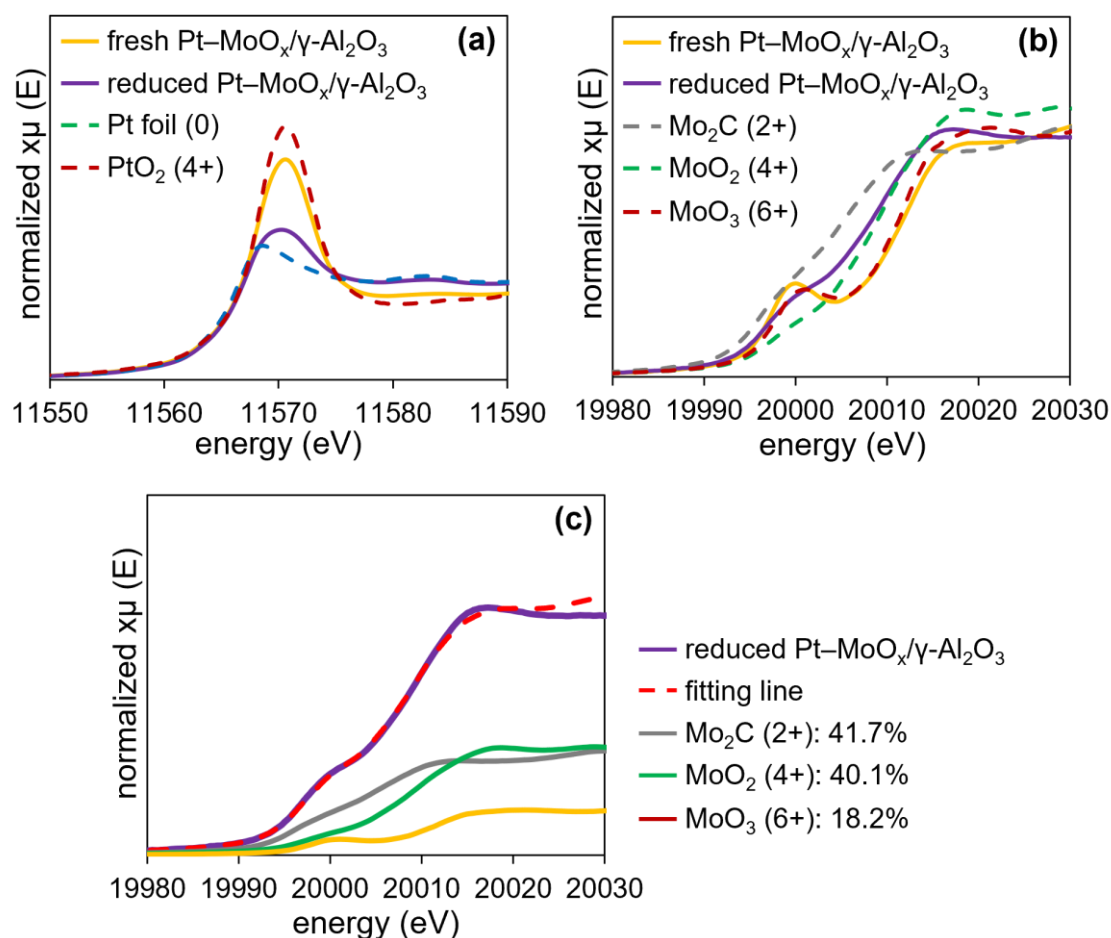
Figure 2-3 (a) Pt L_3-edge XANES spectra of fresh Pt–MoO$_x$/γ-Al$_2$O$_3$, reduced Pt–MoO$_x$/γ-Al$_2$O$_3$, Pt foil, and PtO$_2$. (b) Mo K-edge XANES spectra of fresh Pt–MoO$_x$/γ-Al$_2$O$_3$, reduced Pt–MoO$_x$/γ-Al$_2$O$_3$, Mo$_2$C, MoO$_2$, and MoO$_3$. (c) Linear combination fitting analysis of Mo K-edge XANES spectrum of reduced Pt–MoO$_x$/γ-Al$_2$O$_3$.

Furthermore, TEM images of the reduced Pt–MoO$_x$/γ-Al$_2$O$_3$ confirmed the presence of NPs with a mean diameter of 2.3 nm (Figure 2-4a). A high-resolution TEM image of the NPs showed that the measured d-spacing value of the lattice fringe was approximately 0.20 nm, which corresponds to the (200) plane of face-centered cubic Pt NPs (Figure 2-4b). HAADF-STEM coupled with EDX demonstrated a high dispersion of Pt and Mo (Figures 2-4c and d). Overall, the Pt NPs and MoO$_x$ species are dispersed on the γ-Al$_2$O$_3$ surface.
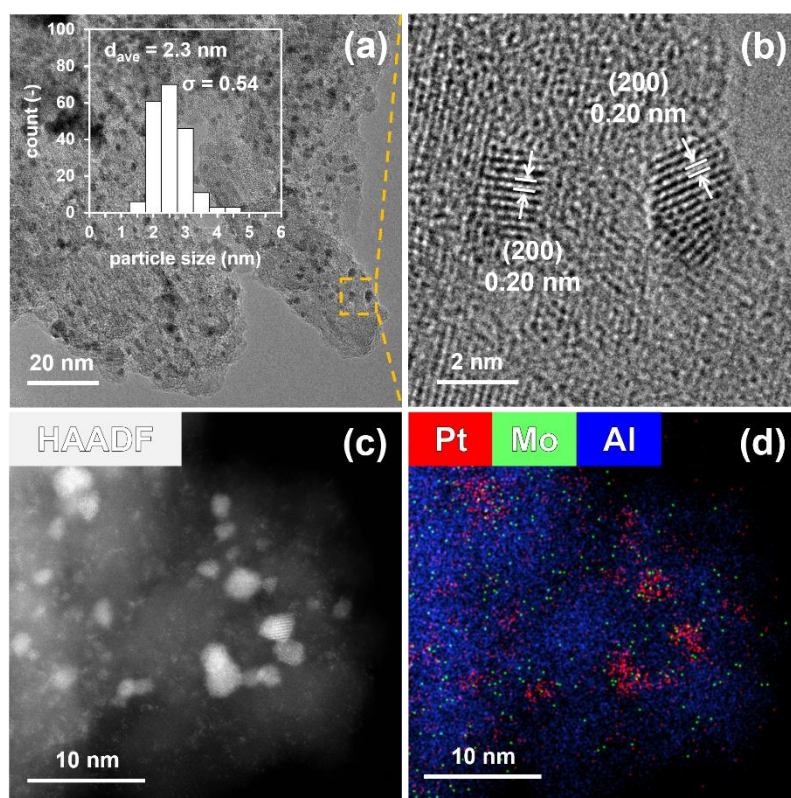
Figure 2-4 (a) TEM image and size distribution histogram (inset) of reduced Pt–MoO$_x$/γ-Al$_2$O$_3$. (b) High-resolution TEM image of reduced Pt–MoO$_x$/γ-Al$_2$O$_3$ showing one-dimensional lattice fringes of the (200) lattice planes in the Pt NPs. (c) HAADF-STEM image of reduced Pt–MoO$_x$/γ-Al$_2$O$_3$. (d) Composite overlay of the elemental mapping of Pt, Mo, and Al in reduced Pt–MoO$_x$/γ-Al$_2$O$_3$.

3.5 DFT calculation

To investigate the interaction between MoO_x and carboxylic acids, DFT calculation on the adsorption energy of **2a** was performed (for DFT calculation methods, see the paper [1] in the List of Publications of this doctoral thesis). The (011) surface of MoO_2 was chosen to construct a slab model of MoO_x in Pt–MoO_x/γ-Al_2O_3 based on the literature [59]. The adsorption energy (ΔE) of **2a** on the oxygen-vacant MoO_x surface was calculated to be −45.9 kcal/mol, suggesting chemisorption of **2a** on MoO_x (Figure 2-5) [60]. Therefore, the DFT calculation revealed significant adsorption of carboxylic acids on MoO_x [61].

ΔE = −45.9 kcal/mol
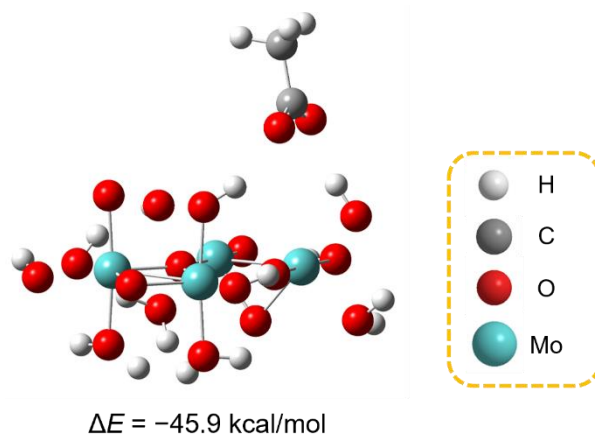
Figure 2-5 Optimized structure model of **2a** adsorbed on an oxygen-defective MoO_x surface.

3.6 Proposed catalyst cycle

Based on the above results, a catalyst cycle is proposed as shown in Scheme 2-7. First, Pt NPs

are formed *via* reduction with H_2 and then, dissociate H_2 (Scheme 2-7a(I)). The spillover hydrogen

from the Pt NPs reduces MoO_3 to form MoO_x (Scheme 2-7a(II)). Carboxylic acid is activated on Lewis

acidic MoO_x (Scheme 2-7a(III)) followed by the attack of amine (Scheme 2-7a(IV)). MoO_x is oxidized

by removing carbonyl oxygen with formation of hemiaminal intermediate (Scheme 2-7a(V)). Finally,

hydrogenation of hemiaminal affords alkylamine (Scheme 2-7a(VI)). Therefore, cooperative catalysis

between the Pt NPs and MoO_x efficiently promoted the reductive amination of carboxylic acids under

H_2. The steps VIa and VIb in Scheme 2-7a were supported by the following experimental results: the

amination of **2l** afforded *N*-ethyl piperidine with H–D scrambling (Scheme 2-3). Thus, there are two

reaction pathways to afford amine, i.e., *via* a direct hydrogenation of hemiaminal (Scheme 2-7a(VIa))

or through enamine (Scheme 2-7a(VIb)). Alternatively, carboxylic acid is hydrogenated to aldehyde

followed by amination (Scheme 2-7b). In this pathway, Pt NPs dissociate H_2 and MoO_x activate

carboxylic acid as Lewis acid, efficiently promoting hydrogenation of carboxylic acid to aldehyde.
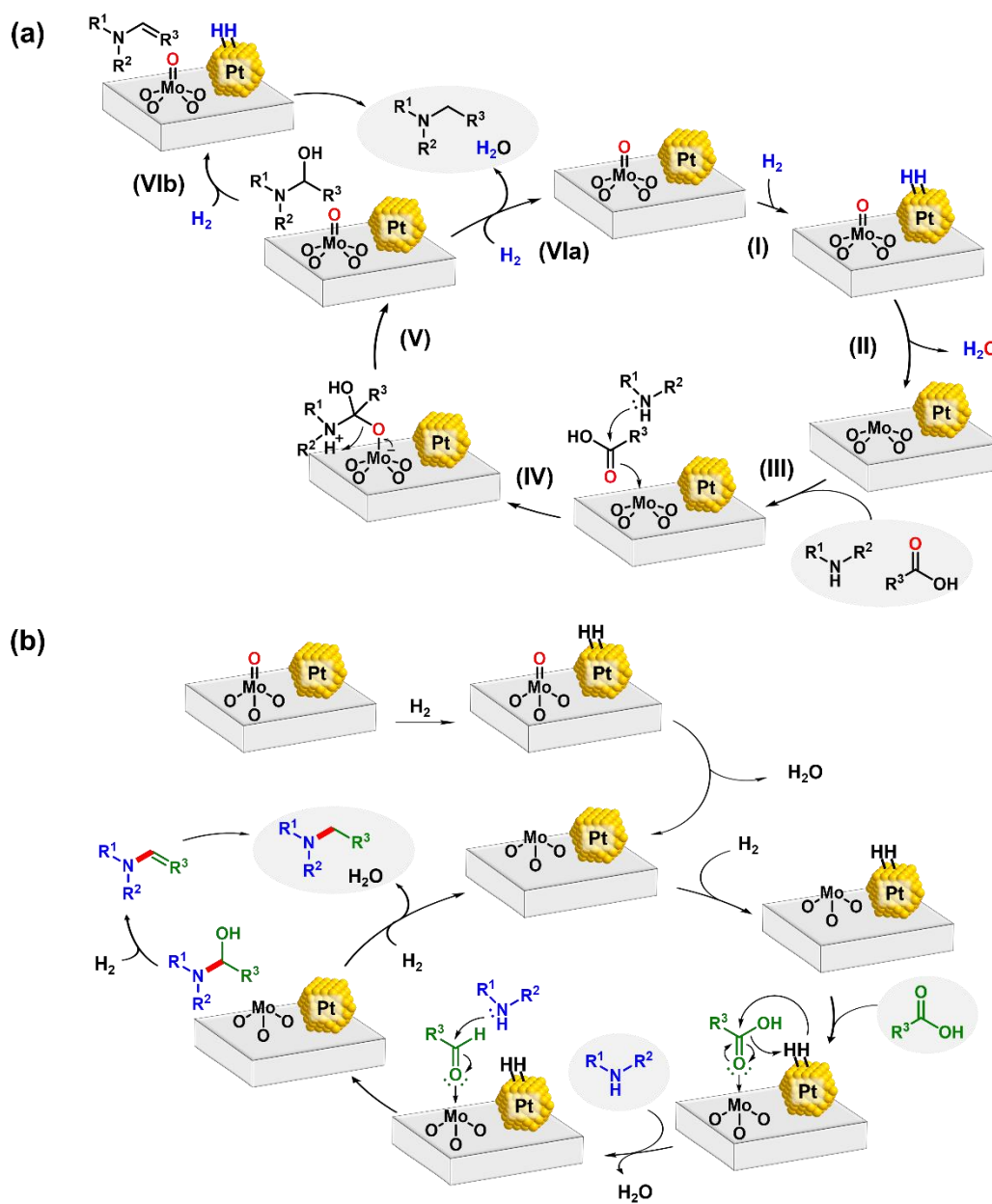
Scheme 2-7 Proposed major reaction pathway for the reductive amination of **2a** with **1a** over Pt–MoO$_x$/γ-Al$_2$O$_3$.

4   Conclusions

The highly effective Pt–MoO$_x$/γ-Al$_2$O$_3$ catalyst was developed for the reductive amination of carboxylic acids using H$_2$ as a reductant. This is the first catalyst that promoted the reductive amination of carboxylic acids under ambient H$_2$ pressure. The Pt–MoO$_x$/γ-Al$_2$O$_3$ catalyst was operated in a gram-scale reaction, achieving a high TON value of 363. Moreover, the catalyst could be easily recoverable from the reaction mixture and reusable at least five times without significant loss of its activity or selectivity. This catalyst system demonstrated a broad substrate scope, including biomass-derived carboxylic acids and functionalized amines. Characterizations, DFT calculations, and control experiments revealed that the exceptional catalytic activity of Pt–MoO$_x$/γ-Al$_2$O$_3$ stems from the cooperative catalysis between Pt NPs and MoO$_x$. Therefore, this study provides a straightforward and clean approach for the reductive amination of carboxylic acids.

5   Reference

1   Lawrence, S. A. *Amines: Synthesis, Properties and Application*, Cambridge University Press, Cambridge, 2004.

2   Müller T. E.; Beller, M. Metal-Initiated Amination of Alkenes and Alkynes. *Chem. Rev.*, **1998**, *98*, 675–703.

3   Müller, T. E.; Hultzsch, K. C.; Yus, M.; Foubelo, F.; Tada, M. Hydroamination: Direct Addition of Amines to Alkenes and Alkynes. *Chem. Rev.*, **2008**, *108*, 3795–3892.

4   Sengupta, M.; Das, S.; Islam, S. M.; Bordoloi, A. Heterogeneously Catalysed Hydroamination. *ChemCatChem*, **2021**, *13*, 1089–1104.

5   Ley, S. V.; Thomas, A. W. Modern Synthetic Methods for Copper-Mediated C(aryl)–O, C(aryl)–N, and C(aryl)–S Bond Formation. *Angew. Chem., Int. Ed.*, **2003**, *42*, 5400–5449.

6   Ruiz-Castillo, P.; Buchwald, S. L. Applications of Palladium-Catalyzed C–N Cross-Coupling Reactions. *Chem. Rev.*, **2016**, *116*, 12564–12649.

7   Dorel, R.; Grugel, C. P.; Haydl, A. M. The Buchwald–Hartwig Amination After 25 Years. *Angew. Chem., Int. Ed.*, **2019**, *58*, 17118–17129.

8   Irrgang, T.; Kempe, R. Transition-Metal-Catalyzed Reductive Amination Employing Hydrogen. *Chem. Rev.*, **2020**, *120*, 9583–9674.

9   Murugesan, K.; Senthamarai, T.; Chandrashekhar, V. G.; Natte, K.; Kamer, P. C. J.; Beller, M.; Jagadeesh, R. V. Catalytic Reductive Aminations Using Molecular Hydrogen for Synthesis of Different Kinds of Amines. *Chem. Soc. Rev.*, **2020**, *49*, 6273–6328.

10   Cabrero-Antonino, J. R.; Adam, R.; Beller, M. Catalytic Reductive N-Alkylations Using CO_2 and Carboxylic Acid Derivatives: Recent Progress and Developments. *Angew. Chem., Int. Ed.*, **2019**, *58*, 12820–12838.

11   Li, J.; Huang, C.-Y.; Li, C.-J. Deoxygenative Functionalizations of Aldehydes, Ketones and Carboxylic Acids. *Angew. Chem., Int. Ed.*, **2022**, *61*, e202112770.

12   Dong, J.; Yang, Z.; Catalytic One-Pot Reductive Amination of Carboxylic Acids, *ChemCatChem*, **2024**, *16*, e202301427.

13   Werpy, T.; Petersen, G. *Top Value Added Chemicals from Biomass: Volume I – Results of Screening for Potential Candidates from Sugars and Synthesis Gas*, 2004, DOI: 10.2172/15008859.

14   Bozell, J. J.; Petersen, G. R. Technology Development for the Production of Biobased Products from Biorefinery Carbohydrates—the US Department of Energy's "Top 10" Revisited. *Green Chem.* **2010**, *12*, 539–554.

15   Tomishige, K.; Yabushita, M.; Cao, J.; Nakagawa, Y. Hydrodeoxygenation of Potential Platform Chemicals Derived from Biomass to Fuels and Chemicals. *Green Chem.* **2022**, *24*, 5652–5690.

16   Gribble, G. W.; Lord, P. D.; Skotnicki, J.; Dietz, S. E.; Eaton, J. T.; Johnson, J. L. Reactions of Sodium Borohydride in Acidic Media. I. Reduction of Indoles and Alkylation of Aromatic Amines with Carboxylic Acids. *J. Am. Chem. Soc.* **1974**, *96*, 7812–7814.

17   Marchini, P.; Liso, G.; A. Reho; Liberatore, F.; Moracci, F. M. Sodium Borohydride-Carboxylic Acid Systems. Useful Reagents for the Alkylation of Amines. *J. Org. Chem.* **1975**, *40*, 3453–3456.

18   Sorribes, I.; Junge, K.; Beller, M. Direct Catalytic N-Alkylation of Amines with Carboxylic Acids. *J. Am. Chem. Soc.* **2014**, *136*, 14314–14319.

19   Fu, M.-C.; Shang, R.; Cheng, W.-M.; Fu, Y. Boron-Catalyzed N-Alkylation of Amines using Carboxylic Acids. *Angew. Chem., Int. Ed.* **2015**, *54*, 9042–9046.

20   Andrews, K. G.; Faizova, R.; Denton, R. M. A Practical and Catalyst-Free Trifluoroethylation Reaction of Amines using Trifluoroacetic Acid. *Nat. Commun.* **2017**, *8*, 15913.

21 Stoll, E. L.; Tongue, T.; Andrews, K. G.; Valette, D.; Hirst, D. J.; Denton, R. M. A Practical Catalytic Reductive Amination of Carboxylic Acids. *Chem. Sci.* **2020**, *11*, 9494–9500.

22 Ouyang, L.; Miao, R.; Yang, Z.; Luo, R. Iridium-Catalyzed Reductive Amination of Carboxylic Acids *J. Catal.* **2023**, *418*, 283–289.

23 Magro, A. A. N.; Eastham, G. R.; Cole-Hamilton, D. J. The Synthesis of Amines by the Homogeneous Hydrogenation of Secondary and Primary Amides. *Chem. Commun.* **2007**, 3154–3156.

24 Sorribes, I.; Cabrero-Antonino, J. R.; Vicent, C.; Junge, K.; Beller, M. Catalytic N-Alkylation of Amines Using Carboxylic Acids and Molecular Hydrogen. *J. Am. Chem. Soc.* **2015**, *137*, 13580–13587.

25 Shi, Y.; Kamer, P. C. J.; Cole-Hamilton, D. J.; Harvie, M.; Baxter, E. F.; Lim, K. J. C.; Pogorzelec, P. A New Route to N-Aromatic Heterocycles from the Hydrogenation of Diesters in the Presence of Anilines. *Chem. Sci.* **2017**, *8*, 6911–6917.

26 Shi, Y.; Kamer, P. C. J.; Cole-Hamilton, D. J. A New Route to α,ω-Diamines from Hydrogenation of Dicarboxylic Acids and Their Derivatives in the Presence of Amines. *Green Chem.* **2017**, *19*, 5460–5466.

27 Liu, W.; Sahoo, B.; Spannenberg, A.; Junge, K.; Beller, M. Tailored Cobalt-Catalysts for Reductive Alkylation of Anilines with Carboxylic Acids under Mild Conditions. *Angew. Chem., Int. Ed.* **2018**, *57*, 11673–11677.

28 Emayavaramban, B.; Chakraborty, P.; Sundararaju, B. Cobalt-Catalyzed Reductive Alkylation of Amines with Carboxylic Acids. *ChemSusChem* **2019**, *12*, 3089–3093.

29 Toyao, T.; Siddiki, S. M. A. H.; Morita, Y.; Kamachi, T.; Touchy, A. S.; Onodera, W.; Kon, K.; Furukawa, S.; Ariga, H.; Asakura, K.; Yoshizawa, K.; Shimizu, K. Rhenium-Loaded TiO_2: A Highly Versatile and Chemoselective Catalyst for the Hydrogenation of Carboxylic Acid Derivatives and the N-Methylation of Amines Using H_2 and CO_2. *Chem. Eur. J.* **2017**, *23*, 14848–14859.

30 Coeck, R.; De Vos, D. E. One-Pot Reductive Amination of Carboxylic Acids: A Sustainable Method for Primary Amine Synthesis. *Green Chem.* **2020**, *22*, 5105–5114.

31 Coeck, R.; Meeprasert, J.; Li, G.; Altantzis, T.; Bals, S.; Pidko, E. A.; De Vos, D. E. Gold and Silver-Catalyzed Reductive Amination of Aromatic Carboxylic Acids to Benzylic Amines. *ACS Catal.* **2021**, *11*, 7672–7684.

32 Robinson, A. M.; Hensley, J. E.; Will Medlin, J. Bifunctional Catalysts for Upgrading of Biomass-Derived Oxygenates: A Review. *ACS Catal.* **2016**, *6*, 5026–5043.

33 Toyao, T.; Siddiki, S. M. A. H.; Kon, K.; Shimizu, K. The Catalytic Reduction of Carboxylic Acid Derivatives and CO_2 by Metal Nanoparticles on Lewis-Acidic Supports. *Chem. Rec.* **2018**, *18*, 1374–1393.

34 Kon, K.; Siddiki, S. M. A. H.; Onodera, W.; Shimizu, K. Sustainable Heterogeneous Platinum Catalyst for Direct Methylation of Secondary Amines by Carbon Dioxide and Hydrogen. *Chem. Eur. J.* **2014**, *20*, 6264–6267.

35 Touchy, A. S.; Siddiki, S. M. A. H.; Kon, K.; Shimizu, K. Heterogeneous Pt Catalysts for Reductive Amination of Levulinic Acid to Pyrrolidones. *ACS Catal.* **2014**, *4*, 3045–3050.

36 Nakamura, Y.; Kon, K.; Touchy, A. S.; Shimizu, K.; Ueda, W. Selective Synthesis of Primary Amines by Reductive Amination of Ketones with Ammonia over Supported Pt catalysts. *ChemCatChem* **2015**, *7*, 921–924.

37 Mizugaki, T.; Nagatsu, Y.; Togo, K.; Maeno, Z.; Mitsudome, T.; Jitsukawa, K.; Kaneda K. Selective Hydrogenation of Levulinic Acid to 1,4-Pentanediol in Water Using a Hydroxyapatite-Supported Pt–Mo Bimetallic Catalyst. *Green Chem.* **2015**, *17*, 5136–5139.

38 Mizugaki, T.; Togo, K.; Maeno, Z.; Mitsudome, T.; Jitsukawa, K.; Kaneda, K. One-Pot Transformation of Levulinic Acid to 2-Methyltetrahydrofuran Catalyzed by Pt–Mo/H-β in Water. *ACS Sustainable Chem. Eng.* **2016**, *4*, 682–685.

39 Shimizu, K.; Onodera, W.; Touchy, A. S.; Siddiki, S. M. A. H.; Toyao, T.; Kon, K. Lewis Acid-Promoted Heterogeneous Platinum Catalysts for Hydrogenation of Amides to Amines. *ChemistrySelect* **2016**, *4*, 736–740.

40 Kon, K.; Toyao, T.; Onodera, W.; Siddiki, S. M. A. H.; Shimizu, K. Hydrodeoxygenation of Fatty Acids, Triglycerides, and Ketones to Liquid Alkanes by a Pt–MoO$_x$/TiO$_2$ Catalyst. *ChemCatChem* **2017**, *9*, 2822–2827.

41 Siddiki, S. M. A. H.; Touchy, A. S.; Bhosale, A.; Toyao, T.; Mahara, Y.; Ohyama, J.; Satsuma, A.; Shimizu, K. Direct Synthesis of Lactams from Keto Acids, Nitriles, and H_2 by Heterogeneous Pt Catalysts. *ChemCatChem* **2018**, *10*, 789–795.

42 Janampelli, S.; Darbha, S. Selective Deoxygenation of Fatty Acids to Fuel-Range Hydrocarbons over Pt-MO$_x$/ZrO$_2$ (M = Mo and W) Catalysts. *Catal. Today* **2021**, *375*, 174–180.

43 Gomez, L. A.; Bababrik, R.; Komarneni, M. R.; Marlowe, J.; Salavati-fard, T.; D'Amico, A. D.; Wang, B.; Christopher, P.; Crossley, S. P. Selective Reduction of Carboxylic Acids to Aldehydes with Promoted MoO_3 Catalysts. *ACS Catal.* **2022**, *12*, 6313–6324.

44 Kaku, C.; Suganuma, S.; Nakajima, K.; Tsuji, E.; Katada, N. Selective Hydrogenation of L-proline to L-prolinol over Al_2O_3-supported Pt-MoOx Catalyst. *ChemCatChem* **2022**, *14*, e202200399.

45 Ro, I.; Sener, C.; Stadelman, T. M.; Ball, M. R.; Venegas, J. M.; Burt, S. P.; Hermans, I.; Dumesic, J. A.; Huber, G. W. Measurement of Intrinsic Catalytic Activity of Pt Monometallic and Pt-MoO_x Interfacial Sites over Visible Light Enhanced $PtMoO_x/SiO_2$ Catalyst in Reverse Water Gas Shift Reaction. *J. Catal.* **2016**, *344*, 784–794.

46 Ge, H.; Kuwahara, Y.; Kusu, K.; Yamashita, H. Plasmon-Induced Catalytic CO_2 Hydrogenation by a Nano-Sheet Pt/H_xMoO_{3-y} Hybrid with Abundant Surface Oxygen Vacancies. *J. Mater. Chem. A* **2021**, *9*, 13898–13907.

47 Kuwahara, Y.; Mihogi, T.; Hamahara, K.; Kusu, K.; Kobayashi, H.; Yamashita, H. A Quasi-Stable Molybdenum Sub-Oxide with Abundant Oxygen Vacancies that Promotes CO_2 Hydrogenation to Methanol. *Chem. Sci.* **2021**, *12*, 9902–9915

48 Toyao, T.; Kayamori, S.; Maeno, Z.; Siddiki, S. M. A. H.; Shimizu, K. Heterogeneous Pt and MoO_x Co-Loaded TiO_2 Catalysts for Low-Temperature CO_2 Hydrogenation To Form CH_3OH. *ACS Catal.* **2019**, *9*, 8187–8196.

49 Mine, S.; Yamaguchi, T.; Ting, K. W.; Maeno, Z.; Siddiki, S. M. A. H.; Oshima, K.; Satokawa, S.; Shimizu, K.; Toyao, T. Reverse Water-Gas Shift Reaction over $Pt/MoO_x/TiO_2$: Reverse Mars–van Krevelen Mechanism via Redox of Supported MoO_x. *Catal. Sci. Technol.* **2021**, *11*, 4172–4180.

50 Ting, K. W.; Imbe, T.; Kamakura, H.; Maeno, Z.; Siddiki, S. M. A. H.; Matsushita, K.; Shimizu, K.; Toyao, T. Catalytic Methylation of Benzene over $Pt/MoO_x/TiO_2$ and Zeolite Catalyst Using CO_2 and H_2. *Chem. Lett.* **2022**, *51*, 149–152.

51 Liu, H.-X.; Li, J.-Y.; Qin, X.; Ma, C.; Wang, W.-W.; Xu, K.; Yan, H.; Xiao, D.; Jia, C.-J.; Fu, Q.; Ma, D. $Pt_n–O_v$ Synergistic Sites on MoO_x/γ-Mo_2N Heterostructure for Low-Temperature Reverse Water–Gas Shift Reaction. *Nat Commun.* **2022**, *13*, 5800.

52 Asano, T.; Tamura, M.; Nakagawa, Y.; Tomishige K. Selective Hydrodeoxygenation of 2-Furancarboxylic Acid to Valeric Acid over Molybdenum-Oxide-Modified Platinum Catalyst. *ACS Sustainable Chem. Eng.* **2016**, *4*, 6253–6257.

53 Asano, T.; Nakagawa, Y.; Tamura, M.; Tomishige, K. Structure and Mechanism of Titania-Supported Platinum–Molybdenum Catalyst for Hydrodeoxygenation of 2-Furancarboxylic Acid to Valeric Acid. *ACS Sustainable Chem. Eng.* **2019**, *7*, 9601–9612.

54 Yang, M.; Qi, H.; Liu, F.; Ren, Y.; Pan, X.; Zhang, L.; Liu, X.; Wang, H.; Pang, J.; Zheng, M.; Wang, A.; Zhang, T. One-Pot Production of Cellulosic Ethanol via Tandem Catalysis over a Multifunctional Mo/Pt/WOx Catalyst. *Joule* **2019**, *3*, 1937–1948.

55 Touchy, A. S.; Siddiki, S. M. A. H.; Onodera, W.; Kon, K.; Shimizu, K. Hydrodeoxygenation of Sulfoxides to Sulfides by a Pt and MoOx Co-Loaded TiO2 Catalyst. *Green Chem.* **2016**, *18*, 2554–2560.

56 Kuwahara, Y.; Yoshimura, Y.; Haematsu, K.; Yamashita, H. Mild Deoxygenation of Sulfoxides over Plasmonic Molybdenum Oxide Hybrid with Dramatic Activity Enhancement under Visible Light. *J. Am. Chem. Soc.* **2018**, *140*, 9203–9210.

57 Oare, D. A.; Henderson, M. A.; Sanner, M. A.; Heathcock, C. H. Stereochemistry of the Michael Addition of N,N-Disubstituted Amide and Thioamide Enolates to α,β-Unsaturated Ketones *J. Org. Chem.* **1990**, *55*, 132–157.

58 Atasoy, M.; Owusu-Agyeman, I.; Plaza, E.; Cetecioglu, Z. Bio-Based Volatile Fatty Acid Production and Recovery from Waste Streams: Current Status and Future Challenges. *Bioresour. Technol.* **2018**, *268*, 773–786.

59 Bolzan, A. A.; Kennedy, B. J.; Howard, C. J. Neutron Powder Diffraction Study of Molybdenum and Tungsten Dioxides. *Aust. J. Chem.* **1995**, *48*, 1473–1477.

60 Haywood, D. O.; Trapnell, B. M. W. *Chemisorption*, Butterworth, 1964.

61 Najmi, S.; Rasmussen, M.; Innocenti, G.; Chang, C.; Stavitski, E.; Bare, S. R.; Medford, A. J.; Medlin, J. W.; Sievers, C. Pretreatment Effects on the Surface Chemistry of Small Oxygenates on Molybdenum Trioxide. *ACS Catal.* **2020**, *10*, 8187–8200.

Chapter III.

Reductive Amination of Triglycerides Using a Heterogeneous Pt–MoO$_x$/TiO$_2$ Catalyst

1   Introduction

Fatty amines are important chemicals used as surfactants and lubricants [1,2]. One of the most famous methods to produce fatty amines is the nitrile process using triglycerides found in plant oils and fats [3,4]. The nitrile process involves multiple steps: hydrolysis of triglycerides to fatty acids, amidation and subsequent dehydration to form nitriles, and hydrogenation of nitrile to fatty amines (Scheme 3-1(I)), requiring large amounts of solvent and energy for the production and isolation of intermediates. Therefore, the development of a straightforward method to convert triglycerides into fatty amines is of great interest [5,6]. In this context, Beller *et al.* reported the reductive amination of triglycerides with aromatic or aliphatic amines using a homogeneous Ru catalyst and an acid additive under 6 MPa H_2 at 130 °C (Scheme 3-1(IIa)) [7]. In addition to the homogeneous catalyst system, two heterogeneous catalyst systems have been reported (Scheme 3-1(IIb)). The $ZnO–Al_2O_3$ catalyst efficiently transformed coconut oil into fatty amines at 25 MPa H_2 and 310 °C [8]. Shimizu *et al.* reported a Pt/ZrO_2 catalyst that promoted the reductive amination of triglycerides in aqueous NH_3 to afford primary amines under 5.5 MPa H_2 at 220 °C [9]. However, these catalytic systems require high H_2 pressures and temperatures, and the catalyst reusability has not been investigated. Therefore, the development of highly active and reusable catalysts is desired to achieve the green and sustainable fatty amine production.

In this chapter, the author developed a titanium oxide-supported $Pt–MoO_x$ ($Pt–MoO_x/TiO_2$) catalyst for the reductive amination of triglycerides to fatty amines under mild conditions, e.g. 1 MPa H_2 and 180 °C (Scheme 3-1(III)). The $Pt–MoO_x/TiO_2$ catalyst is reusable without loss of its high activity. A wide range of amines and triglycerides, including a real cooking oil, were successfully transformed into fatty amines. Control experiments and characterizations revealed that the high catalytic activity of $Pt–MoO_x/TiO_2$ can be attributed to its multiple properties: the TiO_2 support with

a high acid amount to facilitate the conversion of triglycerides to fatty amides, as well as Pt–MoO$_x$ species to promote the hydrodeoxygenation of fatty amides to fatty amines.

(I) nitrile process[3,4]
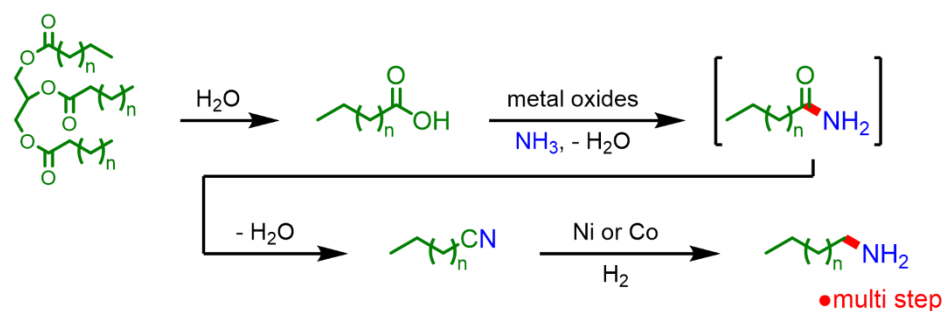
(II) reductive amination of triglycerides
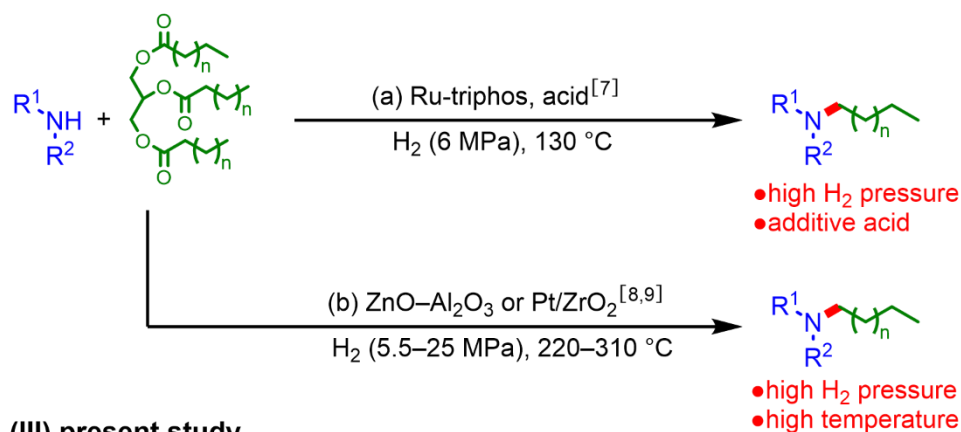
(III) present study
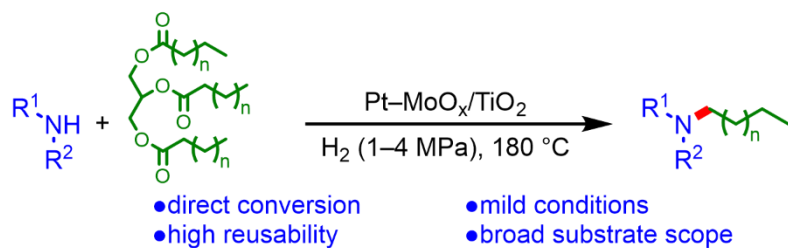
Scheme 3-1 Fatty amine syntheses from triglycerides.

2 Experimental section

2.1 General

Organic chemicals were purchased from Fujifilm Wako Pure Chemical Industries, Ltd., Tokyo Chemical Industry Co., Ltd., and Sigma-Aldrich, and were used as received. H_2PtCl_6, $RuCl_3$, K_3RhCl_6, and $Pd(NH_3)_4Cl_2$ hydrates were obtained from N. E. Chemcat. $(NH_4)_6Mo_7O_{24} \cdot 4H_2O$, NH_4VO_3, $(NH_4)_{10}(H_2W_{12}O_{42}) \cdot 4H_2O$, and $NaReO_4$ were purchased from Nacalai Tesque, Kishida Chemical, Sigma-Aldrich, and Alfa Aesar Co., Ltd., respectively. TiO_2 (SSP-N), ZrO_2 (RC-100), γ-Al_2O_3, and WO_3 were obtained from Sakai Chemical Industry Co., Ltd., Daiichi Kigenso Kagaku Kogyo Co., Ltd., Sumitomo Chemical Co., Ltd., and Fujifilm Wako Pure Chemical Industries, Ltd., respectively. Nb_2O_5 (JRC-NBO-2) was supplied by the Catalyst Society of Japan as the reference catalyst. Gas chromatography (GC-FID) analyses were performed on a Shimadzu GC-2030 instrument equipped with a capillary column (SH-Rtx-200MS, Shimadzu, 30 m × 0.25 mm i.d. film thickness 0.25 μm). Gas chromatography-mass spectrometry (GC-MS) analyses were performed on a Shimadzu QP-2010SE instrument equipped with a capillary column (SH-Rtx-200MS, Shimadzu, 30 m × 0.25 mm i.d. film thickness 0.25 μm, or InertCap WAX-HT, GL Science, 30 m × 0.25 mm i.d. film thickness 0.25 μm). ^1H and ^{13}C nuclear magnetic resonance (NMR) spectra were recorded using a JEOL JNM-ECS400 spectrometer. Chemical shifts are reported as follows: TMS (0 ppm for ^1H NMR) and $CDCl_3$ (77.1 ppm for ^{13}C NMR). NMR multiplicities are reported using the following abbreviations: s, singlet; d, doublet; t, triplet; q, quartet; m, multiplet; br, broad; J, coupling constants in hertz. Transmission electron microscopy (TEM) images were obtained using a Hitachi HF-2000 microscope instrument operating at 200 kV. High-angle annular dark-field scanning transmission electron microscopy (HAADF-STEM) images with elemental maps were collected using a JEOL JEM-ARM200F instrument, operated at 200 kV, and equipped with an energy-dispersive X-ray spectroscopy (EDX) detector. Pt L_3-edge and Mo K-edge X-ray absorption near-edge structure (XANES) spectra were

66

recorded at room temperature in transmittance mode using Si (311) monochromators at the 01B1 beam line stations at SPring-8, Japan Atomic Energy Research Institute (JASRI), Harima, Japan (promotion number: 2024B1602). Data analysis was performed using Demeter ver. 0.9.21. X-ray photoelectron spectroscopy (XPS) spectra of the samples were obtained using a Shimadzu KRATOS ULTRA2 instrument, and the binding energy was referenced to the C 1s peak (285.0 eV). Inductively coupled plasma-atomic emission spectroscopy (ICP-AES) measurements was performed using a Perkin Elmer Optima 8300 instrument. Fourier-transform infrared (FT-IR) spectra were recorded using a JASCO FT-IR 4100 spectrometer equipped with a mercury cadmium telluride detector. The CO pulse chemisorption and NH_3-temperature programmed desorption (TPD) data were measured using a BELCAT-A instrument (BEL Japan Inc.) equipped with a thermal conductivity detector and mass spectrometer (BELMASSII, BEL Japan Inc.), respectively.

2.2 Preparation of Pt–MoO$_x$/TiO$_2$ catalyst

The Pt–MoO$_x$/TiO$_2$ catalyst was prepared by co-impregnation method. Aqueous solution of H_2PtCl_6 (6.00 mL, 100 mM), $(NH_4)_6Mo_7O_{24}$·$4H_2O$ (0.0265 g), and TiO_2 (1.000 g) was added to distilled water (50 mL) at room temperature. After stirring for 12 h in air, water was removed by rotary evaporation under reduced pressure, and the resulting powder was dried at 110 °C for 5 h. After drying, the powder was calcined at 500 °C for 3 h under a static air atmosphere to obtain Pt–MoO$_x$/TiO$_2$ as a gray powder. As determined using ICP-AES, the Pt and Mo contents in Pt–MoO$_x$/TiO$_2$ were 9.31 and 1.30 wt%, respectively. The other catalysts were prepared in a similar way using various metal salts and supports. All catalysts were applied to the reaction without any pre-reduction step.

2.3 Typical reductive amination procedure

The reductive amination of trilaurin (**2**) with piperidine (**1**) was carried out in a 50 mL stainless steel autoclave equipped with a Teflon vessel. The vessel was charged with **1** (0.085 g, 1.0 mmol), **2** (0.320 g, 0.5 mmol), Pt–MoO$_x$/TiO$_2$ (0.150 g), and n-hexane (3.0 mL), and a Teflon-coated magnetic stir bar was added. The reactor was sealed, purged five times with 1.0 MPa H$_2$, and then pressurized (4.0 MPa), heated to 180 °C, and stirred at 900 rpm for 6 h. After the reaction, the autoclave was cooled in an ice-water bath, and H$_2$ gas was released. The resulting reaction mixture was diluted with ethanol and analyzed by GC-FID.

Product yields were calculated by the following equation:

$$\text{yield (based on } \mathbf{1}) = \frac{\text{amount of } \mathbf{3} \text{ (mmol)}}{\text{amount of loaded } \mathbf{1} \text{ (mmol)}} \times 100 \qquad \text{(eq. 3-1)}$$

$$\text{yield (based on } \mathbf{2}) = \frac{\text{amount of } \mathbf{3} \text{ (mmol)}}{\text{amount of loaded } \mathbf{2} \text{ (mmol)} \times 3} \times 100 \qquad \text{(eq. 3-2)}$$

In Table 3-4, entry 7, didodecylamine yield was calculated by the following equation:

$$\text{yield (based on } \mathbf{2}) = \frac{\text{amount of didodecylamine (mmol)} \times 2}{\text{amount of loaded } \mathbf{2} \text{ (mmol)} \times 3} \times 100 \qquad \text{(eq. 3-3)}$$

2.4 Catalyst reuse experiments

After the reductive amination was complete, the catalyst was separated from the reaction mixture by centrifugation and washed with ethanol and n-hexane in air before reuse in subsequent reactions.

2.5 Gram-scale reaction

The gram-scale reductive amination was carried out in a 100 mL stainless steel autoclave equipped with a Teflon vessel. The vessel was charged with **1** (1.00 g, 11.7 mmol), **2** (3.50 g, 5.48 mmol), Pt–MoO$_x$/TiO$_2$ (1.00 g), and n-hexane (10.0 mL), and a Teflon-coated magnetic stir bar was added. The reactor was purged five times with 1.0 MPa H$_2$ and then pressurized to 4.0 MPa at room temperature, heated to 180 °C, and stirred at 900 rpm for 60 h. After the reaction, the autoclave was cooled in an ice-water bath, and the H$_2$ gas was carefully released. Pt–MoO$_x$/TiO$_2$ was separated by filtration, and n-hexane was evaporated. The residue was purified by silica gel chromatography with chloroform/methanol to give pure **3** (1.86 g, 7.36 mmol, 62%).

2.6 Pt–MoO$_x$/γ-Al$_2$O$_3$ pre-reduction

Pt–MoO$_x$/TiO$_2$ was pre-reduced for control experiments in Figure 3-4(iii) and Table 3-7 under the typical reductive amination conditions without substrates: Pt–MoO$_x$/TiO$_2$ (0.150 g), n-hexane (3 mL), 180 °C, H$_2$ (4.0 MPa), 2 h.

2.7 Synthesis of 1-(1-piperidinyl)-1-dodecanone

1-(1-piperidinyl)-1-dodecanone (**4**) was prepared according to the literature procedure [10]. The flask was charged with **1** (0.850 g, 10 mmol), lauroyl chloride (1.20 g, 5.5 mmol), and Et$_2$O (50.0 mL) in an ice-water bath, and a Teflon-coated magnetic stir bar was added. The solution was stirred at room temperature for 3 h. After the reaction, the solution was washed consecutively with aqueous HCl, aqueous NaOH, and brine. The organic phase was gathered, dried with anhydrous magnesium sulfate, evaporated, and dried under vacuum to give pure **4** (1.30 g, 4.84 mmol, 88%).

2.8 Analysis of the components of cooking oil

The cooking oil (Canola oil, J-OIL MILLS, Inc.) used in this study was analyzed according to the literature procedure [11, 12]. The flask was charged with cooking oil (0.040 g), *n*-hexane (1.0 mL), and KOH (1.0 mL, 0.4 M in methanol), and a Teflon-coated magnetic stir bar was added. The solution was sonicated for 2 h, and then stirred at room temperature for 12 h. After the reaction, water (2.0 mL) was added to the reaction mixture. The organic phase was analyzed by GC-MS using an internal standard method. The oil composition is in Table 3-1.

Table 3-1 The carboxylic acid contents of the cooking oil

type of carboxylic acid	C16	C18:0	C18:1	C18:2
content (mmol/g)	0.17	0.07	2.67	0.62

[a] For C18:X, X is the number of C=C bonds in carboxylic acids

2.9 TPD-IR measurements

A thin disk of the sample was prepared by pressing the sample powder onto a stainless steel grid. The sample disk was then placed inside an IR cell to enable thermal treatment in a controlled atmosphere. The sample pellet was treated under vacuum at 180 °C for 1 h before the introduction of probe molecules. The sample was pretreated under 1 bar of H_2 at 180 °C for 1 h and then outgassed. Then, the sample was cooled to 50 °C, and treated with vaporized acetone (27 mbar) at 50 °C for 5 min. FT-IR spectra were recorded after the desorption of physisorbed or weakly chemisorbed species under vacuum at 50 °C. After the IR spectrum at 50 °C was measured, the sample was heated to a desired temperature under vacuum, and the spectrum was measured after keeping at the same temperature for 10 min.

2.10 Product identification
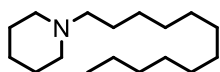
1-Dodecylpiperidine (3)

CAS registry No. [5917-47-5]. **^{1}H NMR** (400 MHz, CDCl$_3$): δ/ppm 2.37 (br-s, 4H), 2.31–2.23 (m, 2H), 1.64–1.55 (m, 4H), 1.55–1.38 (m, 4H), 1.38–1.20 (m, 18H), 0.88 (t, 3H, J = 7.0 Hz). **^{13}C NMR** (100 MHz, CDCl$_3$): δ/ppm 59.7, 54.7, 32.0, 29.74, 29.69, 29.4, 27.9, 27.0, 26.0, 24.6, 22.8, 14.2. **GC-MS** (EI): *m/z* 253 (M$^+$, 1%), 99 (8), 98 (100), 96 (1), 85 (1), 84 (2), 70 (2), 69 (2), 57 (1), 56 (1), 55 (5).
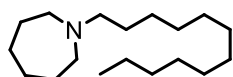
1-Dodecylazepane

CAS registry No. [20422-09-7]. **^{1}H NMR** (400 MHz, CDCl$_3$): δ/ppm 2.63 (t, 4H, J = 5.6 Hz), 2.49–2.42 (m, 2H), 1.69–1.55 (m, 8H), 1.52–1.41 (m, 2H), 1.35–1.19 (m, 18H), 0.88 (t, 3H, J = 6.8 Hz). **^{13}C NMR** (100 MHz, CDCl$_3$): δ/ppm 58.5, 55.6, 32.0, 29.74, 29.71, 29.4, 27.8, 27.7 27.5, 27.1, 22.8, 14.2. **GC-MS** (EI): *m/z* 267 (M$^+$, 1%), 113 (9), 112 (100), 110 (1), 98 (1), 84 (2), 70 (1), 69 (1), 58 (8), 57 (2), 56 (1), 55 (6).
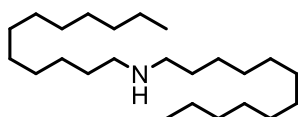
Didodecylamine

CAS registry No. [3007-31-6]. **^{1}H NMR** (400 MHz, CDCl$_3$): δ/ppm 2.58 (t, 4H, J = 7.2 Hz), 1.53–1.44 (m, 4H), 1.35–1.20 (m, 37H), 0.88 (t, 6H, J = 6.8 Hz). **^{13}C NMR** (100 MHz, CDCl$_3$): δ/ppm 50.3, 32.0, 30.3, 29.8, 29.71, 29.68, 29.4, 27.5, 22.8, 14.2. **GC-MS** (EI): *m/z* 353 (M$^+$, 2%), 352 (1), 254 (1), 212 (2), 200 (1), 199 (15), 198 (100), 196 (1), 186 (1), 185 (1), 184 (4), 112 (1), 98 (1), 86 (1), 85 (1),84 (2), 83 (1), 72 (1), 71 (2) 70 (4), 69 (4), 58 (1), 57 (9), 56 (4), 55 (8).
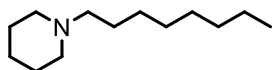
1-Octylpiperidine

CAS registry No. [7335-02-6]. **^{1}H NMR** (400 MHz, CDCl$_3$): δ/ppm **^{1}H NMR** (400 MHz, CDCl$_3$): δ/ppm 2.39 (br-s, 4H), 2.32–2.19 (m, 2H), 1.70–1.55 (m, 4H), 1.55–1.37 (m, 4H), 1.37–1.17 (m, 18H), 0.88 (t, 3H, *J* = 7.0 Hz). **^{13}C NMR** (100 MHz, CDCl$_3$): δ/ppm 59.7, 54.7, 31.9, 29.6, 29.3, 27.8, 26.9, 25.9, 24.5, 22.7, 14.1. **GC-MS** (EI): *m/z* 197 (M$^+$, 3%), 196 (1), 99 (7), 98 (100), 96 (1), 85 (1), 84 (2), 70 (4), 69 (2), 56 (2), 55 (5).
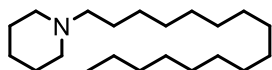
1-Hexadecylpiperidine

CAS registry No. [7335-03-7]. **^{1}H NMR** (400 MHz, CDCl$_3$): δ/ppm 2.36 (br-s, 4H), 2.30–2.22 (m, 2H), 1.64–1.55 (m, 4H), 1.54–1.38 (m, 4H), 1.38–1.18 (m, 26H), 0.88 (t, 3H, *J* = 6.8 Hz). **^{13}C NMR** (100 MHz, CDCl$_3$): δ/ppm 59.8, 54.8, 32.0, 29.8, 29.74, 29.71, 29.69, 29.4, 27.9, 27.0, 26.1, 24.6, 22.8, 14.2. **GC-MS** (EI): *m/z* 309 (M$^+$, 1%), 99 (7), 98 (100), 96 (1), 85 (1), 84 (1), 70 (1), 69 (1), 57 (1), 56 (1), 55 (4).
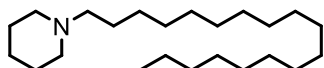
1-Octadecylpiperidine

CAS registry No. [79403-35-3]. **^{1}H NMR** (400 MHz, CDCl$_3$): δ/ppm 2.38 (br-s, 4H), 2.31–2.25 (m, 2H), 1.65–1.55 (m, 4H), 1.54–1.47 (m, 4H), 1.47–1.18 (m, 30H), 0.88 (t, 3H, *J* = 6.8 Hz). **^{13}C NMR** (100 MHz, CDCl$_3$): δ/ppm 59.7, 54.7, 32.0, 29.8, 29.74, 29.70, 29.67, 29.4, 27.9, 26.9, 26.0, 24.5, 22.8, 14.2. **GC-MS** (EI): *m/z* 337 (M$^+$, 1%), 336 (1), 99 (7), 98 (100), 96 (1), 85 (2), 84 (2), 70 (1), 69 (1), 57 (2), 56 (1), 55 (4).
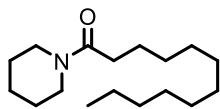
1-(1-Piperidinyl)-1-dodecanone (4)

CAS registry No. [22342-28-5]. **¹H NMR** (400 MHz, CDCl₃): δ/ppm 3.55 (t, 2H, *J* = 5.4 Hz), 3.39 (t, 2H, *J* = 5.4 Hz), 2.31 (t, 2H, *J* = 7.6 Hz), 1.69–1.48 (m, 8H), 1.38–1.19 (m, 16H), 0.88 (t, 3H, *J* = 7.0 Hz). **¹³C NMR** (100 MHz, CDCl₃): δ/ppm 171.6, 46.8, 42.6, 33.6, 32.0, 29.7, 29.60, 29.57, 29.5, 29.4, 26.6, 25.7, 25.6, 24.7, 22.7, 14.2. **GC-MS** (EI): *m/z* 267 (M⁺, 3%), 238 (1), 224 (1), 196 (1), 182 (2), 168 (1), 154 (4), 141 (5), 140 (23), 128 (8), 127 (100), 126 (3), 113 (2), 112 (21), 99 (3), 98 (1), 86 (7), 85 (14), 84 (21), 83 (2), 71 (1), 70 (7), 69 (12), 68 (1), 67 (1), 60 (2), 57 (9), 56 (7), 55 (10), 54 (1).

3 Result and discussion

3.1 Catalyst performance in the reductive amination of triglycerides
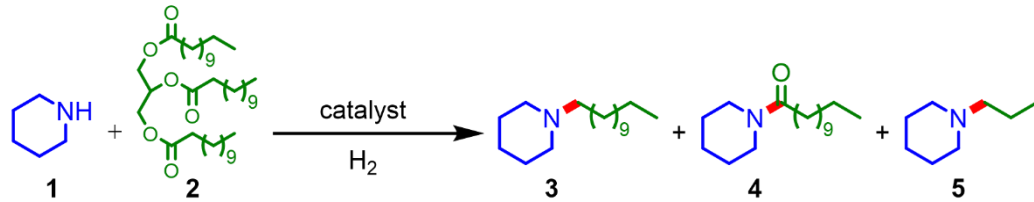
Various bifunctional catalysts were prepared by the co-impregnation method and used in the reductive amination of trilaurin (**2**) with piperidine (**1**) under 4 MPa H_2 at 180 °C for 6 h (Table 3-2). Among the catalysts examined, Pt–MoO_x/TiO_2 showed the highest activity, affording 1-dodecylpiperidine (**3**) in a 35% yield at a 54% conversion of **1** (Table 3-2, entry 1). When the reaction time was prolonged to 16 h, the yield of **3** increased to 70%, along with the formation of 1-(1-piperidinyl)-1-dodecanone (**4**) in a 2% yield and 1-propylpiperidine (**5**) in a 7% yield (Table 3-2, entry 2). Some byproducts derived from **2**, such as *n*-dodecane, 1-dodecanol, propyl dodecanoate, and dodecyldodecanoate, were identified based on GC-MS analysis (Figure 3-1). The use of other noble metals (Rh, Ru, and Pd) with MoO_x, or Pt with other metal oxides (ReO_x, WO_x, and VO_x), resulted in lower activities (Table 3-2, entries 3–8). TiO_2 supported single-metal catalysts (Pt/TiO_2 and MoO_x/TiO_2) and bare TiO_2 were ineffective in the reductive amination (Table 3-2, entries 9–11), and **4** was produced as the major product. These results demonstrated that the co-presence of Pt and MoO_x was important for efficient fatty amine production.

Table 3-2 Reductive amination of trilaurin (**2**) with piperidine (**1**) to 1-dodecylpiperidine (**3**) over various heterogeneous catalysts

entry	catalyst	conv. of **1** (%)	yield (%)		
			3	**4**	**5**
1	Pt–MoO$_x$/TiO$_2$	54	35	4	3
2[a]	Pt–MoO$_x$/TiO$_2$	99	70	2	7
3	Rh–MoO$_x$/TiO$_2$	35	17	2	1
4	Ru–MoO$_x$/TiO$_2$	62	8	24	<1
5	Pd–MoO$_x$/TiO$_2$	79	1	67	1
6	Pt–ReO$_x$/TiO$_2$	61	26	21	1
7	Pt–WO$_x$/TiO$_2$	95	14	53	1
8	Pt–VO$_x$/TiO$_2$	67	14	41	<1
9	Pt/TiO$_2$	80	16	49	1
10	MoO$_x$/TiO$_2$	59	0	47	0
11	TiO$_2$	70	0	61	0
12	Pt–MoO$_x$/ZrO$_2$	53	32	3	2
13	Pt–MoO$_x$/γ-Al$_2$O$_3$	54	30	2	3
14	Pt–MoO$_x$/WO$_3$	23	7	6	<1
15	Pt–MoO$_x$/Nb$_2$O$_5$	21	4	2	0

Table 3-2 *(Contd.)*

entry	catalyst	conv. of **1** (%)	yield (%)		
			3	**4**	**5**
16[b]	Pt–MoO$_x$/TiO$_2$	31	3	4	0
17[c]	Pt–MoO$_x$/TiO$_2$	>99	0	0	0

Reaction conditions: catalyst (0.15 g, Pt: 7 mol% and Mo: 2 mol%), **1** (1 mmol), **2** (0.5 mmol), *n*-hexane (3 mL), 180 °C, H$_2$ 4 MPa, 6 h. Conversion and yield were determined by GC-FID using an internal standard method and calculated based on **1**. [a] 16 h. [b] THF was used as a solvent. [c] Ethanol was used as a solvent. 1-ethylpiperidine was obtained in >99% yield.
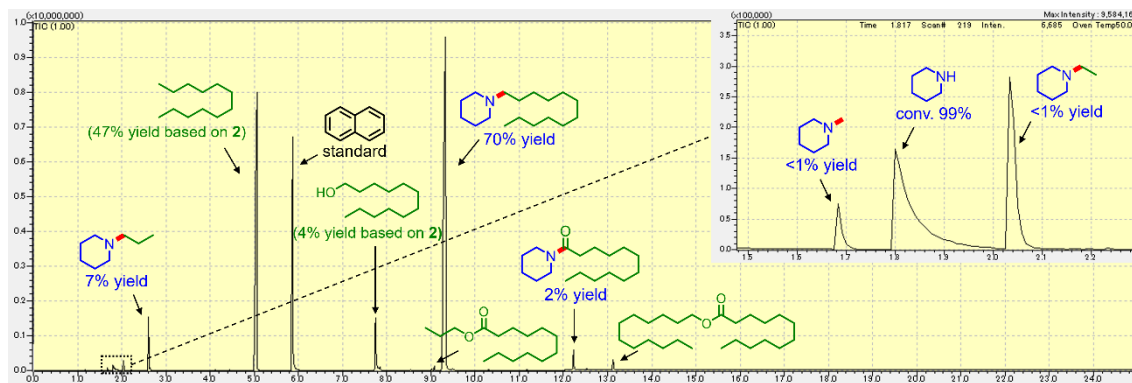
Figure 3-1 GC-MS analysis of the liquid phase after the reductive amination of **2** with **1**.

The support material was important for this reaction. Pt–MoO$_x$ catalysts supported on ZrO$_2$ and γ-Al$_2$O$_3$ were effective, affording **3** in 32% and 30% yields, respectively (Table 3-2, entries 12 and 13), which were comparable to that of Pt–MoO$_x$/TiO$_2$ (Table 3-2, entry 1). The Nb$_2$O$_5$- and WO$_3$-supported catalysts resulted in low conversions of **1** (Table 3-2, entries 14 and 15). Subsequently, the reusability of Pt–MoO$_x$/TiO$_2$, Pt–MoO$_x$/ZrO$_2$, and Pt–MoO$_x$/γ-Al$_2$O$_3$, which showed similar activity, was investigated. After reductive amination, the Pt–MoO$_x$/TiO$_2$ catalyst was recovered by centrifugation and reused in the next reductive amination without additional treatment. The high activity of the Pt–MoO$_x$/TiO$_2$ catalyst was maintained until the 11 cycle (Figure 3-2a). Inductively coupled plasma atomic emission spectroscopy analyses showed that Pt and Mo loadings of the used Pt–MoO$_x$/TiO$_2$ catalyst are similar to those of the fresh catalyst, confirming that the leaching of Pt and Mo into the reaction solution was negligible (Table 3-3). In sharp contrast to the high reusability of Pt–MoO$_x$/TiO$_2$, the conversions decreased in the reuse experiment of Pt–MoO$_x$/ZrO$_2$ and Pt–MoO$_x$/γ-Al$_2$O$_3$ (Figures 3-2b and c). Therefore, Pt–MoO$_x$/TiO$_2$ was selected as the most suitable catalyst in terms of its activity and durability.

The solvents used in the reaction were investigated. *n*-Hexane was effective in this reaction (Table 3-2, entry 1), while tetrahydrofuran was an ineffective solvent for the reductive amination maybe due to strong adsorption of polar solvents on the catalyst active sites (Table 3-2, entry 16). In the ethanol solvent, 1-ethylpiperidine was produced in >99% yield, and **3** was not obtained at all (Table 3-2, entry 17).
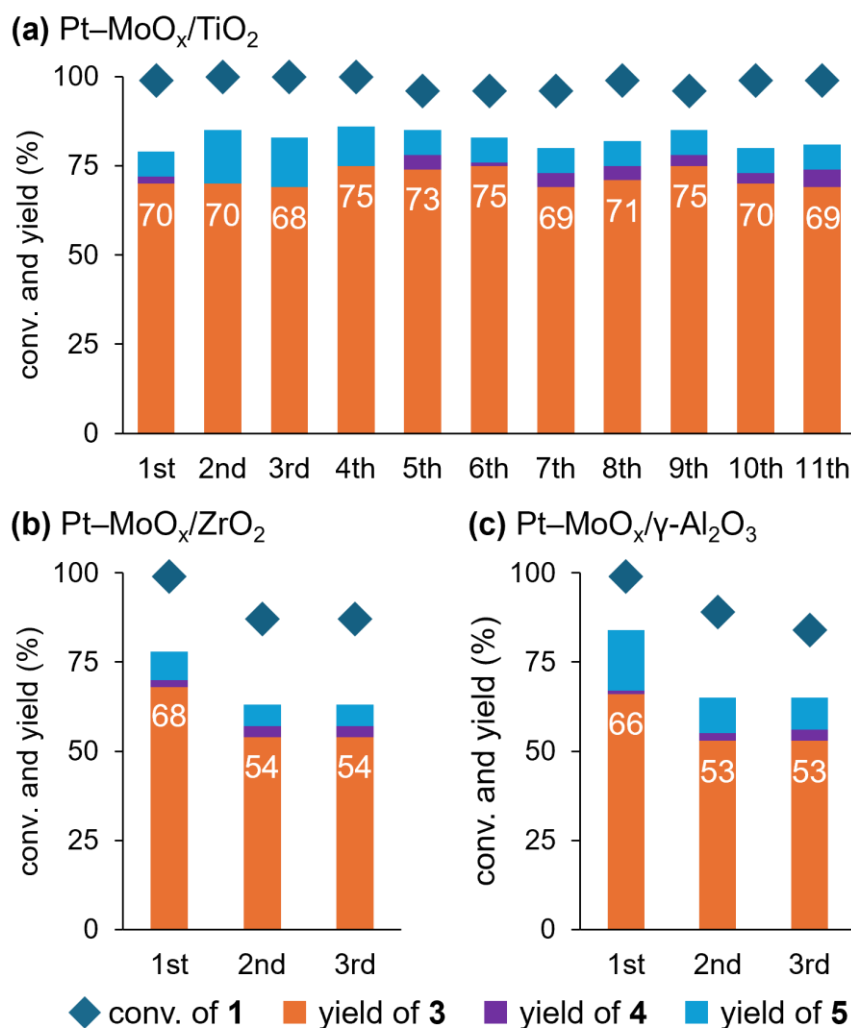
Figure 3-2 Reuse experiment in the (a) Pt–MoO$_x$/TiO$_2$, (b) Pt–MoO$_x$/ZrO$_2$, and (c) Pt–MoO$_x$/γ-Al$_2$O$_3$ catalyzed reductive amination. Reaction conditions: catalyst (0.15 g, Pt: 7 mol% and Mo: 2 mol%), **1** (1 mmol), **2** (0.5 mmol), *n*-hexane (3 mL), 180 °C, H$_2$ (4 MPa), 16 h. Conversion and yield were determined by GC-FID using an internal standard for analysis and calculated based on **1**.

Table 3-3 ICP-AES analyses of fresh and used Pt–MoO$_x$/TiO$_2$

sample	amount (wt%)			atomic ratio		
	Pt	Mo	Ti	Pt/Ti	Mo/Ti	Mo/Pt
fresh Pt–MoO$_x$/TiO$_2$	9.31	1.30	46.2	0.0494	0.0140	0.284
used Pt–MoO$_x$/TiO$_2$	9.16	1.26	45.8	0.0491	0.0137	0.280

The high catalytic activity of Pt–MoO$_x$/TiO$_2$ was further demonstrated in the reductive amination under lower H$_2$ pressure. Pt–MoO$_x$/TiO$_2$ afforded **3** in a 61% yield under 1 MPa H$_2$ (Scheme 3-2a), outperforming previously reported catalyst systems requiring over 5.5 MPa [7–9]. Moreover, the Pt–MoO$_x$/TiO$_2$ catalyst was applicable to the gram-scale reaction (Scheme 3-2b); 1.0 g of **1** and 3.5 g of **2** were stirred under the reductive amination conditions and 1.9 g of **3** was obtained with a 62% isolated yield.
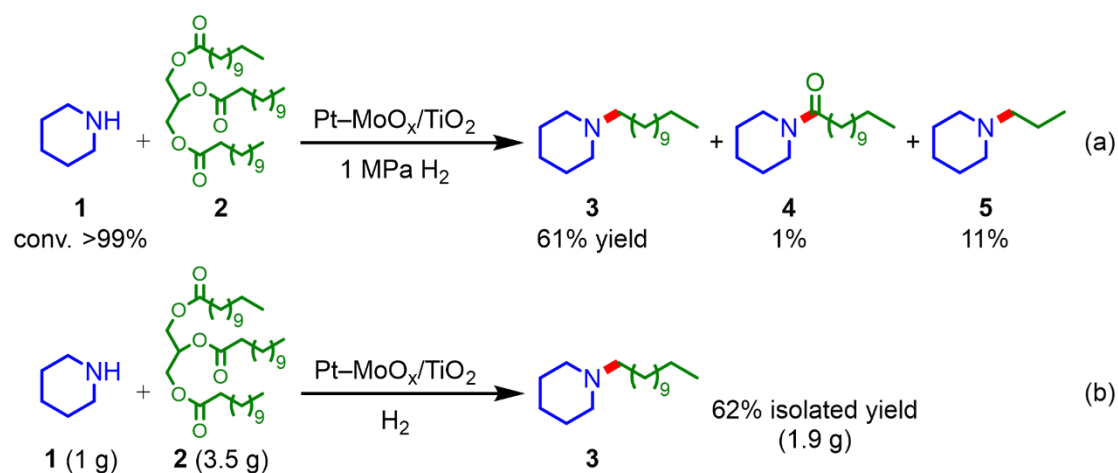
Scheme 3-2 (a) Pt–MoO$_x$/TiO$_2$ catalyzed reductive amination under 1 MPa H$_2$. Reaction conditions: Pt–MoO$_x$/TiO$_2$ (0.15 g, Pt: 7 mol% and Mo: 2 mol%), **1** (1 mmol), **2** (0.5 mmol), *n*-hexane (3 mL), 180 °C, H$_2$ (1 MPa), 60 h. (b) Gram-scale reductive amination. Reaction conditions: Pt–MoO$_x$/TiO$_2$ (1 g, Pt: 4.1 mol% and Mo: 1.2 mol%), **1** (1 g), **2** (3.5 g), *n*-hexane (15 mL), 180 °C, H$_2$ (4 MPa), 60 h.

3.2 Substrate scope

The generality of the Pt–MoO_x/TiO_2 system was investigated using various amines and triglycerides (Table 3-4). Six- and seven-membered cyclic amines (**1** and azepane) were converted into the corresponding tertiary amines (**3** and 1-dodecylazepane) in 70% and 60% yields, respectively (Table 3-4, entries 1 and 2). In the reductive amination using hexylamine, *N*-hexyldodecylamine was obtained in a 35% yield, concomitant with dihexylamine in 11% yield (Table 3-4, entry 3). Dodecylamine was alkylated to didodecylamine in a 70% yield with tridodecylamine formed in a 26% yield as a byproduct (Table 3-4, entry 4). The use of pyridine and aniline resulted in the formation of **3** and *N*-dodecylcyclohexanamine as the major products, along with hydrogenation of the aromatic rings (Table 3-4, entries 5 and 6). Moreover, the reaction under NH_3 gas afforded didodecylamine and tridodecylamine in 74% and 10% yields, respectively (Table 3-4, entry 7). Then, the reductive amination of triglycerides with different carbon chain lengths was tested. Triacetin, tricaprylin, tripalmitin, and tristearin were successfully transformed into their corresponding *N*-alkylated piperidines in over 61% yield (Table 3-4, entries 8–11). The utility of the Pt–MoO_x/TiO_2 catalyst was further investigated using a real cooking oil, because used cooking oil is an attractive carbon source obtained as food waste [13]. The cooking oil, without any pretreatment, was successfully aminated to fatty amines, including 1-hexadecylpiperidine and 1-octadecylpiperidine, in a 65% total yield (Table 3-4, entry 12; the composition of the cooking oil is shown in Table 3-1). These results demonstrated the versatility of the Pt–MoO_x/TiO_2 catalyst.

Table 3-4 Pt–MoO$_x$/TiO$_2$-catalyzed reductive amination of various triglycerides with amines

entry	amine	triglyceride	time (h)	product and yield (%)	
1			16	70%[a]	
2			36	60%[b]	
3			36	35%[a]	11%[a]
4			36	70%[a]	26%[a]
5			24	44%[a]	
6			24	46%[a]	32%[a]
7[c]	NH$_3$		36	74%[a]	10%[a]
8			12	79%[a]	
9			24	62%[d]	

Table 3-4 *(Contd.)*

entry	amine	triglyceride	time (h)	product and yield (%)
10[e]			48	63%[d]
11[e]			48	61%[d]
12[e,f]		cooking oil	48	n = 13 and 15 65%[b]

Reaction conditions: Pt–MoO$_x$/TiO$_2$ (0.15 g, Pt: 7 mol% and Mo: 2 mol%), amine (1 mmol), triglyceride (0.5 mmol), *n*-hexane (3 mL), H$_2$ (4 MPa). Yield was based on amine. [a] GC-FID yield. [b] ^{1}H NMR yield. [c] Pt–MoO$_x$/TiO$_2$ (0.15 g, Pt: 4.8 mol% and Mo: 1.4 mol% with respect to the ester moiety), NH$_3$ (0.7 MPa). Yield was based on **2**. [d] Isolated yield. [e] *n*-Hexane (5 mL). [f] Cooking oil (0.5 g). The oil composition is shown in Table 3-1.

3.3 Reaction pathway

The possible reaction pathways of the Pt–MoO$_x$/TiO$_2$-catalyzed reductive amination were investigated by monitoring the products. The time-course data showed that the yield of 1-dodecanol (**7**) increased to 10% at 6 h and then decreased (Figure 3-3). **4** was also observed in low yields (<4%) throughout the reaction. In addition, various TiO$_2$-supported catalysts and bare TiO$_2$ produced **4** as the major product (Table 3-2, entries 1–11). These results suggested that **7** and **4** could be the potential intermediates in this system. Thus, two reaction pathways were proposed: hydrogenation of triglycerides to aldehydes or alcohols followed by amination (Scheme 3-3a); and amidation of triglycerides and subsequent hydrodeoxygenation of fatty amides (Scheme 3-3b) [9,14,15].

82
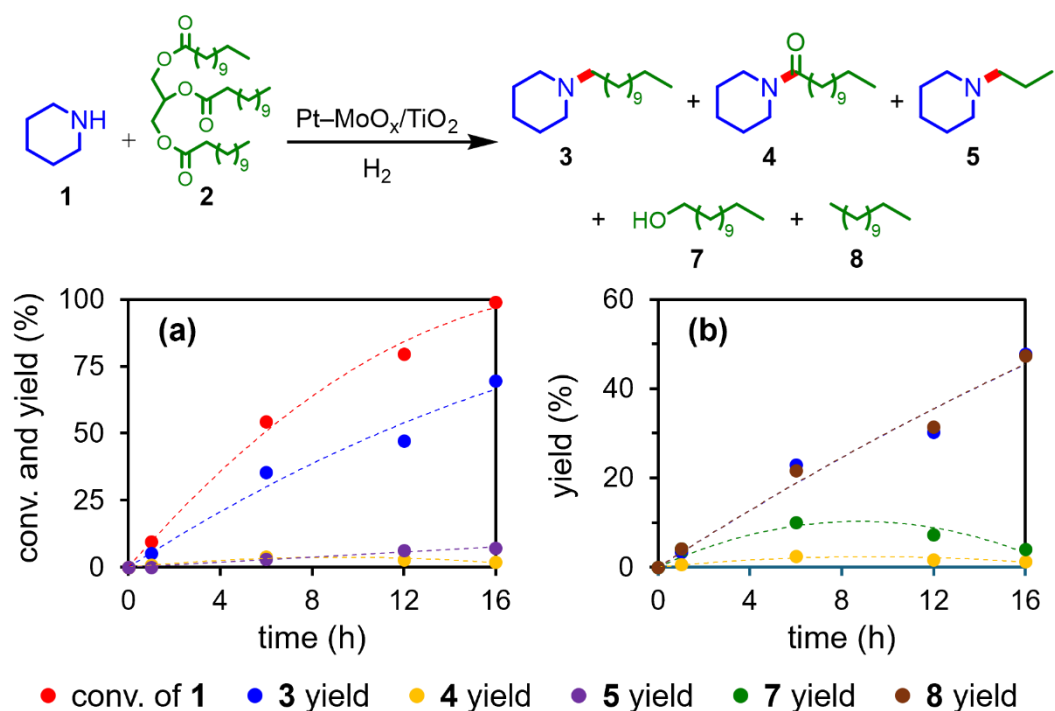
Figure 3-3 Time-course data of the Pt–MoO$_x$/TiO$_2$ catalyzed reductive amination of **2** with **1.** Product distribution was determined based on (a) **1** and (b) **2**. Reaction conditions: Pt–MoO$_x$/TiO$_2$ (0.15 g, Pt: 7 mol% and Mo: 2 mol%), **1** (1 mmol), **2** (0.5 mmol), *n*-hexane (3 mL), H$_2$ (4 MPa).
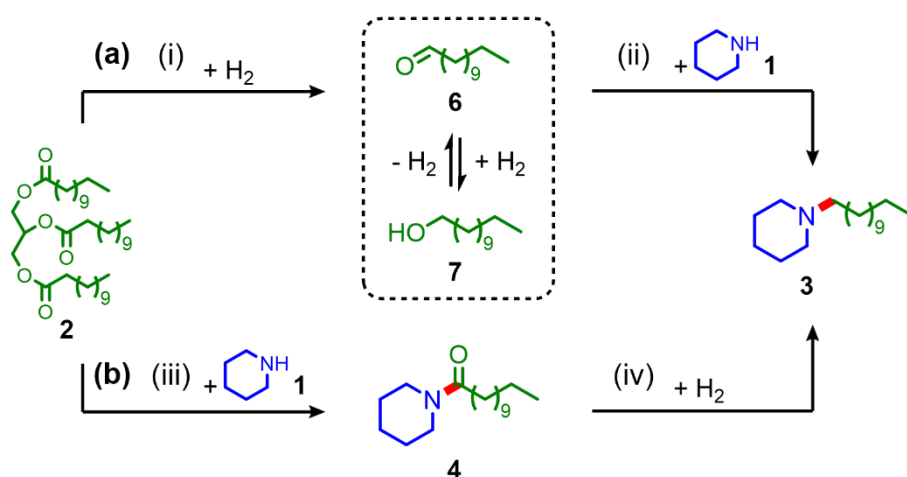
Scheme 3-3 Possible reaction pathways for the Pt–MoO$_x$/TiO$_2$ catalyzed reductive amination.

3.4 Catalysis by Pt–MoO$_x$

To elucidate the reason for the high activity of Pt–MoO$_x$/TiO$_2$, control experiments and characterizations were performed using Pt–MoO$_x$/TiO$_2$, and the results were compared with those of Pt/TiO$_2$ (Figure 3-4). In the hydrogenation of **2** in the absence of amines, Pt–MoO$_x$/TiO$_2$ showed high activity, affording **7** in a 15% yield and *n*-dodecane (**8**) in a 63% yield, whereas Pt/TiO$_2$ showed lower yields (7% and 21%, respectively) compared with Pt–MoO$_x$/TiO$_2$ (Figure 3-4(i)). The hydrodeoxygenation of **4** was facilitated by the Pt–MoO$_x$/TiO$_2$ catalyst, providing **3** in 33% yield, which was much higher than that by Pt/TiO$_2$ (Figure 3-4(iv)). No significant differences in yields were observed in other reaction steps, such as the reductive amination of **6** (Figure 3-4(ii-1)), amination of **7** (Figure 3-4(ii-2)), and amidation of **2** (Figure 3-4(iii)). The above results demonstrated that co-presence of Pt and Mo species is important for promoting hydrogenation of triglycerides and amides more efficiently.

84
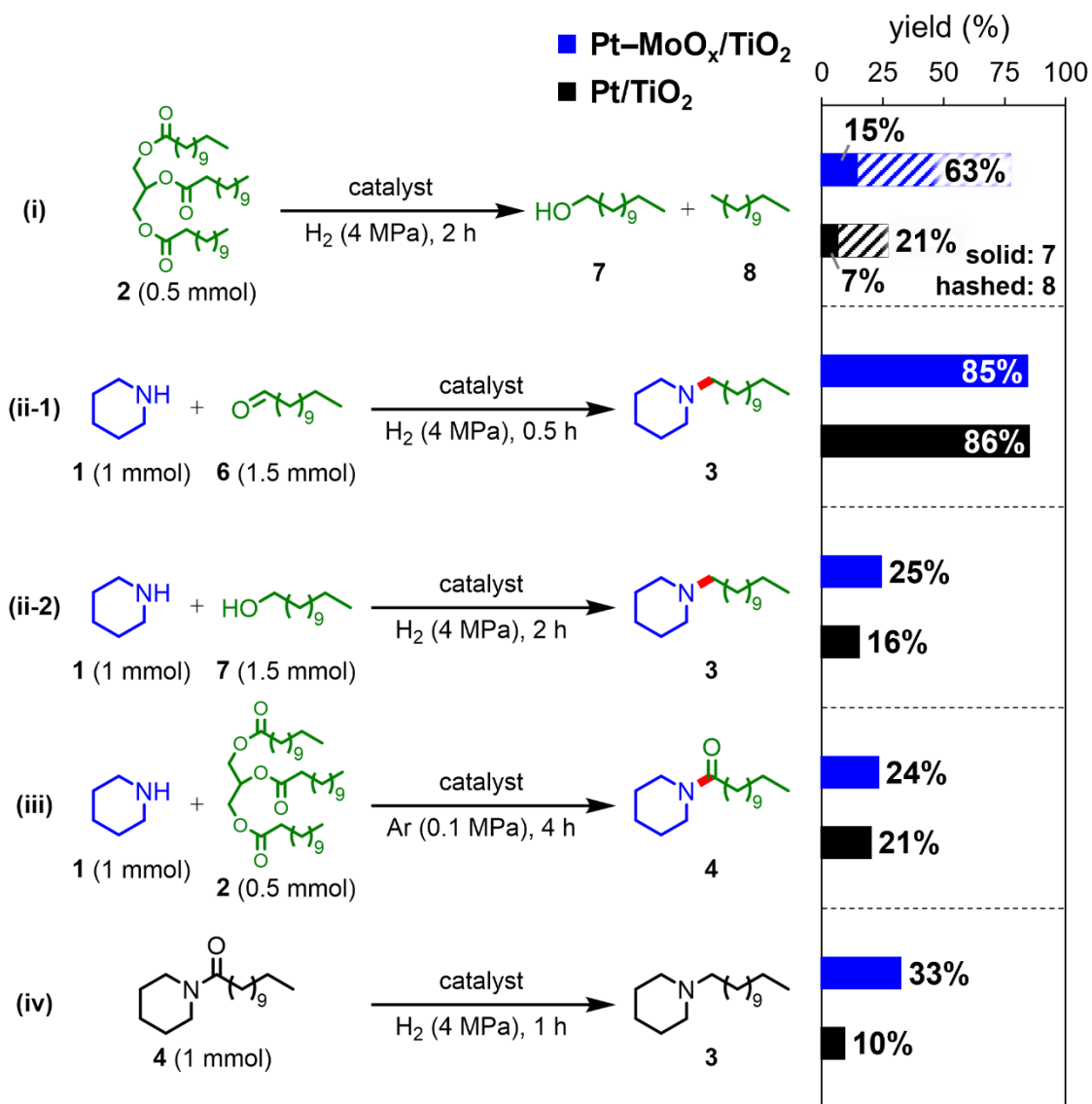
Figure 3-4 Comparison of the activities of Pt–MoO$_x$/TiO$_2$ and Pt/TiO$_2$. Reaction conditions: Pt–MoO$_x$/TiO$_2$ or Pt/TiO$_2$ (0.15 g; Pt: 4.8 mol% and Mo: 1.4 mol% with respect to the ester moiety for (i); Pt: 7 mol% and Mo: 2 mol% for (ii-1), (ii-2), (iii), (iv)), *n*-hexane (3 mL), 180 °C.

The catalyst structure during reductive amination was investigated. TEM images of the used Pt–MoOₓ/TiO₂ and Pt/TiO₂ revealed the presence of platinum nanoparticles (NPs) with mean diameters of 3.5 and 4.2 nm, respectively, on the TiO₂ surface (Figures 3-5a and b). HAADF-STEM image and EDX elemental mapping of used Pt–MoOₓ/TiO₂ revealed a high dispersion of Pt NPs and Mo species on the TiO₂ surface (Figures 3-5c and d). Importantly, EDX line analysis showed co-presence of Pt and Mo (Figures 3-6). In the CO pulse chemisorption analysis, adsorption amount of CO on Pt–MoOₓ/TiO₂ was lower than that of Pt/TiO₂ (Table 3-5), supporting the presence of Mo species on the Pt NPs surface [16].
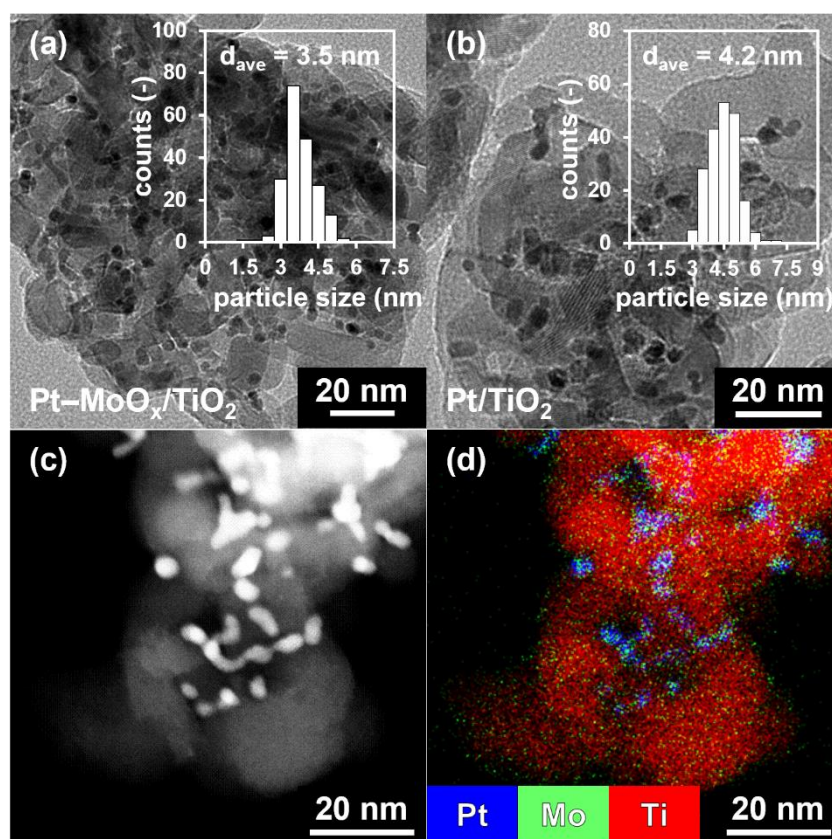
Figure 3-5 TEM image and size distribution histogram (inset) of used (a) Pt–MoOₓ/TiO₂ and (b) Pt/TiO₂. (c) HAADF-STEM image of used Pt–MoOₓ/TiO₂. (d) Composite overlay of the elemental mapping of Pt, Mo, and Ti in used Pt–MoOₓ/TiO₂.
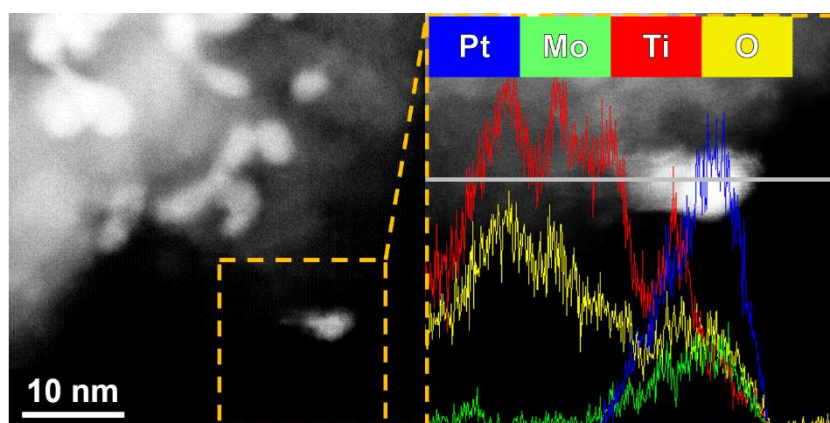
Figure 3-6 EDX line analysis of used Pt–MoO$_x$/TiO$_2$. Line scan was performed across nanoparticles on TiO$_2$ surface, as shown by horizontal gray line.

Table 3-5 Results of CO pulse chemisorption analysis.

sample	adsorption amount (mmol/g)	dispersion
Pt–MoO$_x$/TiO$_2$	0.137	0.272
Pt/TiO$_2$	0.197	0.398

Catalysts were pretreated in 5% H$_2$ in Ar flow at 180 °C before CO pulse injection.

Pt 4f XPS analyses were performed to obtain information on the chemical states of the Pt species in the used Pt–MoO$_x$/TiO$_2$ and Pt/TiO$_2$. The Pt 4f$_{7/2}$ peak of used Pt–MoO$_x$/TiO$_2$ and Pt/TiO$_2$ was observed at 70.6 eV and 70.4 eV, respectively (Figure 3-7a), which can be assigned to Pt^0. These XPS results were consistent with the Pt L_3-edge XANES analysis, in which the white-line intensities of the Pt L_3-edge XANES spectra of the used Pt–MoO$_x$/TiO$_2$ and Pt/TiO$_2$ were similar to that of the Pt foil (Figure 3-7b). Therefore, no obvious changes in the chemical state of the Pt species were observed by Mo loading.

Furthermore, the chemical states of the Mo species in the used Pt–MoO$_x$/TiO$_2$ were evaluated. The absorption edge of the Mo K-edge XANES spectrum of used Pt–MoO$_x$/TiO$_2$ shifted to lower energy compared with that of used MoO$_x$/TiO$_2$, indicating the reduction of Mo species by spillover hydrogen from Pt (Figure 3-7c). The XPS spectrum of the used Pt–MoO$_x$/TiO$_2$ in the Mo 3d region displayed multiple peaks, which were deconvoluted to Mo(0) and molybdenum oxides with valence states ranging from 4+ to 6+ (Figure 3-7d and Table 3-6). These results demonstrated the presence of reduced molybdenum oxides (MoO$_x$) in the used Pt–MoO$_x$/TiO$_2$ catalyst.
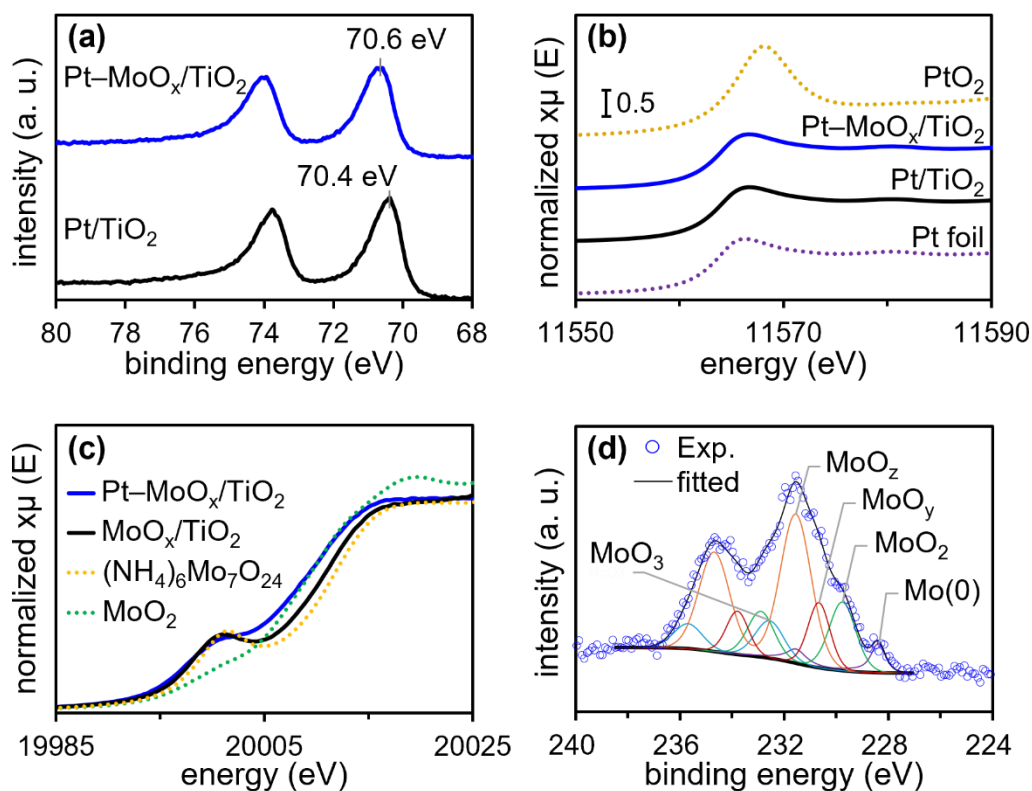
Figure 3-7 (a) XPS spectra in the Pt 4f region of used Pt–MoO$_x$/TiO$_2$ and Pt/TiO$_2$. (b) Pt L_3-edge XANES spectra of PtO$_2$, used Pt–MoO$_x$/TiO$_2$, used Pt/TiO$_2$, and Pt foil. (c) Mo K-edge XANES spectra of used Pt–MoO$_x$/TiO$_2$, used MoO$_x$/TiO$_2$, (NH$_4$)$_6$Mo$_7$O$_{24}$, and MoO$_2$. (d) Mo 3d XPS spectrum of used Pt–MoO$_x$/TiO$_2$.

Table 3-6 The content of Mo species in used Pt–MoO$_x$/TiO$_2$ estimated by Mo 3d XPS spectrum

	binding energy (eV)	ratio (%)
Mo(0)	228.4	5.5
MoO$_2$	229.8	19.2
MoO$_y$	230.7	15.2
MoO$_z$	231.5	48.7
MoO$_3$	232.6	11.4

To investigate the interaction between MoO_x and carbonyl compounds, a TPD-IR study was performed using Pt/TiO_2 and $Pt–MoO_x/TiO_2$ (Figure 3-8). When acetone vapor was introduced into Pt/TiO_2 and $Pt–MoO_x/TiO_2$ at 50 °C, an intense band attributed to the C=O stretching vibration of acetone was observed at approximately 1690 cm^{-1} [17]. As temperature gradually increased from 50 °C, the peak for Pt/TiO_2 decreased in intensity and completely disappeared at 170 °C (Figure 3-8a). In contrast, the spectrum for $Pt–MoO_x/TiO_2$ retained the peak even at 200 °C (Figure 3-8b). These results suggested that the carbonyl moieties of the substrates were strongly adsorbed on the MoO_x sites, which may play key roles in the hydrogenation of triglycerides and amides.
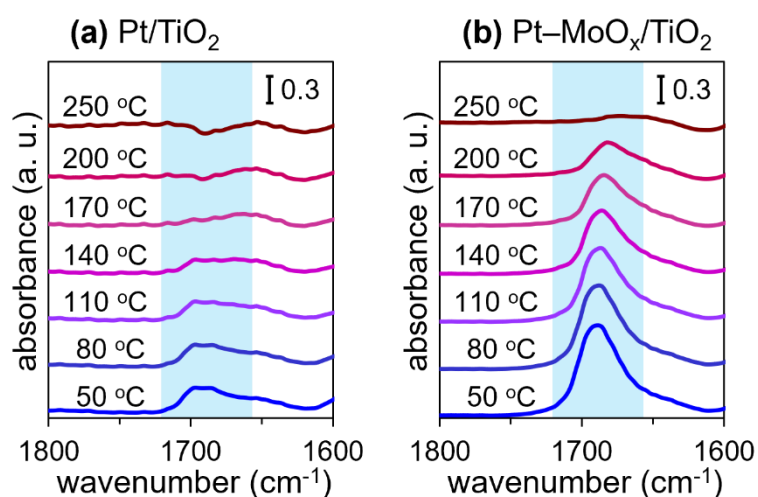
Figure 3-8 TPD-IR spectra of acetone adsorbed on H_2-treated (a) Pt/TiO_2 and (b) $Pt–MoO_x/TiO_2$.

3.5 Support effect

As mentioned previously, the catalytic activity in the reductive amination was strongly affected by the support materials: the Pt–MoO$_x$ catalysts supported on TiO$_2$, ZrO$_2$, and γ-Al$_2$O$_3$ promoted the reductive amination of **2** with **1**, whereas the WO$_3$- and Nb$_2$O$_5$-supported catalysts resulted in low conversions of **1** (Table 3-2, entries 1 and 12–15). Moreover, bare TiO$_2$ showed a high conversion of **1** to produce **4** (Table 3-2, entry 11). These results indicate that the support materials would promote amidation step in Scheme 3-3(iii). To support this consideration, three Pt–MoO$_x$ catalysts, i.e. Pt–MoO$_x$/TiO$_2$, Pt–MoO$_x$/γ-Al$_2$O$_3$, and Pt–MoO$_x$/Nb$_2$O$_5$, were selected and their activities in amidation were evaluated in the absence of H$_2$. Pt–MoO$_x$/TiO$_2$ and Pt–MoO$_x$/γ-Al$_2$O$_3$ provided **4** in 24% and 21% yields, respectively (Table 3-7, entries 1 and 2), whereas Pt–MoO$_x$/Nb$_2$O$_5$ resulted in a 10% yield (Table 3-7, entry 3). NH$_3$-TPD measurements revealed that the acid amounts of Pt–MoO$_x$/TiO$_2$ and Pt–MoO$_x$/γ-Al$_2$O$_3$ calculated by the peak at approximately 200 °C were 130 and 132 μmol/g, respectively, which were much higher than that of Pt–MoO$_x$/Nb$_2$O$_5$ (13 μmol/g; Figure 3-9). It has been reported that acid catalysts facilitate amidation reactions [18]. Hence, the use of support materials with high acid amounts is important to promote amidation, resulting in a high activity in the reductive amination of triglycerides. This result suggested that the pathway including amidation (Scheme 3-3b) is likely to be the major reaction pathway, consistent with the pathway previously reported in the Pt/ZrO$_2$ system [9].

Table 3-7 Amidation of **2** with **1** using Pt–MoO$_x$ catalysts in the absence of H$_2$.

entry	catalyst	conv. of **1** (%)	yield of **4** (%)
1	Pt–MoO$_x$/TiO$_2$	58	24
2	Pt–MoO$_x$/γ-Al$_2$O$_3$	50	21
3	Pt–MoO$_x$/Nb$_2$O$_5$	17	10

Reaction conditions: Pt–MoO$_x$ catalyst (0.15 g; Pt: 7 mol% and Mo: 2 mol%), **1** (1 mmol), **2** (0.5 mmol), *n*-hexane (3 mL), 180 °C, Ar (0.1 MPa), 4 h. Yield was based on **1**. Catalyst was pre-reduced under 4 MPa H$_2$ at 180 °C for 2 h.
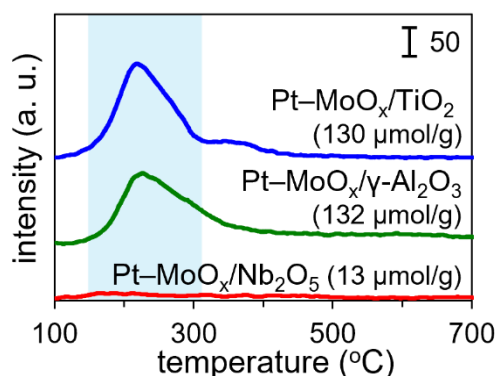
Figure 3-9 NH$_3$-TPD profiles of Pt–MoO$_x$/TiO$_2$, Pt–MoO$_x$/γAl$_2$O$_3$, and Pt–MoO$_x$/Nb$_2$O$_5$. Acid amounts at approximately 200 °C are presented in parentheses. NH$_3$ desorption was monitored by mass number *m/z* = 16 during heating.

3.6 Proposed reaction mechanism

In the time-course data shown in Figure 3-3, **3** was formed without an induction period, and the yield of **4** was low throughout the reductive amination. Moreover, the rates of Pt–MoO$_x$/TiO$_2$-

catalyzed amidation (Figure 3-4(iii)) and hydrodeoxygenation of amide (Figure 3-4(iv)) are calculated to be 0.4 mmol/h·g_{cat} and 2.2 mmol/h·g_{cat}, respectively. These results suggested that the amidation is the rate-determining step in the present catalyst system.

Based on the aforementioned results, a catalyst cycle of the reductive amination of triglycerides was proposed as follows: the carbonyl moiety of triglycerides is activated on the acid site of the TiO_2 surface (Scheme 3-4(I)), followed by attack of amines to form to fatty amides (Scheme 3-4(II)) [18]. H_2 is separated on the Pt NPs [19,20], and the carbonyl moiety of fatty amides is adsorbed and activated on the MoO_x (Scheme 3-4(III)) [21]. Finally, hydrodeoxygenation of adsorbed fatty amides affords desired fatty amines (Scheme 3-4(IV)). Thus, the combination of Pt NPs, MoO_x, and TiO_2 is essential to promote the reductive amination of triglycerides.
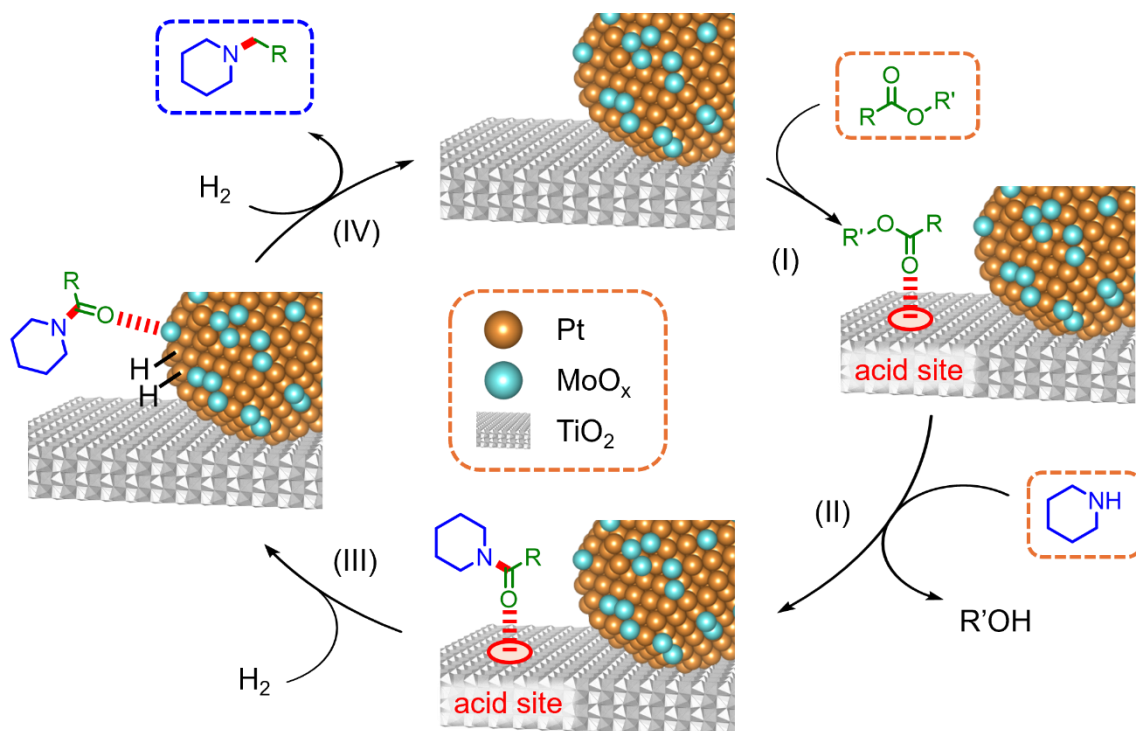
Scheme 3-4 Proposed catalyst cycle for the reductive amination of triglycerides to fatty amines over Pt–MoO_x/TiO_2.

4 Conclusions

The reductive amination of triglycerides to fatty amines was achieved using a Pt–MoO$_x$/TiO$_2$ catalyst under mild reaction conditions, e.g. 1 MPa H$_2$ and 180 °C. The high activity of Pt–MoO$_x$/TiO$_2$ was maintained even after 11 cycles, demonstrating its excellent durability and reusability. A wide range of amines and triglycerides, including cooking oil, was transformed to the corresponding fatty amines in this system. Control experiments and characterizations revealed that the high activity of Pt–MoO$_x$/TiO$_2$ was attributed to the combination of Pt NPs, MoO$_x$, and TiO$_2$, where TiO$_2$ promoted the amidation of triglycerides and Pt–MoO$_x$ species facilitated hydrodeoxygenation of fatty amides to fatty amines.

5 Reference

1. Roose, P.; Eller, K.; Henkes, E.; Rossbacher, R.; Höke, H. *Amines, Aliphatic. Ullmann's Encyclopedia of Industrial Chemistry*; Wiley, 2015.

2. Gonçalves, R. A.; Holmberg, K.; Lindman, B. A Cationic Surfactants: A Review. *J. Mol. Liq.* **2023**, 121335.

3. Corma, A.; Iborra, S.; Velty, A. Chemical Routes for the Transformation of Biomass into Chemicals. *Chem. Rev.* **2007**, *107*, 2411–2502.

4. Foley, P.; Kermanshahi-pour, A.; Beach, E. S.; Zimmerman, J. B. Derivation and Synthesis of Renewable Surfactants. *Chem. Soc. Rev.* **2012**, *41*, 1499–1518.

5. Tietze, L. F. Domino Reactions in Organic Synthesis. *Chem. Rev.* **1996**, *96*, 115–136.

6. Climent, M. J.; Corma, A.; Iborra, S.; Sabater, M. J. Heterogeneous Catalysis for Tandem Reactions. *ACS Catal.* **2014**, *4*, 870–891.

7. Adam, R.; Cabrero-Antonino, J. R.; Junge, K.; Jackstell, R.; Beller, M. Esters, Including Triglycerides, and Hydrogen as Feedstocks for the Ruthenium-Catalyzed Direct N-Alkylation of Amines. *Angew. Chem., Int. Ed.* **2016**, *55*, 11049–11053.

8. Rutzen, H.; Process for the Production of Saturated and/or Unsaturated Aliphatic Amines. DE Pat., 1288595B, 1969.

9. Jamil, M. A. R.; Siddiki, S. M. A. H.; Touchy, A. S.; Rashed, M. N.; Poly, S. S.; Jing, Y.; Ting, K. W.; Toyao, T.; Maeno, Z.; Shimizu, K. Selective Transformations of Triglycerides into Fatty Amines, Amides, and Nitriles by using Heterogeneous Catalysis. *ChemSusChem* **2019**, *12*, 3115–3125.

10. Michniak, B. B.; Player, M. R.; Godwin, D. A.; Lockhart, C. C.; Sowell, J. W. In Vitro Evaluation of Azone Analogs as Dermal Penetration Enhancers: V. Miscellaneous Compounds. *Int. J. Pharm.* **1998**, *161*, 169–178.

11. Wei, F.; Gao, G.-Z.; Wang, X.-F.; Dong, X.-Y.; Li, P.-P.; Hua, W.; Wang, X.; Wu, X.-M.; Chen, H. Quantitative Determination of Oil Content in Small Quantity of Oilseed Rape by Ultrasound-Assisted Extraction Combined with Gas Chromatography. *Ultrason. Sonochem.* **2008**, *15*, 938–942.

12. Yuan, K.; Yamazaki, Y.; Jin, X.; Nozaki, K. Multifunctional WO_3–ZrO_2-Supported Platinum Catalyst for Remarkably Efficient Hydrogenolysis of Esters to Alkanes. *J. Am. Chem. Soc.* **2023**, *145*, 3454–3461.

13. Lin, C. S. K.; Pfaltzgraff, L. A.; Herrero-Davila, L.; Mubofu, E. B.; Abderrahim, S.; Clark, J. H.; Koutinas, A. A.; Kopsahelis, N.; Stamatelatou, K.; Dickson, F.; Thankappan, S.; Mohamed, Z.; Brocklesby, R.; Luque, R. Food Waste as a Valuable Resource for the Production of Chemicals, Materials and Fuels. Current Situation and Global Perspective. *Energy Environ. Sci.* **2013**, *6*, 426–464.

14. Shi, Y.; Kamer, P. C. J.; Cole-Hamilton, D. J.; Harvie, M.; Baxter, E. F.; Lim, K. J. C.; Pogorzelec, P. A New Route to N-Aromatic Heterocycles from the Hydrogenation of Diesters in the Presence of Anilines. *Chem. Sci.* **2017**, *8*, 6911–6917.

15. Shi, Y.; Kamer, P. C. J.; Cole-Hamilton, D. J. A New Route to α,ω-Diamines from Hydrogenation of Dicarboxylic Acids and Their Derivatives in the Presence of Amines. *Green Chem.* **2017**, *19*, 5460–5466.

16. Asano, T.; Nakagawa, Y.; Tamura, M.; Tomishige, K. Structure and Mechanism of Titania-Supported Platinum−Molybdenum Catalyst for Hydrodeoxygenation of 2-Furancarboxylic Acid to Valeric Acid. *ACS Sustainable Chem. Eng.* **2019**, *7*, 9601–9612.

17. Nakamura, Y.; Kon, K.; Touchy, A. S.; Shimizu, K.; Ueda, W. Selective Synthesis of Primary Amines by Reductive Amination of Ketones with Ammonia over Supported Pt catalysts. *ChemCatChem* **2015**, *7*, 921–924.

18. Lundberg, H.; Tinnis, F.; Selander, N.; Adolfsson, H. Catalytic Amide Formation from Non-activated Carboxylic Acids and Amines. *Chem. Soc. Rev.* **2014**, *43*, 2714–2742.

19. Nishimura, S. *Handbook of Heterogeneous Catalytic Hydrogenation for Organic Synthesis*; John Wiley & Sons Inc., 2001.

20. Zhang, L.; Zhou, M.; Wang, A.; Zhang, T. Selective Hydrogenation over Supported Metal Catalysts: From Nanoparticles to Single Atoms. *Chem. Rev.* **2020**, *120*, 683–733.

21. Toyao, T.; Siddiki, S. M. A. H.; Kon, K.; Shimizu, K. The Catalytic Reduction of Carboxylic Acid Derivatives and CO_2 by Metal Nanoparticles on Lewis-Acidic Supports. *Chem. Rec.* **2018**, *18*, 1374–1393.

Chapter IV.

Direct Hydrodeoxygenation of Esters to Unsymmetrical Ethers

over a Pt–MoO$_x$/ZrO$_2$ Catalyst

1   Introduction

Ethers are essential compounds in bulk and fine chemistry, and are widely used in solvents, fuels, fragrances, and pharmaceuticals [1]. Symmetrical ethers are traditionally produced through acid-catalyzed alcohol dehydration [2,3]. For an unsymmetrical ether synthesis, Williamson reaction and Ullmann reaction have been applied for an unsymmetrical ether synthesis, but these techniques generate stoichiometric amounts of salt waste due to the use of inorganic bases, organic halides, and alkoxide substrates [4]. Deoxygenation of the carbonyl oxygen of esters is an attractive approach for unsymmetrical ether synthesis because esters are abundant in nature [5,6]. This reaction had been reported using $LiAlH_4$ or $NaBH_4$ in the presence of BF_3 etherate (Scheme 4-1(Ia)) [7–10]. Hydrosilanes have also been used as reductants in the catalytic reduction of esters to ethers (Scheme 4-1(Ib)) [11–23]. Although these reactions are performed under mild conditions, the waste formations are problematic. From an environmental and atom economy viewpoint, the catalytic conversion of esters to ethers using H_2 as a reductant is attractive, since water is the sole co-product (Scheme 4-1(II)). So far, various homogeneous and heterogeneous catalyst systems, consisting of metal species with acids, have been reported for unsymmetrical ether synthesis from esters [24–32]. However, these methods suffer from requiring excessive amounts of alcohol additive or low selectivity due to the formation of undesired symmetrical ethers. To establish green and sustainable processes, it is crucial to develop efficient catalyst systems for unsymmetrical ether production from esters using H_2.

In this chapter, the author achieved the direct hydrodeoxygenation (HDO) of esters to the corresponding unsymmetrical ethers using a zirconium oxide supported $Pt–MoO_x$ ($Pt–MoO_x/ZrO_2$) catalyst (Scheme 4-1(III)). The catalyst exhibited high activity and selectivity under mild conditions, e.g. 0.5 MPa H_2 and 100 °C. A broad substrate scope including biomass-derived triglyceride was demonstrated.

(I) direct reduction of esters to ethers

(a) hydride reduction

$$R^1-C(=O)-O-R^2 \xrightarrow[\text{BF}_3\cdot\text{Et}_2\text{O}]{\text{hydride reagents}} R^1-CH_2-O-R^2 \;+\; \text{waste}$$

(b) hydrosilylation

$$R^1-C(=O)-O-R^2 \xrightarrow[\text{R}^3\text{SiH, rt–100 °C}]{\text{homogeneous catalysts}} R^1-CH_2-O-R^2 \;+\; \text{siloxane}$$
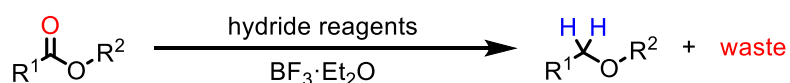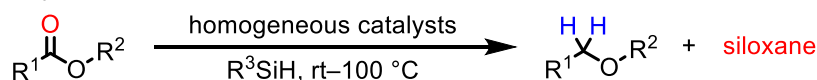
(II) ether synthesis from ester under H$_2$

$$R^1-C(=O)-O-R^2 \;+\; R^2{-}OH \xrightarrow[\text{H}_2\ (4\text{–}6\ \text{MPa}),\ 140\text{–}160\ °C]{\text{catalysts}} R^1-CH_2-O-R^2 \;+\; H_2O$$
●alcohol additive

$$R^1-C(=O)-O-R^2 \xrightarrow[\substack{\text{H}_2\ (5.6\text{–}6.2\ \text{MPa})\\ 103\text{–}200\ °C}]{\text{catalysts}} R^1-CH_2-O-R^2 \;+\; R^1{\sim}O{\sim}R^1 \;+\; R^2{-}O{-}R^2 \;+\; H_2O$$
●low selectivity

(III) present study
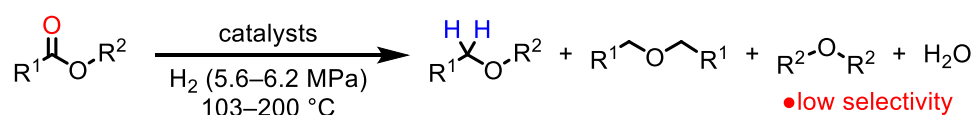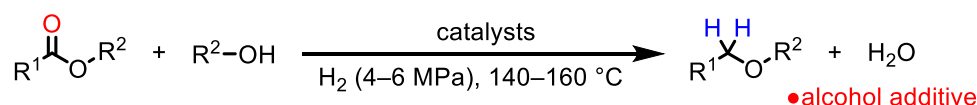
$$R^1-C(=O)-O-R^2 \xrightarrow[\text{H}_2\ (0.1\text{–}0.5\ \text{MPa}),\ 100\ °C]{\text{Pt–MoO}_x/\text{ZrO}_2} R^1-CH_2-O-R^2 \;+\; H_2O$$
●only water byproduct ●no additives ●high selectivity
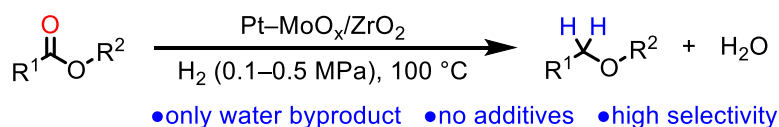
Scheme 4-1 Hydrodeoxygenation of esters to ethers.

2   Experimental section

2.1 General

Organic chemicals were purchased from Fujifilm Wako Pure Chemical Industries, Ltd., Tokyo Chemical Industry Co., Ltd., and Sigma-Aldrich, and were used as received. H_2PtCl_6, $RuCl_3$, K_3RhCl_6, and $Pd(NH_3)_4Cl_2$ hydrates were obtained from N. E. Chemcat. $(NH_4)_6Mo_7O_{24}\cdot4H_2O$, NH_4VO_3, $(NH_4)_{10}(H_2W_{12}O_{42})\cdot4H_2O$, and $NaReO_4$ were purchased from Nacalai Tesque, Kishida Chemical, Sigma-Aldrich, and Alfa Aesar Co., Ltd., respectively. Hydroxyapatite and MoO_3 were purchased from Fujifilm Wako Pure Chemical Industries, Ltd. ZrO_2 (JRC-ZRO-8), TiO_2 (JRC-TIO-2), CeO_2 (JRC-CEO-2), and MgO (JRC-MGO-3 1000A) were supplied by the Catalyst Society of Japan as

reference catalysts. Gas chromatography-mass spectrometry (GC-MS) analyses were performed on a Shimadzu QP-2010SE instrument equipped with a capillary column (InertCap WAX-HT, GL Science, 30 m × 0.25 mm i.d. film thickness 0.25 μm). ^{1}H and ^{13}C nuclear magnetic resonance (NMR) spectra were recorded on a JEOL JNM-ESC400 spectrometer. Chemical shifts are reported as follows: TMS (0 ppm for ^{1}H NMR) and CDCl$_3$ (77.10 ppm for ^{13}C NMR). NMR multiplicities are reported using the following abbreviations: s, singlet; d, doublet; t, triplet; q, quartet; m, multiplet; br, broad; *J*, coupling constants in hertz. High-resolution mass spectra (HRMS) were recorded on a JEOL JMS700 spectrometer. Transmission electron microscopy (TEM) images were obtained using Hitachi HF-2000 microscope or FEI Tecnai G2 20ST. Powder X-ray diffraction (XRD) patterns were acquired using a Philips XPert-MPD instrument with Cu-Kα radiation. Pt *L*$_3$-edge and Mo *K*-edge X-ray absorption near-edge structure (XANES) analyses were performed at room temperature in transmittance mode using Si (311) monochromators at the 14B2 and 01B1 beamline stations at SPring-8, Japan Atomic Energy Research Institute (JASRI), Harima, Japan (promotion numbers: 2019B1858, 2020A1487, and 2021A1647). Data analysis was performed using the Demeter ver. 0.9.21. Inductively coupled plasma-atomic emission spectroscopy (ICP-AES) was performed using a Perkin Elmer Optima 8300 instrument. Fourier-transform infrared (FT-IR) spectra were recorded on a JASCO FT-IR 4100 spectrometer equipped with a mercury cadmium telluride detector. The single-point Brunauer–Emmett–Teller (BET) method and CO pulse chemisorption was measured using a BELCAT-A instrument (BEL Japan Inc.).

2.2 Preparation of Pt–MoO$_x$/ZrO$_2$ catalyst

The Pt–MoO$_x$/ZrO$_2$ catalyst was prepared using a sequential impregnation method. An aqueous solution of (NH$_4$)$_6$Mo$_7$O$_{24}$·4H$_2$O (0.0066 g) and ZrO$_2$ (1.500 g) was added to distilled water (50 mL) at room temperature. After stirring for 12 h in air, water was removed by rotary evaporation under

reduced pressure, and the resulting powder was dried at 110 °C for 5 h. After drying, the product and an aqueous solution of H_2PtCl_6 (2.00 mL, 100 mM) was added to distilled water (50 mL) at room temperature and stirred for 12 h. Then, water was removed by rotary evaporation and the resulting powder was dried at 110 °C for 5 h. Finally, the obtained powder was calcined at 500 °C for 3 h under a static air atmosphere to obtain $Pt–MoO_x/ZrO_2$ as a gray powder. As determined by ICP-AES, the Pt and Mo contents in $Pt–MoO_x/ZrO_2$ were 2.45 and 0.24 wt%, respectively. The other catalysts were prepared in a similar manner using various metal salts and supports, with the loading amounts of platinum group metal and metal oxide adjusted to 6.0 and 1.13 $\mu mol/m^2$, respectively. The specific surface areas and amounts of each support are summarized in Table 4-1. All catalysts were applied to the reaction without any pre-reduction steps.

Table 4-1 Specific surface area and the amount of support.

sample	SSA $[m^2/g]^a$	$W_{support}$ $[g]^b$	$W_{catalyst}$ $[g]^c$
ZrO_2 (JRC-ZRO-8)	22.1	1.50	0.150
TiO_2 (JRC-TIO-2)	18	1.80	0.180
hydroxyapatite	59.0^d	0.56	0.060
CeO_2 (JRC-CEO-2)	123.1	0.27	0.031
MgO (JRC-MGO-3 1000A)	13–19	2.07	0.207

^{a} Specific surface area. The data was obtained from the Catalysis Society of Japan. ^{b} The weight of support material used for the catalyst preparation. ^{c} The weight of catalyst used for the reaction in Table 4-2. ^{d} Measured by the single point BET method.

2.3 Typical HDO reaction procedure

The reaction with cyclohexyl acetate (**1**) was carried out in a 50 mL stainless steel autoclave

equipped with a Teflon vessel. The vessel was charged with **1** (1 mmol), Pt–MoO$_x$/ZrO$_2$ (0.150 g), *n*-hexane (3 mL), and a Teflon-coated magnetic stir bar. The reactor was sealed, purged five times with 0.5 MPa H$_2$, pressurized (0.5 MPa), heated to 100 °C, and stirred at 900 rpm for 4 h. After the reaction, the autoclave was cooled in an ice-water bath, and H$_2$ gas was released. The resulting reaction mixture was diluted with ethyl acetate and analysed by GC-MS.

Product yields were calculated by the following equation based on **1**:

$$\textbf{2} \text{ yield (based on } \textbf{1}) = \frac{\text{amount of } \textbf{3} \text{ (mmol)}}{\text{amount of loaded } \textbf{1} \text{ (mmol)}} \times 100 \qquad \text{(eq. 4-1)}$$

2.4 Catalyst reuse experiment

After the HDO reaction was complete, the catalyst was recovered from the reaction mixture by centrifugation, washed with ethyl acetate, and dried at 110 °C for 3 h in air. The recovered Pt–MoO$_x$/ZrO$_2$ catalyst was calcined under a flow of O$_2$ (50 sccm) at 300 °C for 20 min before being reused in a subsequent reaction.

2.5 HDO under atmospheric H$_2$ pressure

The HDO under reaction atmospheric H$_2$ pressure was carried out in a 50 mL stainless steel autoclave equipped with a Teflon vessel. The vessel was charged with **1** (0.25 mmol), Pt–MoO$_x$/ZrO$_2$ (0.0375 g), *n*-hexane (0.8 mL), and a Teflon-coated magnetic stir bar. The reactor was sealed, purged five times with 0.5 MPa H$_2$, pressurized (0.1 MPa), heated to 100 °C, and stirred at 900 rpm for 4 h. After the reaction, the autoclave was cooled in an ice-water bath, and H$_2$ gas was released. The resulting reaction mixture was diluted with ethyl acetate and analysed by GC-MS.

2.6 Gram-scale reaction

The gram-scale HDO of ethyl stearate was carried out in a 100 mL stainless steel autoclave equipped with a Teflon vessel. The vessel was charged with ethyl stearate (3.00 g, 9.6 mmol), Pt–MoO$_x$/ZrO$_2$ (0.300 g), and n-hexane (10 mL), and a Teflon-coated magnetic stir bar. The reactor was purged five times with 1.0 MPa H$_2$ and then pressurized to 3.0 MPa at room temperature, heated to 100 °C, and stirred at 900 rpm for 72 h. After the reaction, the autoclave was cooled in an ice-water bath, and the hydrogen gas was carefully released. Pt–MoO$_x$/ZrO$_2$ was separated by centrifugation, and n-hexane was evaporated. The residue was purified by silica gel chromatography with hexane/diethyl ether to give ethyl octadecyl ether (1.9 g, 6.2 mmol, 65%).

The turnover number (TON) based on surface Pt atoms was described by the following equation:

$$\text{TON} = \frac{\text{mole of product}}{W_{\text{catalyst}} \times \frac{\text{Pt loading}}{\text{atomic weight of Pt}} \times \text{dispersion}} \qquad (\text{eq. 4-2})$$

W_{catalyst}: the gram of catalyst used in the HDO

Pt loading: the loading amount of Pt measured by ICP-AES analysis (2.45 wt%)

dispersion: Pt dispersion measured by CO pulse chemisorption analysis (63.4%)

2.7 FT-IR measurements

A thin disk of the sample was prepared by pressing the sample powder with KBr onto a stainless-steel grid. The sample disk was then placed inside an IR cell to enable thermal treatment in a controlled atmosphere. The sample pellet was treated under vacuum at 100 °C for 1 h and pre-reduced under 1 bar of H$_2$ at 100 °C for 1 h and then outgassed. Then, the sample was treated with vaporized ethyl butyrate (13 mbar) at 100 °C for 5 min. FT-IR spectra were recorded after the desorption of physisorbed or weakly chemisorbed species under vacuum at 100 °C.

2.8 Product identification
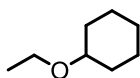
Cyclohexyl ethyl ether

CAS registry No. [932-92-3]. **¹H NMR** (400 MHz, CDCl₃): δ/ppm 3.51 (q, 2H, *J* = 6.8 Hz), 3.22 (m, 1H), 1.92 (m, 2H), 1.73 (m, 2H), 1.54 (m, 1H), 1.30–1.17 (m, 8H). **¹³C NMR** (100 MHz, CDCl₃): δ/ppm 77.4, 63.0, 32.5, 25.9, 24.4, 15.8.

Ethyl hexyl ether

CAS registry No. [5756-43-4]. **¹H NMR** (400 MHz, CDCl₃): δ/ppm 3.46 (q, 2H, *J* = 7.2 Hz), 3.40 (t, 2H, *J* = 6.8 Hz), 1.57 (m, 2H), 1.38–1.25 (m, 6H), 1.20 (t, 3H, *J* = 6.8 Hz), 0.89 (t, 3H, *J* = 6.8 Hz). **¹³C NMR** (100 MHz, CDCl₃): δ/ppm 70.9, 66.1, 31.8, 29.9, 26.0, 22.7, 15.3, 14.1.
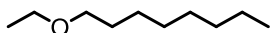
Ethyl octyl ether

CAS registry No. [929-61-3]. **¹H NMR** (400 MHz, CDCl₃): δ/ppm 3.46 (q, 2H, *J* = 7.2 Hz), 3.40 (t, 2H, *J* = 6.8 Hz), 1.57 (m, 2H), 1.37–1.27 (m, 10H), 1.20 (t, 3H, *J* = 7.2 Hz), 0.88 (t, 3H, *J* = 6.4 Hz). **¹³C NMR** (100 MHz, CDCl₃): δ/ppm 70.9, 66.1, 31.9, 29.9, 29.6, 29.4, 26.3, 22.7, 15.3, 14.2.
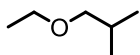
Ethyl isobutyl ether

CAS registry No. [627-02-1]. **¹H NMR** (400 MHz, CDCl₃): δ/ppm 3.46 (q, 2H, *J* = 6.8 Hz), 3.17 (d, 2H, *J* = 6.8 Hz), 1.90–1.80 (m, 1H), 1.20 (t, 3H, *J* = 7.2 Hz), 0.90 (d, 6H, *J* = 6.8 Hz). **¹³C NMR** (100 MHz, CDCl₃): δ/ppm 77.7, 66.3, 28.5, 19.5, 15.3.
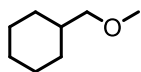
Cyclohexylmethyl methyl ether

CAS registry No. [19752-94-4]. **¹H NMR** (400 MHz, CDCl₃): δ/ppm 3.32 (s, 3H), 3.18 (d, 2H, $J = 6.4$ Hz), 1.80–1.51 (m, 6H), 1.30–1.10 (m, 3H), 0.98–0.86 (m, 2H). **¹³C NMR** (100 MHz, CDCl₃): δ/ppm 79.0, 58.9, 38.1, 30.1, 26.7, 26.0.
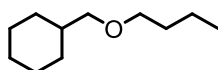
Butyl cyclohexylmethyl ether

CAS registry No. [60784-60-3]. **¹H NMR** (400 MHz, CDCl₃): δ/ppm 3.39 (t, 2H, $J = 6.4$ Hz), 3.19 (d, 2H, $J = 6.4$ Hz), 1.77–1.61 (m, 5H), 1.60–1.51 (m, 3H), 1.41–1.32 (m, 2H), 1.29–1.10 (m, 3H), 0.92 (m, 5H). **¹³C NMR** (100 MHz, CDCl₃): δ/ppm 76.9, 70.9, 38.2, 31.9, 30.3, 26.8, 26.0, 19.5, 14.0.
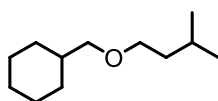
Cyclohexylmethyl isoamyl ether

CAS registry No. [2762677-10-9]. **¹H NMR** (400 MHz, CDCl₃): δ/ppm 3.41 (t, 2H, $J = 6.8$ Hz), 3.19 (d, 2H, $J = 6.4$ Hz), 1.77–1.65 (m, 6H), 1.60–1.51 (m, 1H), 1.45 (q, 2H, $J = 6.8$ Hz), 1.30–1.10 (m, 3H), 0.98–0.87 (m, 8H). **¹³C NMR** (100 MHz, CDCl₃): δ/ppm 77.0, 69.6, 38.7, 38.2, 30.3, 26.8, 26.0, 25.2, 22.7. **HRMS** (EI) [M+H]⁺ calcd.: 184.1828, found: 184.1834. **GC-MS** (EI): m/z (rel. Int, %): 43.05 (72.20), 55.05 (73.78), 70.10 (100.00), 71.10 (72.82), 81.10 (44.06), 97.15 (59.09), 113.10 (0.57), 127.15 (1.77), 141.20 (0.35), 184.20 (0.09).
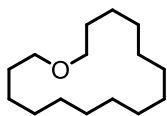
Oxacyclohexadecane

CAS registry No. [295-67-0]. **^{1}H NMR** (400 MHz, CDCl$_3$): δ/ppm 3.43 (t, 4H, J = 5.6 Hz), 1.58–1.52 (m, 4H), 1.48–1.41 (m, 4H), 1.25–1.38 (m, 18H). **^{13}C NMR** (100 MHz, CDCl$_3$): δ/ppm 70.0, 29.3, 27.4, 27.3, 26.6, 26.33, 26.31, 25.4.
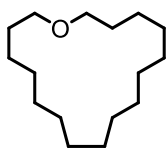
Oxacycloheptadecane

CAS registry No. [295-99-8]. **^{1}H NMR** (400 MHz, CDCl$_3$): δ/ppm 3.43 (t, 4H, J = 5.6 Hz), 1.55 (m, 4H), 1.26–1.46 (m, 24H). **^{13}C NMR** (100 MHz, CDCl$_3$): δ/ppm 70.4, 29.7, 28.3, 28.1, 27.3, 27.21, 27.16, 26.0.
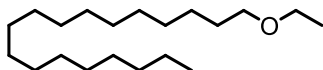
Ethyl octadecyl ether

CAS registry No. [62435-06-7]. **^{1}H NMR** (400 MHz, CDCl$_3$): δ/ppm 3.46 (q, 2H, J = 6.8 Hz), 3.40 (t, 2H, J = 6.8 Hz), 1.57 (m, 2H), 1.37–1.18 (m, 33H), 0.88 (t, 3H, J = 6.4 Hz). **^{13}C NMR** (100 MHz, CDCl$_3$): δ/ppm 70.9, 66.1, 32.0, 29.9, 29.80, 29.76, 29.7, 29.6, 29.5, 26.3, 22.8, 15.3, 14.2.
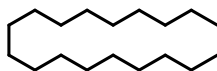
Octadecane

CAS registry No. [593-45-3]. **^{1}H NMR** (400 MHz, CDCl$_3$): δ/ppm 1.33–1.21 (m, 32H), 0.88 (t, 6H, J = 6.8 Hz). **^{13}C NMR** (100 MHz, CDCl$_3$): δ/ppm 32.0, 29.80, 29.76, 29.5, 22.8, 14.2.
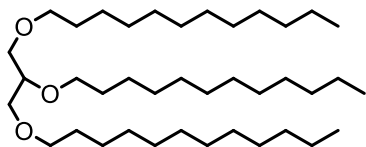
Tridodecyl glyceryl ether

CAS registry No. [37639-50-2]. **¹H NMR** (400 MHz, CDCl₃): δ/ppm 3.58–3.38 (m, 11H), 1.62–1.52 (m, 6H), 1.37–1.18 (m, 54H), 0.88 (t, 9H, J = 6.8 Hz). **¹³C NMR** (100 MHz, CDCl₃): δ/ppm 78.0, 71.7, 70.9, 70.7, 32.0, 30.2, 29.8, 29.7, 29.6, 29.5, 26.23, 26.19, 22.8, 14.2. **GC-MS** (EI): m/z (rel. Int, %): 43.05 (41.81), 57.05 (100.00), 71.05 (67.63), 85.05 (52.80), 99.05 (26.68), 113.10 (18.65), 127.10 (7.30), 169.10 (18.37), 197.10 (25.53), 224.10 (6.26), 226.10 (7.26), 229.10 (6.32), 241.10 (6.58), 245.15 (4.14), 396.25 (6.47), 410.25 (1.72), 597.40 (0.12).
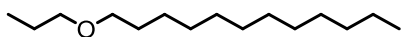
Dodecyl propyl ether

CAS registry No. [53685-79-3]. **¹H NMR** (400 MHz, CDCl₃): δ/ppm 3.41–3.34 (m, 4H), 1.64–1.53 (m, 4H), 1.36–1.25 (m, 18H), 0.94–0.86 (m, 6H). **¹³C NMR** (100 MHz, CDCl₃): δ/ppm 72.6, 71.0, 32.0, 31.7, 29.9, 29.8, 29.73, 29.71, 29.6, 29.4, 26.3, 23.0, 22.8, 14.2, 10.7. **GC-MS** (EI): m/z (rel. Int, %): 29.00 (13.49), 43.00 (100.00), 57.05 (49.39), 69.05 (23.35), 71.05 (24.38), 72.10 (1.54), 73.05 (19.49), 83.05 (26.89), 97.05 (21.49), 111.10 (14.12), 125.10 (4.58), 140.10 (4.86), 168.10 (7.38), 169.10 (1.07), 185.10 (0.20), 199.10 (0.35), 229.15 (0.05).

3　Result and discussion

3.1　Catalyst performance in the HDO of esters

　　Various bifunctional catalysts consisting of metal nanoparticle and metal oxides were prepared using the sequential impregnation method. The catalyst activity was evaluated in the HDO of cyclohexyl acetate (**1**) to cyclohexyl ethyl ether (**2**) under 0.5 MPa H_2 at 100 °C for 4 h using *n*-hexane as a solvent (Table 4-2). The Pt–MoO_x/ZrO_2 catalyst demonstrated the high activity and selectivity, providing **2** in 70% yield with 23% yield of cyclohexane (**4**) as a byproduct (Table 4-2, entry 1). Pt–MoO_x/ZrO_2 was operated even under atmospheric pressure of H_2, affording **2** in a 57% yield (Scheme 4-2). Other bifunctional catalysts based on platinum-group metals (Rh, Pd, and Ru) with MoO_x hardly promoted the HDO under 0.5 MPa H_2 (Table 4-2, entries 2–4). The combination of Pt with metal oxides, such as ReO_x, WO_x, and VO_x, resulted in low conversion (Table 4-2, entries 5–7). Support materials are also important for the HDO; although the Pt–MoO_x/TiO_2 catalyst exhibited a high activity, its selectivity for **2** was inferior to that of Pt–MoO_x/ZrO_2 (Table 4-2, entry 8). Pt–MoO_x/hydroxyapatite showed low activity compared with that of Pt–MoO_x/TiO_2 and Pt–MoO_x/ZrO_2 (Table 4-2, entry 9). Pt–MoO_x/CeO_2 and Pt–MoO_x/MgO were ineffective for the HDO (Table 4-2, entries 10 and 11). Furthermore, Pt/MoO_3, Pt/ZrO_2, and MoO_x/ZrO_2 catalysts were tested for the HDO, resulting in low yields of **2** (Table 4-2, entries 12–14). A physical mixture of Pt/ZrO_2 and MoO_x/ZrO_2 provided **2** in lower yield than that of Pt–MoO_x/ZrO_2 (Table 4-2, entry 15). These results clearly demonstrate that the co-presence of Pt and MoO_x on the ZrO_2 support is essential for the efficient HDO of esters to unsymmetrical ethers.

Table 4-2. Hydrodeoxygenation (HDO) of **1** to **2** using various heterogeneous catalysts.
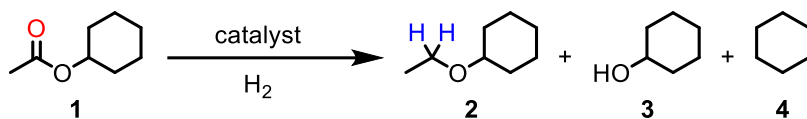
entry	catalyst	conv. of **1** (%)	yield (%)		
			2	**3**	**4**
1[a]	Pt–MoO$_x$/ZrO$_2$	97	70	0	23
2	Ru–MoO$_x$/ZrO$_2$	2	0	2	0
3	Rh–MoO$_x$/ZrO$_2$	2	0	2	0
4	Pd–MoO$_x$/ZrO$_2$	2	0	2	0
5	Pt–ReO$_x$/ZrO$_2$	10	6	4	1
6	Pt–WO$_x$/ZrO$_2$	9	1	6	1
7	Pt–VO$_x$/ZrO$_2$	5	0	5	0
8	Pt–MoO$_x$/TiO$_2$	87	52	<1	28
9	Pt–MoO$_x$/hydroxyapatite	30	19	1	10
10	Pt–MoO$_x$/CeO$_2$	4	1	2	1
11	Pt–MoO$_x$/MgO	3	0	3	0
12	Pt/MoO$_3$	16	3	3	10
13	Pt/ZrO$_2$	8	2	4	2
14	MoO$_x$/ZrO$_2$	2	0	2	0
15	Pt/ZrO$_2$ + MoO$_x$/ZrO$_2$	30	21	5	4

Reaction conditions: catalyst (0.15 g, Pt: 2 mol% and Mo: 0.375 mol%), **1** (1 mmol), *n*-hexane (3 mL), 100 °C, H$_2$ (0.5 MPa), 4 h. Conversion and yield were determined by GC-MS using an internal standard for analysis. [a] Ethane was detected in GC-MS analysis of gas phase.
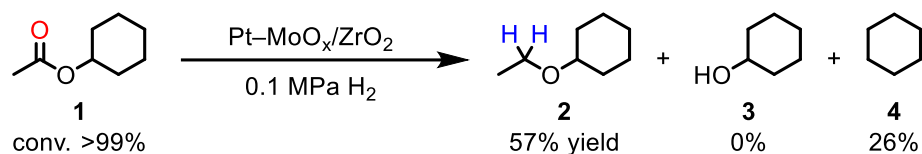
Scheme 4-2 Pt–MoO$_x$/ZrO$_2$ catalyzed HDO under H$_2$ at atmospheric pressure. Reaction conditions: Pt–MoO$_x$/ZrO$_2$ (0.0375 g, Pt: 2 mol% and Mo: 0.375 mol%), **1** (0.25 mmol), *n*-hexane (0.8 mL), 100 °C, H$_2$ (0.1 MPa), 8 h.

The solvents used in the HDO were also investigated. Among the tested solvents, high yields of **2** were obtained with non-polar solvents, such as *n*-hexane and *n*-dodecane (Table 4-3, entries 1 and 2). In contrast, polar solvents, such as tetrahydrofuran, ethanol, 2-propanol, and water, were ineffective for the HDO, maybe due to the competitive adsorption of esters and solvents on the active sites (Table 4-3, entries 3–6).

Table 4-3 HDO of **1** to **2** using Pt–MoO$_x$/ZrO$_2$ in various solvents.

entry	solvent	conv. of **1** (%)	yield (%)		
			2	**3**	**4**
1	*n*-hexane	97	70	0	23
2	*n*-dodecane	>99	62	0	30
3	2-propanol	59	31	24	2
4	ethanol	22	12	7	0
5	water	8	0	3	0
6	tetrahydrofuran	<1	0	0	0

Reaction conditions: Pt–MoO$_x$/ZrO$_2$ (0.15 g, Pt: 2 mol% and Mo: 0.375 mol%), **1** (1 mmol), *n*-hexane (3 mL), 100 °C, H$_2$ (0.5 MPa), 4 h. Conversion and yield were determined by GC-MS using an internal standard for analysis.

After the HDO, the Pt–MoO$_x$/ZrO$_2$ catalyst could be recovered from the reaction mixture by centrifugation and reused without a significant loss in activity or selectivity (Scheme 4-3). ICP-AES analysis revealed that the Pt and Mo loading amounts in the fresh and used Pt–MoO$_x$/ZrO$_2$ were almost constant (Table 4-4), indicating that leaching of Pt and Mo during the HDO reaction was negligible. In addition, a hot filtration experiment was conducted. After the reaction for 1 h, the Pt–MoO$_x$/ZrO$_2$ catalyst was removed by filtration, and the reaction was continued for a further 3 h under the same reaction conditions without Pt–MoO$_x$/ZrO$_2$ (Figure 4-1). The conversion and yield were nearly constant, confirming that the HDO occurred on the catalyst surface. These results clearly demonstrate that the Pt and Mo species were strongly immobilized on the ZrO$_2$ support, and Pt–MoO$_x$/ZrO$_2$ promoted the HDO of esters as a heterogeneous catalyst.
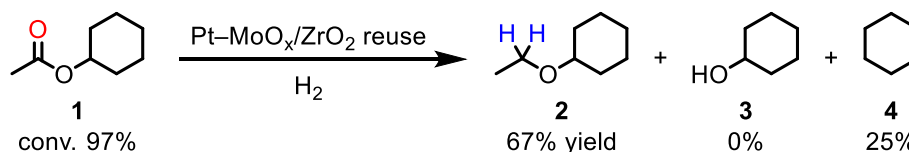
Scheme 4-3 Reusability of Pt–MoO$_x$/ZrO$_2$. Reaction conditions: Pt–MoO$_x$/ZrO$_2$ (0.15 g, Pt: 2 mol% and Mo: 0.375 mol%), **1** (1 mmol), *n*-hexane (3 mL), 100 °C, H$_2$ (0.5 MPa), 4 h.

Table 4-4 ICP-AES analysis of fresh and used Pt–MoO$_x$/ZrO$_2$.

sample	amount (wt%)		atomic ratio
	Pt	Mo	Mo/Pt
fresh Pt–MoO$_x$/TiO$_2$	2.45	0.24	0.098
used Pt–MoO$_x$/TiO$_2$	2.36	0.24	0.102
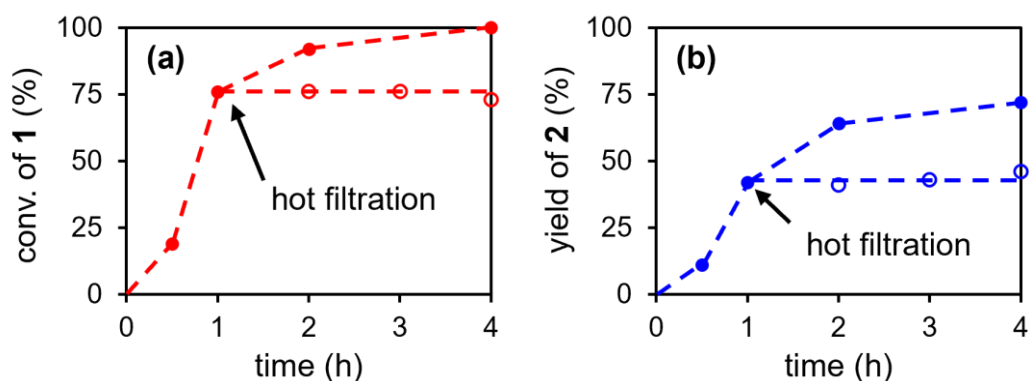
Figure 4-1 (a) Conversion and (b) yield in the hot filtration test of Pt–MoO$_x$/ZrO$_2$ in the HDO of **1** to **2**. (blue circles) without catalyst filtration, and (red circles) with catalyst removal by hot filtration after 1 h. Reaction conditions: Pt–MoO$_x$/ZrO$_2$ (0.15 g), **1** (1 mmol), *n*-hexane (3 mL), H$_2$ (0.5 MPa), 100 °C.

3.2 Substrate scope

The generality of Pt–MoO$_x$/ZrO$_2$ in the HDO was investigated using various esters (Table 4-5). Linear and branched alkyl acetate esters, including cyclohexyl, butyl, hexyl, octyl, isobutyl, and *sec*-butyl acetate, were converted to the corresponding alkyl ethyl ethers in over 57% yield (Table 4-5, entries 1–6). The HDO of esters with different carbon chain length of acyl part afforded the desired unsymmetrical ethers in around 74% yields (Table 4-5, entries 7–9). Hexyl hexanoate was converted to dihexyl ether in a 71 yield (Table 4-5, entry 10). Hexyl formate was unfavorable for the Pt–MoO$_x$/ZrO$_2$ system (Table 4-5, entry 11). Notably, higher yields were obtained in the HDO of bulkier esters: isopropyl 2-methyl butyrate and isopropyl cyclohexanecarboxylate were efficiently transformed into their corresponding ethers in 86% and 95% yields, respectively (Table 4-5, entries 12 and 13). *tert*-Butyl acetate and vinyl pivalate were hardly hydrodeoxygenated (Table 4-5, entries 14 and 15). The HDO of methyl esters required high H$_2$ pressure and temperature (5 MPa and 140 °C), probably due to poisoning of the Pt surface by CO formed during the reaction (Table 4-5, entries 16 and 17) [33]. Alkyl benzoates were converted to unsymmetrical ethers along with hydrogenation of the aromatic rings (Table 4-5, entries 18–20). HDO of δ-valerolactone resulted in 4% yield of desired

cyclic ether, and 1-pentanol and pentylpentanoate were produced in 26% and 12% yields, respectively (Table 4-5, entry 21). Macrocyclic lactones, such as exaltolide and cyclohexadecanolide, were successfully converted to macrocyclic ethers (Table 4-5, entries 22 and 23).

The versatility of the Pt–MoO$_x$/ZrO$_2$ catalyst system was further investigated for the HDO of biomass-derived esters. Fatty acid methyl esters, which are commonly used as biodiesel, could be degraded by the hydrolysis of the ester moieties [34]. The HDO of methyl stearate and ethyl stearate afforded methyl octadecyl ether in 76% yield and ethyl octadecyl ether in 87% yield, respectively (Table 4-5, entries 24 and 25), which could be potential biomass-derived fuels with enhanced hydrolytic stability. Moreover, the Pt–MoO$_x$/ZrO$_2$ catalyst was successfully applied to the gram-scale HDO. Using 3.0 g of ethyl stearate, 1.9 g of ethyl octadecyl ether was obtained in a 65% isolated yield with 0.65 g of octadecane in a 27% yield (Scheme 4-4a). The TON for ethyl octadecyl ether based on surface Pt atoms reached 260. Furthermore, trilaurin, found in coconut oil, was transformed into tridodecyl glyceryl ether in a 51% isolated yield (Scheme 4-4b). These results clearly demonstrate the high applicability of the Pt–MoO$_x$/ZrO$_2$ system to produce unsymmetrical ethers from esters.

Table 4-5 HDO of various esters using Pt–MoO$_x$/ZrO$_2$

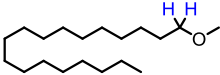$$R^1\text{-CO-O-}R^2 \xrightarrow[\text{H}_2]{\text{Pt–MoO}_x/\text{ZrO}_2} R^1\text{-CH}_2\text{-O-}R^2$$
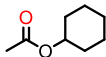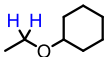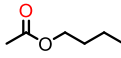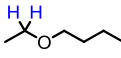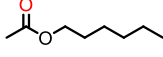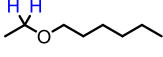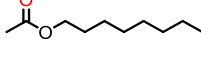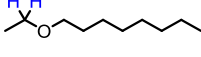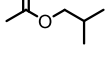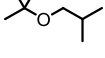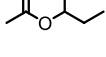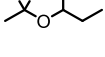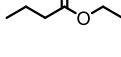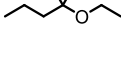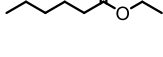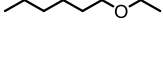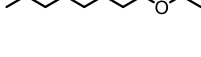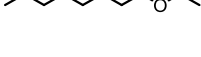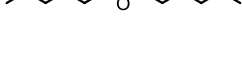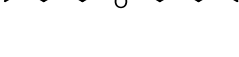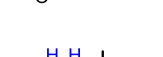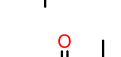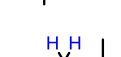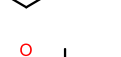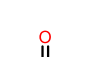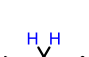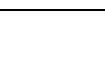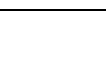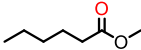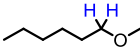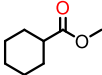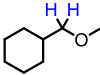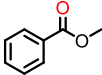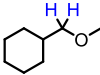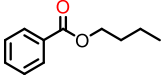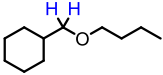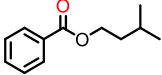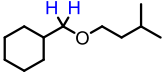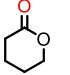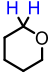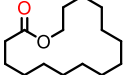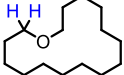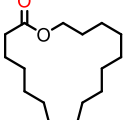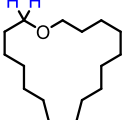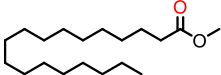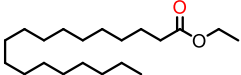
entry	ester	ether	time (h)	conv. (%)	yield (%)
1			4	97	70
2			4	>99	57
3			4	>99	61
4			4	>99	61
5			4.5	98	84
6			4	98	64
7			4	>99	72
8			5	>99	75
9			4	>99	74
10			4	>99	71
11[b]			4	9	0
12			12	>99	86[a]
13			12	>99	95[a]
14			4	72	0
15[c]			4	>99	0

Table 4-5 *(Contd.)*

$$R^1 \overset{O}{\underset{O}{\parallel}} R^2 \xrightarrow[\text{H}_2]{\text{Pt–MoO}_x/\text{ZrO}_2} R^1 \overset{H\ H}{\underset{O}{\parallel}} R^2$$
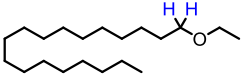
| entry	ester	ether	time (h)	conv. (%)	yield (%)
16[d]			3	>99	61
17[d]			3	>99	62
18[d]			6	>99	61
19			4	>99	64
20			8	>99	80
21[e]			4	>99	4
22			24	99	68[a]
23			24	92	60[a]
24[d]			10	98	76[a]
25			12	98	87[a]

Reaction conditions: Pt–MoO$_x$/ZrO$_2$ (0.15 g, Pt: 2 mol% and Mo: 0.375 mol%), ester (1 mmol), *n*-hexane (3 mL), 100 °C, H$_2$ (0.5 MPa). Conversion and yield were determined by GC-MS using an internal standard for analysis. [a] ^{1}H NMR yield. [b] 1-Hexanol was produced in a 9% yield. [c] Ethyl pivalate was produced in a 69% yield. [d] 140 °C, H$_2$ (5 MPa). [e] 1-Pentanol and pentyl pentanoate were produced in 26% and 12% yield, respectively.
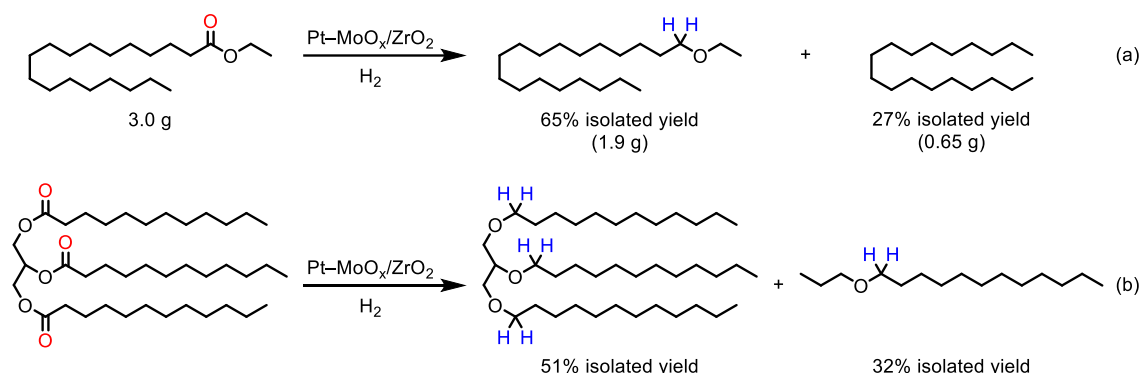
Scheme 4-4 HDO of biomass-derived esters. (a) Gram-scale HDO of ethyl stearate. Reaction conditions: Pt–MoO$_x$/ZrO$_2$ (0.15 g, Pt: 2 mol% and Mo: 0.375 mol%), ethyl stearate (3 g, 9.6 mmol), *n*-hexane (10 mL), 100 °C, H$_2$ (3 MPa), 72 h. (b) HDO of trilaurin. Reaction conditions: Pt–MoO$_x$/ZrO$_2$ (0.15 g, Pt: 2 mol% and Mo: 0.375 mol% with respect to the ester moiety), trilaurin (0.33 mmol), *n*-hexane (3 mL), 100 °C, H$_2$ (0.5 MPa), 48 h.

3.3 Reaction pathway

The reaction pathway for the Pt–MoO$_x$/ZrO$_2$-catalyzed HDO of esters was investigated. Three reaction pathways were proposed: hydrogenation of ester to alcohol followed by alcohol condensation (Scheme 4-5a); hydrogenation to hemiacetal, dehydration, and subsequent hydrogenation (Scheme 4-5b); and direct HDO (Scheme 4-5c). The time-course data shown in Figure 4-2, **2** was formed without an induction period. Moreover, no ethers were produced in the control experiment using **3** and ethanol in the presence of Pt–MoO$_x$/ZrO$_2$ (Scheme 4-6a), suggesting that Pt–MoO$_x$/ZrO$_2$ catalyzed HDO is unlikely to occur through the alcohol condensation pathway shown in Scheme 4-5a. Moreover, the HDO of cyclohexyl acetate-*d$_3$* gave cyclohexyl ethyl-*d$_3$* ether in a 67% yield without the formation of H–D scrambling products (Scheme 4-6b), revealing that the pathway abstracting α-hydrogen (Scheme 4-5b) is negligible. Therefore, the direct HDO pathway (Scheme 4-5c) is the most plausible among the proposed pathways in Scheme 4-5.
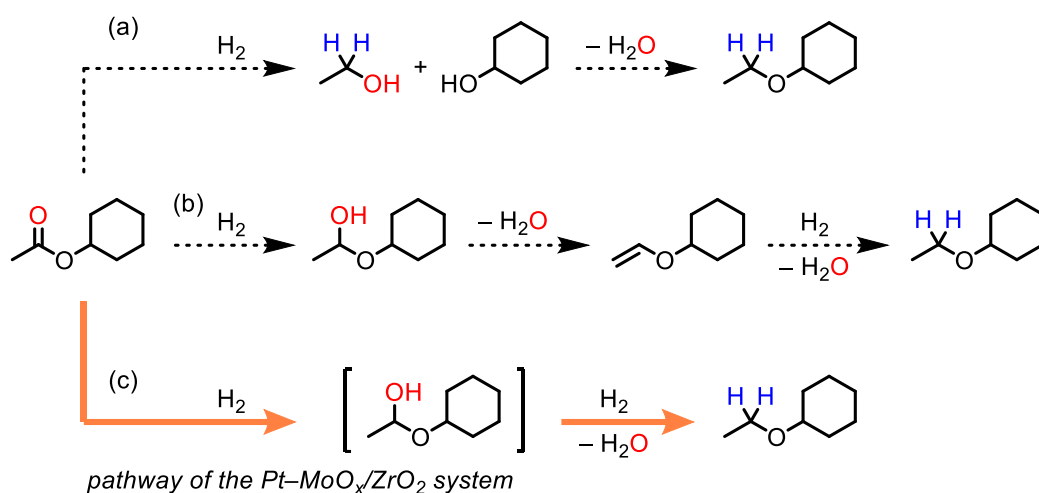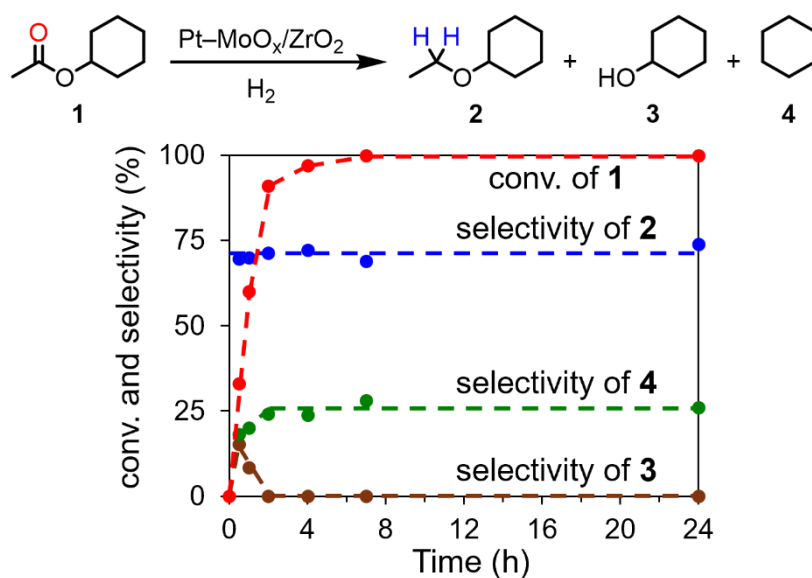
Scheme 4-5 Possible reaction pathways.

Figure 4-2 Time-course data of the HDO of **1** using Pt–MoO$_x$/ZrO$_2$. Pt–MoO$_x$/ZrO$_2$ (0.15 g, Pt: 2 mol% and Mo: 0.375 mol%), **1** (1 mmol), *n*-hexane (3 mL), 100 °C, H$_2$ (0.5 MPa). Conversion and selectivity were determined by GC-MS using an internal standard for analysis. Red circles: conversion of **1**, blue circles: selectivity of **2**, brown circles: selectivity of **3**, green circles: selectivity of **4**.
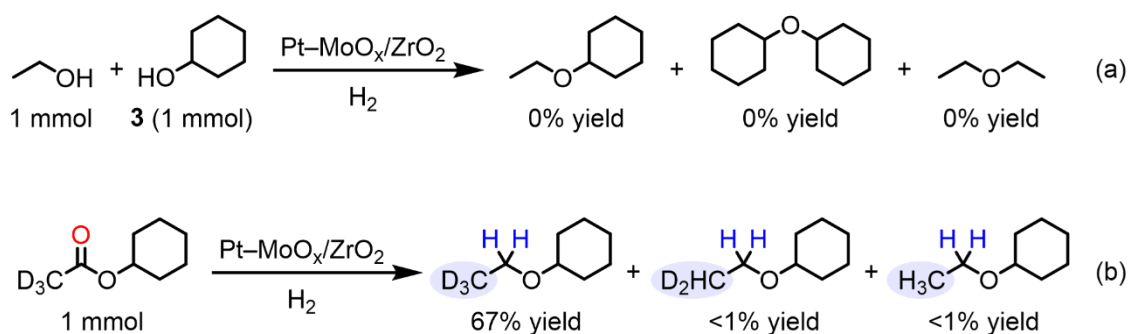
Scheme 4-6 Control experiments. (a) Condensation of ethanol and **3**. (b) HDO of cyclohexyl acetate-d_3. Reaction conditions: Pt–MoO$_x$/ZrO$_2$ (0.15 g, Pt: 2 mol% and Mo: 0.375 mol%), *n*-hexane (3 mL), 100 °C, H$_2$ (0.5 MPa), 4 h. Yield was determined by GC-MS using an internal standard for analysis.

3.4 Characterizations

To investigate the valence states of Pt and Mo species in Pt–MoO$_x$/ZrO$_2$, XANES analysis was performed. The Pt L_3-edge XANES spectrum of used Pt–MoO$_x$/ZrO$_2$ showed lower white line intensity compared with fresh Pt–MoO$_x$/ZrO$_2$, and was similar to that of Pt foil, suggesting formation of Pt^0 during HDO (Figure 4-3a). In the Mo K-edge XANES spectra, the absorption edge energy of fresh and used Pt–MoO$_x$/ZrO$_2$ were similar to that of MoO$_3$ and MoO$_2$, respectively, which reveals that Mo^{6+} species were reduced to Mo^{4+} *in situ* (Figure 4-3b). The Mo K-edge XANES spectrum of used Pt−MoO$_x$/ZrO$_2$ was difficult to distinguish from that of fresh Pt−MoO$_x$/ZrO$_2$ because the absorption edges of Mo K-α and Zr K-β were overlapped. Therefore, the Mo K-edge XANES spectra of Pt−MoO$_x$/TiO$_2$ before and after the reaction were also measured to support the Mo K-edge XANES results (Figure 4-3c). Notably, pre-edge peak of the Mo K-edge XANES spectrum remained even after the formation of Mo^{4+}. It is reported that the pre-edge peak in the spectrum of MoO$_3$ is derived from a distorted MoO$_6$ octahedral structure [35]. Therefore, the Mo species in used Pt–MoO$_x$/ZrO$_2$ were reduced to 4+ valence state without changing the pristine distorted octahedral structure of MoO$_3$, indicating the formation of oxygen vacancy (O$_v$) sites on the MoO$_3$ surface.
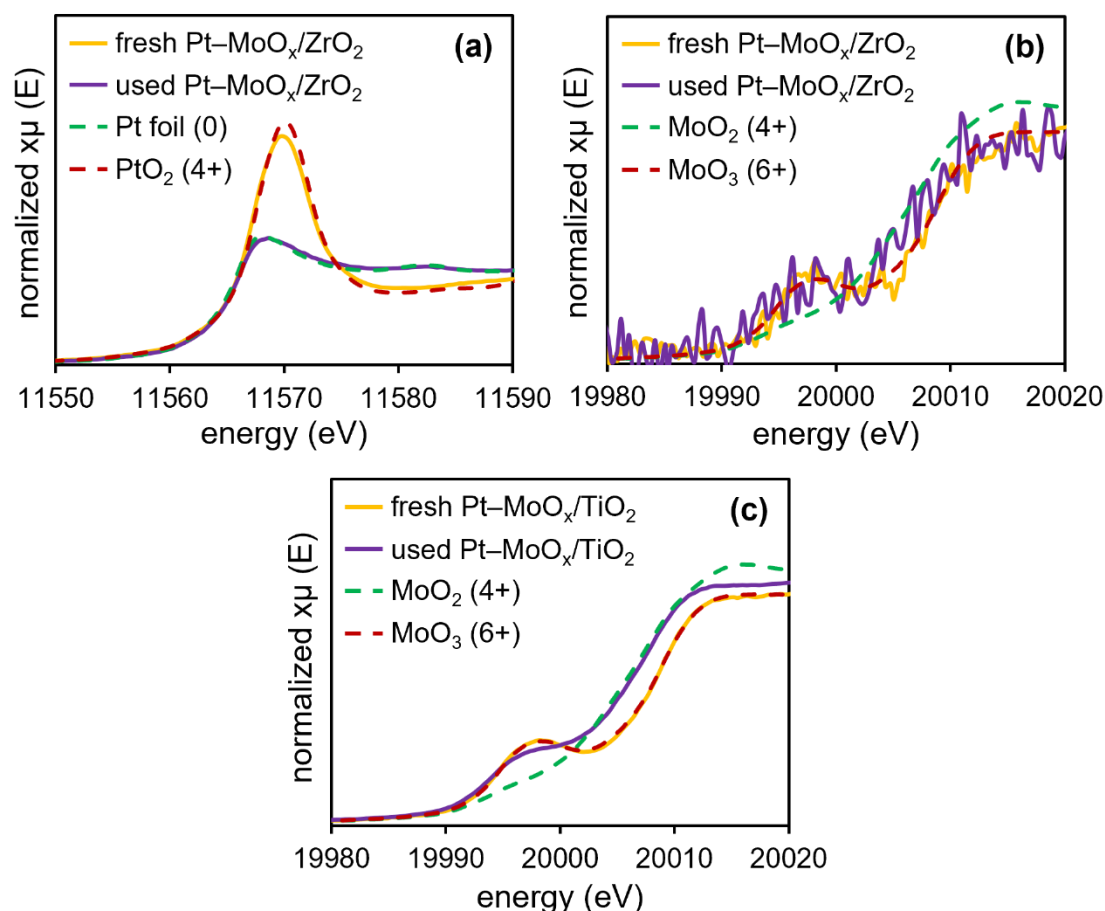
Figure 4-3 (a) Pt L_3-edge XANES spectra of fresh Pt–MoO$_x$/ZrO$_2$, used Pt–MoO$_x$/ZrO$_2$, Pt foil, and PtO$_2$. (b) Mo K-edge XANES spectra of fresh Pt–MoO$_x$/ZrO$_2$, used Pt–MoO$_x$/ZrO$_2$, MoO$_2$, and MoO$_3$. (c) Mo K-edge XANES spectra of fresh Pt–MoO$_x$/TiO$_2$, used Pt–MoO$_x$/TiO$_2$, MoO$_2$, and MoO$_3$.

Furthermore, TEM images of used Pt–MoO$_x$/ZrO$_2$ confirmed the presence of nanoparticles (NPs) with a mean diameter of 2.4 nm (Figure 4-4a). A high-resolution TEM image of the NPs revealed that the measured d-spacing value of the lattice fringe was approximately 0.20 nm, which corresponds to the (200) plane of fcc Pt NPs (Figure 4-4b). XRD pattern of used Pt–MoO$_x$/ZrO$_2$ showed no diffraction peaks attributed to the Pt or Mo species, suggesting high dispersion of the Pt NPs and MoO$_x$ (Figure 4-4c). CO pulse chemisorption analysis of Pt–MoO$_x$/ZrO$_2$ and Pt/ZrO$_2$ showed similar CO adsorption amounts (Table 4-6), indicating that the Mo species in Pt–MoO$_x$/ZrO$_2$ are mainly present

on the ZrO$_2$ surface rather than Pt NPs surface [36]. Overall, these characterizations suggest that Pt NPs and MoO$_x$ species are generated *in situ* and dispersed on ZrO$_2$.
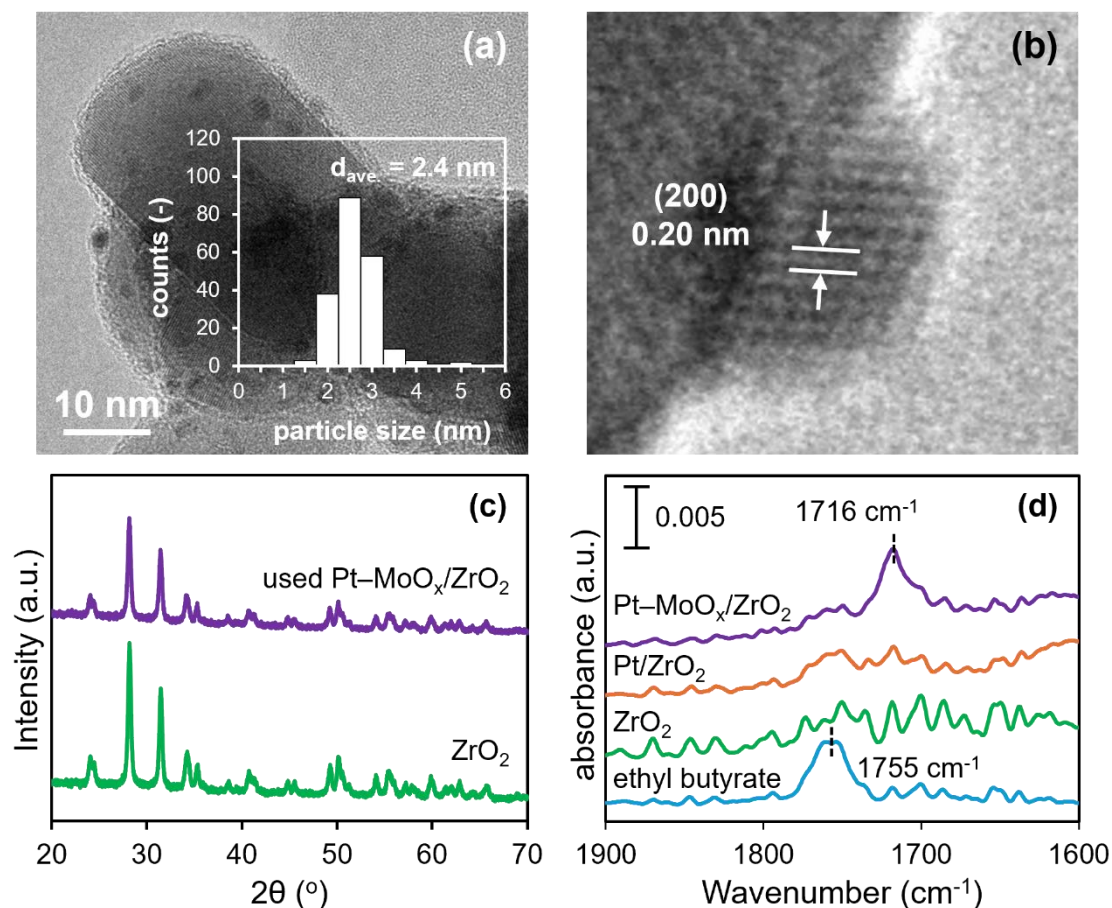

Figure 4-4 (a) TEM image and size distribution histogram (inset) of used Pt–MoO$_x$/ZrO$_2$. (b) High-resolution TEM image of used Pt–MoO$_x$/ZrO$_2$ showing one-dimensional lattice fringes of the (200) lattice planes in the Pt NPs. (c) XRD patterns of used Pt–MoO$_x$/ZrO$_2$ and ZrO$_2$. (d) FT-IR spectra of ethyl butyrate vapor and ethyl butyrate adsorbed on Pt−MoO$_x$/ZrO$_2$, Pt/ZrO$_2$, and ZrO$_2$.

Table 4-6 Results of CO pulse chemisorption analysis.

| sample	adsorption amount (mmol/g)	dispersion
Pt–MoO$_x$/ZrO$_2$	0.0821	0.634
Pt/ZrO$_2$	0.0835	0.644

Catalysts were pretreated in 5% H$_2$ in Ar flow at 100 °C before CO pulse injection.

3.5 Proposed catalyst cycle

The interaction between Pt–MoO$_x$/ZrO$_2$ and esters was investigated using FT-IR analysis with ethyl butyrate as a probe molecule. When ethyl butyrate vapor was introduced into Pt–MoO$_x$/ZrO$_2$ at 100 °C, an intense band attributed to the C=O stretching vibration of the ester moiety was observed at 1716 cm^{-1} (Figure 4-4d), which was much lower than that of obtained for pure ethyl butyrate vapor (1755 cm^{-1}). In contrast, no bands were observed in the spectra for Pt/ZrO$_2$ and ZrO$_2$. It is reported that the O$_v$ sites of MoO$_x$ act as Lewis acid sites for the activation of carbonyl moieties [37,38]. Thus, the FT-IR and XANES results indicate that the O$_v$ sites of MoO$_x$ adsorb and activate the carbonyl moiety of the ester.

Based on the above results, a catalyst cycle in the Pt–MoO$_x$/ZrO$_2$-catalyzed HDO of esters to ethers was proposed (Scheme 4-7). First, Pt NPs are formed by the reduction of PtO$_2$ and dissociate H$_2$ (Scheme 4-7(I)). The spillover hydrogen from the Pt NPs reduces MoO$_3$ to form O$_v$ sites (Scheme 4-7(II)). Molecular adsorption of ester and activation of the carbonyl moiety occur on the O$_v$ sites of MoO$_x$ (Scheme 4-7(III)) followed by hydrogen addition (Scheme 4-7(IV)). Finally, MoO$_x$ remove carbonyl oxygen to produce the desired ether (Scheme 4-7(V)). Overall, the HDO of esters proceeds through a "reverse Mars–van Krevelen"-type mechanism [39–42], in which Pt NPs supply hydrogen

and MoO$_x$ removes carbonyl oxygen through coordination at its O$_v$ sites. This cooperative catalysis between the Pt NPs and MoO$_x$ efficiently facilitates the direct HDO of esters to ethers.
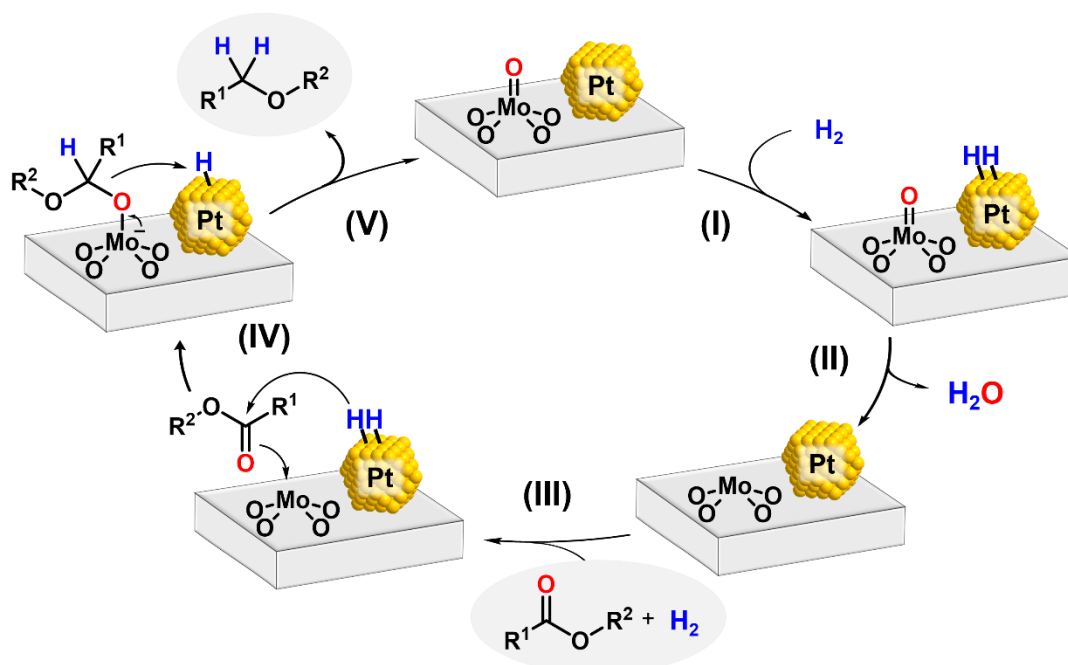
Scheme 4-7 Proposed catalyst cycle for the HDO of esters to ethers over Pt–MoO$_x$/ZrO$_2$.

4   Conclusions

The efficient heterogeneous catalyst system for the direct HDO of esters to ethers was developed using Pt–MoO$_x$/ZrO$_2$. A wide range of esters, including biomass derived triglycerides, were transformed into their corresponding unsymmetrical and symmetric ethers under mild reaction conditions (>0.1 MPa H$_2$ at 100 °C). Moreover, Pt–MoO$_x$/ZrO$_2$ was reusable without loss of its high activity and applicable to gram-scale production with a high TON (260), thus providing a simple and clean methodology for unsymmetrical ether synthesis. XANES and FT-IR studies revealed that the high selectivity of ether in the Pt–MoO$_x$/ZrO$_2$ system was attributable to cooperative catalysis between Pt NPs and MoO$_x$, where Pt NPs separate H$_2$ and MoO$_x$ molecularly adsorb ester.

5   Reference

1. Karas, L.; Piel, W. J. *Ethers. In Kirk-Othmer Encyclopedia of Chemical Technology*; Wiley, 2000.

2. Knözinger, H. Dehydration of Alcohols on Aluminum Oxide. *Angew. Chem., Int. Ed.* **1968**, *7*, 791–805.

3. Rorrer, J. E.; Bell, A. T.; Toste, F. D. Synthesis of Biomass-Derived Ethers for Use as Fuels and Lubricants. *ChemSusChem* **2019**, *12*, 2835–2858.

4. Feuer, H.; Hooz, J. *Methods of formation of the ether linkage. In The Chemistry of the Ether Linkage*; Wiley, 1967.

5. Lluna-Galán, C.; Izquierdo-Aranda, L.; Adam, R.; Cabrero-Antonino, J. R. Catalytic Reductive Alcohol Etherifications with Carbonyl-Based Compounds or CO_2 and Related Transformations for the Synthesis of Ether Derivatives. *ChemSusChem* **2021**, *14*, 3744–3784.

6. Yun, Y. S.; Berdugo-Díaz, C. E.; Flaherty, D. W. Advances in Understanding the Selective Hydrogenolysis of Biomass Derivatives. *ACS Catal.* **2021**, *11*, 11193–11232.

7. Pettit, G. R.; Kasturi, T. R. Steroids and Related Natural Products. II. A Method for the Direct Conversion of Esters to Ethers. *J. Org. Chem.* **1960**, *25*, 875–876.

8. Pettit, G. R.; Piatak, D. M. Steroids and Related Natural Products. XI. Reduction of Esters to Ethers. *J. Org. Chem.* **1962**, *27*, 2127–2130.

9. Go, H. C.; Branen, A. L. Synthesis of Long Chain Alkyl Glyceryl Ethers from Triglycerides Using Boron Trifluoride Etherate and Lithium Aluminum Hydride. *J. Am. Oil Chem. Soc.* **1975**, *52*, 427–429.

10. Ramachandran, P. V.; Alawaed, A. A.; Hamann, H. J. Catalyst- and Stoichiometry-Dependent Deoxygenative Reduction of Esters to Ethers or Alcohols with Borane–Ammonia. *Org. Lett.* **2023**, *25*, 6902–6906.

11. Mao, Z.; Gregg, B. T.; Cutler, A. R. Catalytic Hydrosilylation of Organic Esters Using Manganese Carbonyl Acetyl Complexes. *J. Am. Chem. Soc.* **1995**, *117*, 10139–10140.

12. Yato, M.; Homma, K.; Ishida, A. Reduction of Carboxylic Esters to Ethers with Triethyl Silane in the Combined Use of Titanium Tetrachloride and Trimethylsilyl Trifluoromethanesulfonate. *Tetrahedron* **2001**, *57*, 5353–5359.

13. Matsubara, K.; Iura, T.; Maki, T.; Nagashima, H. A Triruthenium Carbonyl Cluster Bearing a Bridging Acenaphthylene Ligand: An Efficient Catalyst for Reduction of Esters, Carboxylic Acids, and Amides by Trialkylsilanes. *J. Org. Chem.* **2002**, *67*, 4985–4988.

14. Sakai, N.; Moriya, T.; Konakahara, T. An Efficient One-Pot Synthesis of Unsymmetrical Ethers: A Directive Deoxygenation of Esters using an InBr$_3$/Et$_3$SiH Catalytic System. *J. Org. Chem.* **2007**, *72*, 5920–5922.

15. Sakai, N.; Moriya, T.; Fujii, K.; Konakahara, T. Direct Reduction of Esters to Ethers with an Indium(III) Bromide/Triethylsilane Catalytic System. *Synthesis* **2008**, *21*, 3533–3536.

16. Das, S.; Li, Y.; Junge, K.; Beller, M. Synthesis of Ethers from Esters via Fe-Catalyzed Hydrosilylation. *Chem. Commun.* **2012**, *48*, 10742–10744.

17. Biermann, U.; Metzger, J. O. Synthesis of Ethers by GaBr$_3$-Catalyzed Reduction of Carboxylic Acid Esters and Lactones by Siloxanes. *ChemSusChem* **2014**, *7*, 644–649.

18. Xu, S.; Boschen, J. S.; Biswas, A.; Kobayashi, T.; Pruski, M.; Windus, T. L.; Sadow, A. D. Mild Partial Deoxygenation of Esters Catalyzed by an Oxazolinylborate-Coordinated Rhodium Silylene. *Dalton Trans.* **2015**, *44*, 15897–15904.

19. Hosokawa, S.; Toya, M.; Noda, A.; Morita, M.; Ogawa, T.; Motoyama, Y. Catalytic Silane-Reduction of Carboxylic Esters and Lactones: Selective Synthetic Methods to Aldehydes, Lactols, and Ethers via Silyl Acetal Intermediates. *ChemistrySelect* **2018**, *3*, 2958–2961.

20. Dannecker, P.-K.; Biermann, U.; von Czapiewski, M.; Metzger, J. O.; Meier, M. A. R. Renewable Polyethers via GaBr$_3$-Catalyzed Reduction of Polyesters. *Angew Chem., Int. Ed.* **2018**, *57*, 8775–8779.

21. Martínez-Ferraté, O.; Chatterjee, B.; Werlé, C.; Leitner, W. Hydrosilylation of Carbonyl and Carboxyl Groups Catalysed by Mn(I) Complexes Bearing Triazole Ligands. *Catal. Sci. Technol.* **2019**, *9*, 6370–6378.

22. Dannecker, P.-K.; Biermann, U.; Sink, A.; Bloesser, F. R.; Metzger, J. O.; Meier, M. A. R. Fatty Acid–Derived Aliphatic Long Chain Polyethers by a Combination of Catalytic Ester Reduction and ADMET or Thiol-Ene Polymerization. *Macromol. Chem. Phys.* **2019**, *220*, 1800440.

23. Rysak, V.; Dixit, R.; Trivelli, X.; Merle, N.; Agbossou-Niedercorn, F.; Vanka, K.; Michon, C. Catalytic Reductive Deoxygenation of Esters to Ethers Driven by Hydrosilane Activation through Non-Covalent Interactions with a Fluorinated Borate Salt. *Catal. Sci. Technol.* **2020**, *10*, 4586–4592.

24. Li, Y.; Topf, C.; Cui, X.; Junge, K.; Beller, M. Lewis Acid Promoted Ruthenium(II)-Catalyzed Etherifications by Selective Hydrogenation of Carboxylic Acids/Esters. *Angew. Chem., Int. Ed.* **2015**, *54*, 5196–5200.

25. Erb, B.; Risto, E.; Wendling, T.; Gooßen, L. J. Reductive Etherification of Fatty Acids or Esters with Alcohols using Molecular Hydrogen. *ChemSusChem* **2016**, *9*, 1442–1448.

26. Stadler, B. M.; Hinze, S.; Tin, S.; de Vries, J. G. Hydrogenation of Polyesters to Polyether Polyols. *ChemSusChem* **2019**, *12*, 4082–4087.

27. Sutter, M.: Dayoub, W.; Metay, E.; Raoul, Y.; Lemaire, M. Selective Synthesis of 1-*O*-Alkyl(poly)glycerol Ethers by Catalytic Reductive Alkylation of Carboxylic Acids with a Recyclable Catalytic System. *ChemSusChem* **2012**, *5*, 2397–2409.

28. Sutter, M.: Dayoub, W.; Metay, E.; Raoul, Y.; Lemaire, M. 1-*O*-Alkyl (di)glycerol Ethers Synthesis from Methyl Esters and Triglycerides by Two Pathways: Catalytic Reductive Alkylation and Transesterification/Reduction. *Green Chem.* **2013**, *15*, 786–797.

29. Yun, Y. S.; Berdugo-Díaz, C. E.; Luo, J.; Barton, D. G.; Chen, I.; Lee, J.; Flaherty, D. W. The Importance of Brønsted Acid Sites on C–O Bond Rupture Selectivities during Hydrogenation and Hydrogenolysis of Esters. *J. Catal.* **2022**, *411*, 212–225.

30. Berdugo-Díaz, C. E.; Yun, Y. S.; Manetsch, M. T.; Luo, J.; Barton, D. G.; Chen, X.; Flaherty, D. W. Pathways for Reactions of Esters with H_2 over Supported Pd Catalysts: Elementary Steps, Site Requirements, and Particle Size Effects. *ACS Catal.* **2022**, *12*, 9717–9734.

31. Berdugo-Díaz, C. E.; Manetsch, M. T.; Yun, Y. S.; Lee, J.; Luo, J.; Chen, X.; Flaherty, D. W. Ester Reduction with H_2 on Bifunctional Metal-Acid Catalysts: Implications of Metal Identity on Rates and Selectivities. *Angew. Chem., Int. Ed.* **2023**, e202216165.

32. Berdugo-Díaz, C. E.; Manetsch, M. T.; Lee, J.; Yun, Y. S.; Yancey, D. F.; Rozeveld, S. J.; Luo, J.; Chen, X.; Flaherty, D. W. Ester Reduction on Bifunctional Metal-acid Catalysts: Effect of Metal to Acid Ratio, *J. Catal.* **2024**, *430*, 115346.

33. Pritchard, J.; Ciftci, A.; Verhoeven, M. W. G. M.; Hensen, E. J. M.; Pidko, E. A. Supported Pt-Re Catalysts for the Selective Hydrogenation of Methyl and Ethyl Esters to Alcohols. *Catal. Today* **2017**, *279*, 10–18.

34. Knothe, G. Analyzing Biodiesel: Standards and Other Methods. *J. Am. Oil Chem. Soc.* **2006**, *83*, 823–833.

35. Borg, S.; Liu, W.; Etschmann, B.; Tian, Y.; Brugger, J. An XAS Study of Molybdenum Speciation in Hydrothermal Chloride Solutions from 25–385 °C and 600 bar. *Geochim. Cosmochim. Acta* **2012**, *92*, 292–307.

36. Asano, T.; Nakagawa, Y.; Tamura, M.; Tomishige, K. Structure and Mechanism of Titania-

Supported Platinum−Molybdenum Catalyst for Hydrodeoxygenation of 2-Furancarboxylic Acid to Valeric Acid. *ACS Sustainable Chem. Eng.* **2019**, *7*, 9601–9612.

37. Toyao, T.; Siddiki, S. M. A. H.; Kon, K.; Shimizu, K. The Catalytic Reduction of Carboxylic Acid Derivatives and CO_2 by Metal Nanoparticles on Lewis-Acidic Supports. *Chem. Rec.* **2018**, *18*, 1374–1393.

38. Najmi, S.; Rasmussen, M.; Innocenti, G.; Chang, C.; Stavitski, E.; Bare, S. R.; Medford, A. J.; Medlin, J. W.; Sievers, C. Pretreatment Effects on the Surface Chemistry of Small Oxygenates on Molybdenum Trioxide. *ACS Catal.* **2020**, *10*, 8187–8200.

39. Prasomsri, Y.; Nimmanwudipong, T.; Roman-Leshkov, Y. Effective Hydrodeoxygenation of Biomass-Derived Oxygenates into Unsaturated Hydrocarbons by MoO_3 Using Low H_2 Pressures. *Energy Environ. Sci.* **2013**, *6*, 1732–1738.

40. Mironenko, A. V.; Vlachos, D. G. Conjugation-Driven "Reverse Mars−van Krevelen"-Type Radical Mechanism for Low-Temperature C−O Bond Activation, *J. Am. Chem. Soc.* **2016**, *138*, 8104–8113.

41. Mine, S.; Yamaguchi, T.; Ting, K. W.; Maeno, Z.; Siddiki, S. M. A. H.; Oshima, K.; Satokawa, S.; Shimizu, K.; Toyao, T. Reverse Water-gas Shift Reaction over $Pt/MoO_x/TiO_2$: Reverse Mars–van Krevelen Mechanism via Redox of Supported MoO_x. *Catal. Sci. Technol.* **2021**, *11*, 4172–4180.

42. Kuwahara, Y.; Mihogi, T.; Hamahara, K.; Kusu, K.; Kobayashi, H; Yamashita, H. A Quasi-Stable Molybdenum Sub-Oxide with Abundant Oxygen Vacancies that Promotes CO_2 Hydrogenation to Methanol. *Chem. Sci.* **2021**, *12*, 9902–9915.

General Conclusions

This thesis deals with studies on the catalysis of supported platinum–molybdenum oxide (Pt–MoO$_x$) in the reductive transformation of carboxylic acids and esters, (i) reductive amination of carboxylic acids to alkylamines, (ii) reductive amination of triglycerides to fatty amines, and (iii) direct hydrodeoxygenation of esters to unsymmetrical ethers.

In Chapter I, the author reviewed the heterogeneous catalyst systems for the hydrogenation of carboxylic acids and esters to alcohols focusing on their reaction mechanisms. Co-presence of metallic species and Lewis acids is effective for the activation of H$_2$ and carbonyl compounds. This cooperative catalysis will be applicable to reductive transformations to afford various organic compounds except for alcohols. Although reductive transformations have been less explored, they possess a high potential to convert carboxylic acids and esters into value-added compounds.

In Chapter II, the author developed an aluminum oxide-supported Pt–MoO$_x$ (Pt–MoO$_x$/γ-Al$_2$O$_3$) catalyst for the reductive amination of carboxylic acids. Pt–MoO$_x$/γ-Al$_2$O$_3$ could be operated under mild conditions such as 0.1 MPa H$_2$ and 140 °C. This is the first catalyst that promotes the reductive amination of carboxylic acid at atmospheric pressure of H$_2$. Broad substrate scope was demonstrated with respect to both carboxylic acids and amines. Notably, biomass-derived fatty acids were successfully aminated. The catalyst was easily separated from the reaction mixture and reused four times maintaining its high activity and selectivity. Furthermore, a high turnover number (TON) value of 363 was achieved in the gram-scale reaction. Characterizations and DFT calculations revealed that platinum nanoparticles (Pt NPs) separate H$_2$ and molybdenum oxides (MoO$_x$) activate carboxylic acids, leading to the high performance of the Pt–MoO$_x$/γ-Al$_2$O$_3$ catalyst.

In Chapter III, the author described the reductive amination of triglycerides to fatty amines catalyzed by a titanium oxide-supported Pt–MoO$_x$ (Pt–MoO$_x$/TiO$_2$). Pt–MoO$_x$/TiO$_2$ was operable under mild conditions, such as 1 MPa H$_2$ and 180 °C, compared with those previously reported

heterogeneous catalytic systems. Moreover, Pt–MoO$_x$/TiO$_2$ could be reused ten times maintaining its high activity, demonstrating its high durability. A wide range of amines and triglycerides, including a real cooking oil, were successfully transformed into the desired fatty amines. Detailed investigations of the reaction mechanisms revealed that the TiO$_2$ support facilitates the amidation of triglycerides to fatty amides as a solid acid catalyst. Then, the Pt NPs and MoO$_x$ activate H$_2$ and fatty amides, respectively, which promotes the hydrodeoxygenation of fatty amides to fatty amines. Therefore, the co-presence of TiO$_2$, Pt NPs, and MoO$_x$ is crucial for the efficient reductive amination of triglycerides.

In Chapter IV, the author achieved direct hydrodeoxygenation of esters to unsymmetrical ethers using a zirconium oxide-supported Pt–MoO$_x$ (Pt–MoO$_x$/ZrO$_2$) catalyst. This is the first example that promotes direct hydrodeoxygenation of esters to ethers. Various esters, including biomass-derived triglycerides, were converted into their corresponding unsymmetrical ethers in high yields. The Pt–MoO$_x$/ZrO$_2$ catalyst operated well under mild reaction conditions, e.g. 0.1–0.5 MPa H$_2$ and 100 °C, and reused without loss of its high activity. Furthermore, a high TON of 260 was demonstrated in the gram-scale hydrodeoxygenation. Control experiments revealed that the present reaction proceeded through direct removal of the carbonyl oxygen of the esters. The author proposed a reverse Mars–van Krevelen-type mechanism, where Pt NPs activated H$_2$ and MoO$_x$ with oxygen vacancy sites abstracted the carbonyl oxygen of esters to produce ethers.

Finally, the author envisages further development of Pt–MoO$_x$ catalysts for reductive transformations as follows:

1. It is necessary to develop a catalyst with a lower Pt loading for application in the chemical industry since Pt is rare and expensive. In catalytic reactions, surface metal atoms act as active sites, and the catalytic activity per total metal atom theoretically increases with decreasing particle size. The ultimate small-size limit is a single-atom catalyst. Thus, the development of catalysts with Pt

single atoms and MoO_x will increase the turnover number based on Pt atoms and contribute to decrease Pt loading amount.

2. The reusability of catalysts is important for industrial applications. As mentioned in Chapter II, leaching of MoO_x from Pt–MoO_x/γ-Al_2O_3 was observed after 6th run due to the presence of acid in the reaction mixture. Leaching was significant for the Pt–MoO_x/TiO_2 catalyst which showed the highest turnover frequency in the first run. To develop durable Pt–MoO_x catalysts in the presence of carboxylic acids, it is desirable to construct a strong bond between MoO_x and the support materials, for example by preparing a mixed oxide.

List of Publications

[1] **<u>Katsumasa Sakoda</u>**, Sho Yamaguchi, Kazuki Honjo, Yasutaka Kitagawa, Takato Mitsudome, Tomoo Mizugaki

"Reductive Amination of Carboxylic Acids under H_2 Using a Heterogeneous Pt–Mo Catalyst"

Green Chemistry **2024**, *26*, 2571–2576.

[2] **<u>Katsumasa Sakoda</u>**, Harumi Furugaki, Sho Yamaguchi, Takato Mitsudome, Tomoo Mizugaki

"Reductive Amination of Triglycerides to Fatty Amines over a Titanium Oxide-Supported Pt–Mo Catalyst"

Organic & Biomolecular Chemistry **2025***, DOI: 10.1039/D4OB01843E

[3] **<u>Katsumasa Sakoda</u>**, Sho Yamaguchi, Takato Mitsudome, Tomoo Mizugaki

 "Selective Hydrodeoxygenation of Esters to Unsymmetrical Ethers over a Zirconium Oxide-Supported Pt–Mo Catalyst"

JACS Au **2022**, *2*, 665–672.

Related Works

[1] Sho Yamaguchi, Hiroki Kondo, Kohei Uesugi, **<u>Katsumasa Sakoda</u>**, Koichiro Jitsukawa, Takato Mitsudome, Tomoo Mizugaki

"H_2-Free Selective Dehydroxymethylation of Primary Alcohols over Palladium Nanoparticle Catalysts"

ChemCatChem, **2021**, *13*, 1135–1139.

International Meeting (Oral Presentation)

[1] **Katsumasa Sakoda**, Sho Yamaguchi, Takato Mitsudome, Tomoo Mizugaki

"Zirconium Oxide-Supported Pt–Mo Catalyst for the Selective Hydrodeoxygenation of Esters to Unsymmetrical Ethers"

12th International Conference on Environmental Catalysis (ICEC2022), August 2022, Osaka, Japan.

[2] **Katsumasa Sakoda**, Sho Yamaguchi, Takato Mitsudome, Tomoo Mizugaki

"Reductive Amination of Carboxylic Acids over a Heterogeneous Pt–Mo Catalyst under Mild Conditions"

International Symposium on Catalysis and Fine Chemicals (C&FC2023), December 2023, Tokyo, Japan.

[3] **Katsumasa Sakoda**, Sho Yamaguchi, Takato Mitsudome, Tomoo Mizugaki

"Sustainable Alkylamine Synthesis through Reductive Amination of Carboxylic Acids under H_2 over a Pt–Mo Catalyst"

18th International Congress on Catalysis (ICC2024), July 2024, Lyon, France.

Acknowledgement